Dipl. –Ing. Manuel Zettl

Continuous Drying of Pharmaceutical Materials with Regard to Maintaining Particle Properties

DOCTORAL THESIS

to achieve the university degree of

Doktor der technischen Wissenschaften

submitted to

Graz University of Technology

Supervisor

Univ.-Prof. Dipl.-Ing. Dr. techn. Johannes G. Khinast

Institute for Process and Particle Engineering,
Technical University Graz
Research Center Pharmaceutical Engineering GmbH, Graz

Graz, April 2021

Manuel Zettl

Continuous Drying of Pharmaceutical Materials with Regard to Maintaining Particle Properties

Dissertation

First assessor

Univ.-Prof. Dipl.-Ing. Dr.techn. Johannes Khinast

Institute of Process and Particle Engineering

Research Center Pharmaceutical Engineering GmbH

Graz University of Technology

Second assessor

Univ.-Prof. Mag.pharm. Dr.rer.nat. Eva Roblegg

Institute of Pharmaceutical Sciences

University of Graz

Affidavit

I declare that I have authored this thesis independently, that I have not used other than the declared sources/resources, and that I have explicitly indicated all material which has been quoted either literally or by content from the sources used. The text document uploaded to TUGRAZonline is identical to the present doctoral thesis.

(Ich erkläre an Eides statt, dass ich die vorliegende Arbeit selbstständig verfasst, andere als die angegebenen Quellen/Hilfsmittel nicht benutzt, und die den benutzten Quellen wörtlich und inhaltlich entnommenen Stellen als solche kenntlich gemacht habe. Das im TUGRAZ hochgeladene Textdokument ist identisch mit der vorliegenden Arbeit.)

Date

Signature

Acknowledgements

I am grateful for the supervision of Prof. Johannes Khinast and his guidance during my thesis, and for giving me the opportunity to conduct my studies at the RCPE. I could learn a lot thanks to his valuable comments and discussions throughout the years.

I also thank Prof. Eva Roblegg for being available as second assessor for this thesis, as well as for the scientific support on numerous topics.

Additionally, I want to thank Isabella Aigner for the valuable support and the numerous discussions we had over the last years, which helped me to improve the scientific quality of this thesis.

Additional gratitude goes towards Markus Krumme (Novartis) and Peter van der Wel (Hosokawa) for the financial and scientific support during my work, as well as the joyful meetings and fruitful discussions.

I want to thank the numerous colleagues and former colleagues at RCPE who supported me over the last years. However, space is limited and therefore I will only mention a few. Representatively I want to thank Thomas Hagemann, Daniel Kaiser, Sarah Koller, Manuel Kreimer, Julia Kruisz, Michael Martinetz, Jelena Milinkovic, Michael Piller, Jakob Rehrl, Paul Rinner, Mario Unterreiter, Daniel Wiegele and Patrick Vorraber.

All of my friends, who encouraged and motivated me throughout my whole life, and especially the last years. Thank you Adam, Alina, Arthur, Benno, Claudia, Kevin, Klara, Lisa, Nina, Paul and Philip.

My family, which has always been there for me and was my safe haven whenever I needed them. Their lifelong support made this thesis possible.

My newly acquired family in law, which has treated me like their own son and the nice discussions and evenings we had over the last years.

My beloved wife Jennifer. Thank you for your never-ending support and motivation, whenever I was doubtful and always being there for me.

Abstract

In the last years, the interest in continuous manufacturing (CM) has been increasing within the pharmaceutical industry. Replacing the existing, mainly batch-wise, production route by continuous methods, provides several benefits (e.g. higher product quality, lower energy consumption, higher flexibility, etc.) and can be incorporated into the processes. As suitable equipment is often not available at very small production scales and the regulatory perspective for process qualification and validation is often unclear, companies are hesitant to adapt their manufacturing routes. To overcome this issue, improved equipment and process understanding need to be developed, especially in primary manufacturing (i.e. the production of the active pharmaceutical ingredients (API)).

In this thesis, the two important steps of purification and drying within the primary production route are investigated and equipment, which is able to continuously process small-scale mass flows of pharmaceutical materials, is presented. Typically, during crystallization, particles are formed with a certain morphology and size distribution, which is ideal for the biological function in a patient's body. Therefore, the structure of the particles should be maintained as much as possible until the final dosage form is reached (e.g. tablet, suppository). This is especially hard in the drying process, as usually a high heat and mass transfer is involved and/or the particles are subject to a high shear and normal stresses, which may lead to attrition or agglomeration.

For the purification step a precipitating environment was created, where two model substance combinations (lactose/water/isopropanol and ibuprofen/ethanol/water) were investigated, to examine the difference between a hydrophilic and a lipophilic case. By shifting the solubility by the addition of an anti-solvent (i.e. isopropanol and water), solids were precipitated. By using an ultrasonic process chamber as a mixing device, the process duration could be extended to 24 h for both substance combinations with a mass flow of 200 g/min with initially 15 g/min suspended solids, without any process disruptions. The particle size distribution (PSD) measurements demonstrated that the particles increased in size over the process, due to the precipitation on the previously suspended solids. Attrition or particle breakage could not be investigated, and in general, a positive effect of ultrasound on this process could be confirmed.

To enable continuous drying at small production scales, a completely new technology has been developed. Starting with an adapted paddle dryer and the investigated problems therein, an interlocking screw design was implemented for a novel technology, which has been granted a patent. Process times of up to 14 h were possible, with cohesive materials (Ibuprofen and di-calcium phosphate at various moisture contents). The investigated mass

flows ranged between 0.5 to 2.0 kg/h on a dry basis. Several process-influencing parameters were characterized and the tested configurations resulted in evaporation rates of up to 680 g/h of water, with residual moistures below 1 wt. % after the drying process, keeping the particle morphology more or less intact.

Zusammenfassung

In den letzten Jahren wurde das Interesse an kontinuierlichen Prozessen in der pharmazeutischen Industrie immer größer. Das Ersetzen der derzeit vorherrschenden Batch-Produktion durch kontinuierliche Methoden, brächte einige Vorteile mit sich (z.B. höhere Produktqualität, niedrigerer Energieverbrauch, höhere Flexibilität etc.). Da geeignete Geräte für geringe Produktionsmengen nicht immer verfügbar sind und der regulative Aspekt für die Prozessqualifizierung und -validierung oft unklar ist, sind Unternehmen nach wie vor zögerlich ihre Produktionsweisen anzupassen. Um diese Problematik zu überwinden, müssen bessere Gerätschaften und ein höheres Prozessverständnis entwickelt werden, im Besonderen im Bereich der Primärfertigung (Wirkstoffproduktion).

In dieser Dissertation werden die zwei wichtigen Prozessschritte der Purifikation und der Trocknung in der Primärfertigung untersucht, und Geräte die fähig sind im Kleinmaßstab pharmazeutische Materialien zu verarbeiten werden vorgestellt. Typischerweise wird in der Kirstallisation dafür Sorge getragen, dass die erzeugten Partikel eine gewisse Morphologie und Größenverteilung besitzen, um ideale Bedingungen für die biologische Verfügbarkeit im Patienten zu erzeugen. Daher sollte die Struktur der Partikel weitgehend bis zur finalen Darreichungsform beibehalten werden (z.B. Tablette, Suppositorien). Dies ist im Falle der Trocknung besonders schwierig, da typischerweise hoher Wärme- und Massentransfer auftritt, und/oder die Partikel großer Kraft ausgesetzt sind, die zu Abrieb oder Agglomeration führen kann.

Für den Purifikationsschritt wurde eine prezipitierende Umgebung geschaffen, in der zwei Modellsubstanz-Kombinationen (Laktose/Wasser/Isopropanol und Ibuprofen/Ethanol/Wasser) untersucht wurden, um einen Unterschied zwischen hydrophilen und lipophilen Substanzen feststellen zu können. Durch das Beimengen eines Anti-Solvents (Isopropanol und Wasser) wurde die Löslichkeit verringert, wodurch Feststoffe ausgefällt wurden. Es konnten weder Abrieb noch zerstörte Partikel nachgewiesen werden, und generell wurde ein positiver Einfluss des Ultraschalls auf den Prozess bestätigt.

Um kontinuierliche Trocknung im Kleinmaßstab zu verwirklichen, wurde eine komplett neue Technologie entwickelt. Ausgehend von einem adaptierten Paddel-Trockner und den darin auftretenden Problematik wurde ein ineinandergreifendes Schneckensystem in einer neuen Technologie integriert, welche als Patent zugelassen wurde. Prozesszeiten bis zu 14 h waren möglich, wobei kohäsive Materialien (Ibuprofen und Di-Kalzium-Phosphat bei verschiedenen Feuchtegraden) verwendet wurden. Die untersuchten Massenflüsse lagen

zwischen 0.5 und 2.0 kg/h. Verschiedene prozessbeeinflussende Parameter wurden charakterisiert und die getesteten Konfigurationen zeigten Verdampfungsraten bis zu 680 g/h Wasser und Restfeuchten unter einem Gewichtsprozent nach dem Trocknungsprozess, wobei die Partikelmorphologie weitgehend erhalten werden konnte.

Table of Contents

Abbreviations

API	Active pharmaceutical ingredient
BET	Brunauer-Emmett and Teller
BFE	Basic flowability energy
CM	Continuous manufacturing
dW/dt	Drying rate
ffc	Flow function
IP	Point of inflection
PAT	Process analytical tools
PSD	Particle size distribution
Q_r	Cumulative distribution of index r
q_r	Density distribution of index r
r	Index of PSD (Number based 0, length based 1, area based 2, volume based 3)
RTD	Residence time distribution
SE	Specific energy
t	Time
W	Moisture content
wt. %	Weight percent
$x_{50,}$	Median value of PSD
$x_{h,r}$	Modal value of PSD
x_i	Particle diameter with size i
x_{max}	Maximum particle size
x_{min}	Minimum particle size
ΔQ_r	Probability range of particle size class
Δx_i	Particle size class

„Knowing is not enough; we must apply.
Willing is not enough; we must do"
Johann Wolfgang von Goethe (1749-1832)

„Genius is 1% inspiration and 99% perspiration"
Thomas Alva Edison (1847-1931)

1 Introduction and Motivation

Since the beginning of the 21st century, where a set of guidelines was published by the U.S. Food and Drug Administration [1], [2], the pharmaceutical industry has been shifting away from the implemented batch-wise system towards novel methods of production. While other industries, such as food, oil and chemical, implemented continuous manufacturing much earlier, there has been a tentative behavior for pharmaceutical processes [3]–[6]. This can be explained by the high investment costs, regulatory hurdles and the unavailability of equipment [7]–[10]. While batch processes have discontinuous material charging and discharging (i.e. the process chamber is loaded with material at the beginning and discharged after the process), continuous processes have materials entering and leaving the process chamber simultaneously. One of the major improvements of continuous manufacturing is that the same equipment can be used for laboratory, pilot plant and industry scale, as scale-up and scale-down can be regulated by adapting the production times or number of units. Therefore, complicated scale-up processes can be avoided by CM [10], [11]. The first attempts for an end-to-end production line were proposed by Mascia et al.[12] at the MIT center funded by Novartis. End-to-end means in this case, that all steps from the synthesis of the API until the final product are performed continuously after each other. While this offers many advantages, there is no real application for such a process at the moment, as primary and secondary manufacturing are often separated location-wise or are even performed by different companies. Additionally, some processes need a certain storage time before being feasible. Tablets for example, should have a certain relaxation period before they can be coated in order to avoid undesired effects (e.g. capping, cracking, breakage etc.)[13]–[15].

At the moment, several equipment manufacturers and production companies are producing or implementing continuous equipment, mainly in the secondary manufacturing route. An example is the GEA ConsiGma™ tableting line, where the entirety of the second manufacturing route is performed (except for a possible coating step), resulting in tablets [16]–[18]. Systems like this will provoke a significant change in the future, as flexible systems can produce a year's demand of dosage forms within a few weeks, and can then be changed to another production route, saving costs, energy, and scale-up or scale-down efforts. Also, the time to market can be significantly reduced, as storage and delivery times are reduced tremendously. Scaling up and scaling down in continuous manufacturing is as

easy as prolonging and reducing the process time. In case larger throughput is needed, the systems can also be easily numbered up [9].

Another advantage of CM is the small space requirement of the equipment. If equipment is designed in a flexible and mobile way, it can easily be integrated into a so-called ballroom concept, or modular manufacturing. Thereby a large manufacturing area can be built, with all relevant infrastructure integrated. Depending on which product needs to be produced, the single units are then placed inside and connected, and the process is run until the desired amount is produced. Afterwards the whole site can be cleaned, and replaced with a new process, which enables great flexibility as to which and how many unit operations can be connected, essentially allowing an easily implementable end-to-end manufacturing line [19].

In pharmaceutical manufacturing, there are two distinctive production areas, being the primary and secondary manufacturing, in which continuous processes can be integrated. Those two production routes are often not carried out at the same location, or even by the same companies. While primary manufacturing deals with the creation of the active pharmaceutical ingredient (API) as (usually) a dry powder, secondary manufacturing is the production route towards the final medical dose, such as a tablet, by combining one or more APIs with various excipients. Those two manufacturing steps are then followed by the packaging and are subsequently distributed around the world [20], [21].

Secondary manufacturing for oral dosage forms usually deals with dry substances, which are further processed to obtain a final product. Typical unit operations include feeding, blending, wet or dry granulation, milling, drying, tableting and coating. During this manufacturing process, one or more APIs are combined with other excipients to improve the behavior of the final dosage form. Excipients are added due to numerous reasons. Looking at tablets, several behavior-improving attributes exist, as there are materials used as anti-adherents (e.g. magnesium stereate), binders (e.g. lactose), disintegrants (e.g. starch), glidants (e.g. silica gel) or lubricants (e.g. talc). Coatings are also among these excipients.

The primary manufacturing is for the creation of the active drug substance. It starts with the synthesis, followed by crystallization, purification steps and filtration to reduce the liquid content. Purification is an important step, as the purity of the final product decides whether it meets regulatory requirements or has to be discharged. As APIs are usually very expensive, this must be avoided at all costs. Methods to achieve this are usually extraction, distillation, chromatography, adsorption-desorption or solvent exchange [22], [23]. The

method described in this thesis is purification by solvent exchange, as presented in chapter 2. A suspension, coming from crystallization with tailored particle properties, is mixed with an anti-solvent, in which the API is not dissolved, but possible impurities are. Thereby, not only the product is purified, but also the amount of valuable material is increased, as additional solids precipitate by changing the solubility. After the washing step, a filtration step can be implemented, and the process can be repeated until the desired purity is reached [24].

After the mechanical separation between liquid and solids, a paste or a granular substance is usually obtained. The classification of the flow properties of such granular compounds is a complex field, due to the many influences that exist which influence their flowability [25]–[29]. Among those are the particle size distribution (PSD), the particle shape, the moisture content and also environmental influences, such as temperature or relative air humidity. The classification of materials therefore often involves a lot of different analysis methods. Classic approaches are measuring the PSD, density, rheology, humidity, BET surface and porosity to have a good overview of the properties of a certain granular matter.

As the material properties are decisive during manufacturing, drying is a crucial process in primary as well as secondary manufacturing. Those properties are usually fixed already during crystallization and should be maintained for the final dosage form production. During drying several unwanted effects can take place. The most common problems are attrition and agglomeration during drying processes. While attrition can occur due to high shear rates or stresses, agglomeration usually occurs due to the solidification of liquid bridges between the particles, forming strong bonds [15], [30]–[32]. At the moment, small scale equipment either does not exist or is limited with regard to poorly flowable substances or changing particle properties [33]–[36]. Therefore, the further work explained in this thesis is based on the development and classification of a novel dryer design being able to process cohesive, thermosensitive materials in a continuous manner in a mass flow range between 0.5 to 2.0 kg/h on a dry basis. The development and classification of the system is presented in chapters 3 and 4.

An overview of the main challenges and influencing parameters of these fields is given in the following subchapters. At first, continuous manufacturing with a focus on the pharmaceutical industry will be presented, followed by the most important aspects of primary and secondary manufacturing. Afterwards, the purification of pharmaceuticals is addressed. Before concluding the introduction part of this thesis, the classification of granular materials is explained in more detail, followed by the drying process.

1.1 Continuous manufacturing in the pharmaceutical industry

In modern industries, continuous manufacturing is widely integrated, due to the numerous advantages. Those include a faster time to market as scale-up considerations can be avoided, higher product quality, better process understanding, higher yield and reduced waste and energy consumption. However, the pharmaceutical industry has been hesitant to implement a large number of continuous processes due to regulatory insecurities and non-available equipment. For example, the small-scale processing of powders is still a very complex topic with nearly no satisfying equipment being ready to be bought. Also, process analytical tools (PAT) need to be incorporated and validated [9], [37]–[39].

The difference between batch and continuous processing is the filling and discharging of material. While in batch processing the material is filled into the process chamber at the beginning, and is discharged after the process has finished (e.g. tray dryers), in continuous manufacturing (CM) material is continuously added to and removed from the process chamber (e.g. plug flow reactors). Regarding this major difference, it is obvious that CM reduces the storage time and needs tremendously, as after each batch process the produced material needs to be tested to see if it meets the specification and then stored. Frequently, the material must be shipped to another location, making the production process last for a long time, which in turn has an adverse effect on the product quality. On the other hand, fully integrated CM only needs a fraction of that time, as the intermediate products are directly fed into the next unit operation. Also, in contrast to batch-wise manufacturing, it needs thorough monitoring and controlling throughout the process, but by the implementation of those systems, CM leads to an increased mechanistic understanding of the involved processes [17], [40].

To replace existing batch processes by continuous methods, these methods need to be carefully investigated and analyzed. Especially important in the analysis of such processes is the residence time distribution (RTD), as too long residence times could cause degradation in some processes [41], [42]. Also, the evaluation of the system dynamics is crucial to find a suitable control strategy. Another aspect is the feeder noise and dampening, to be able to accurately predict the situation within the unit operations [43]. Furthermore, the homogeneity and content uniformity at all process steps is important. Therefore, a lot of thought has to be invested to decide which tools are placed where in the process, and the relevant chemometric models have to be implemented.

1.2 Primary manufacturing

In the manufacturing of active pharmaceutical ingredients (APIs) several different process steps are involved. An exemplary route is shown in Figure 1. At first, the substance is synthesized, before it enters the crystallization step, where the properties are usually optimized in terms of particle size distribution (PSD) and particle morphology. After this step, the solids are purified in a washing step and filtrated mechanically to reduce the amount of liquids. These washing and filtration steps can be repeated numerous times until the wanted purity of the API is achieved. Finally, the paste or granular material is dried and ready for the secondary manufacturing route.

Figure 1. Typical manufacturing route in primary manufacturing.

Synthesis can be carried out in several different ways, being biosynthetic, where natural products are used, semi-biosynthetic, where these products are chemically modified, and totally chemical, where the API is formed entirely from chemical compounds. The synthesis is mostly carried out in flow reactors, where very high or low pressures and temperatures are possible, depending on the ideal process conditions [44]. In crystallization, one of the main aspects is to avoid the formation of polymorphs with a high yield and purity. The particle and crystal attributes designed during the crystallization, should usually be kept until the final dosage form. Crystallization is traditionally provoked by cooling the mother liquor or increasing the concentration by removing the solvent (e.g. by evaporation) [45]–[47]. Afterwards the purifying steps, washing and filtration take place, whereby during the last filtration as much liquid as possible is typically removed, as thermal separation in the drying step is very energy and time consuming, and should be reduced to the maximum possible extent [48].

1.3 Secondary manufacturing

In secondary manufacturing, the final dosage form is produced. An exemplary process route for the production of tablets is shown in Figure 2. The API and the excipients are fed into a blender, where they are homogeneously mixed. Afterwards, typically a granulation step is added to improve the flowability of the powder and avoid segregation. Afterwards the granular matter is dried. Depending on the influence of the drying process

on the particle properties it might be necessary to mill the particles afterwards. Finally, lubricants or other excipients are added and blended into the mixture prior to the tableting step, where the tablets are produced. Depending on the tablet, coating might be added due to taste-masking, visual or functional purposes.

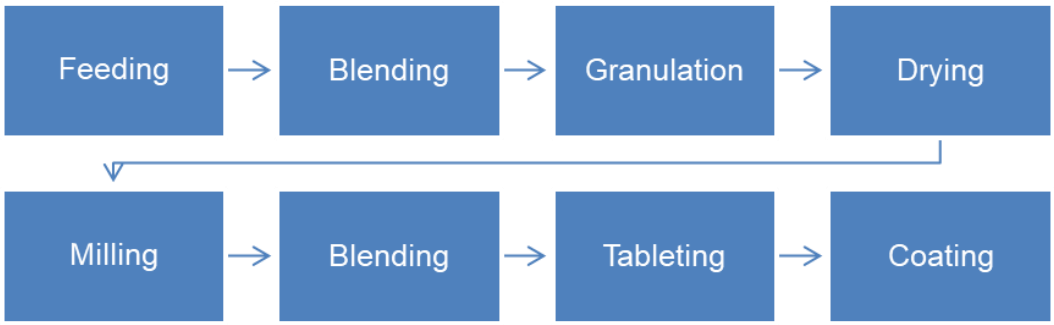

Figure 2. Typical process steps in secondary manufacturing of pharmaceuticals.

The main issue for all of these processes is that there is no straightforward theory describing granular flows, and therefore most of these operations have needed to be studied empirically until now. Due to recent advances in computer sciences, numerical methods were developed that are able to simulate behavior in certain processes [49]–[53]. Examples of occurring problems are attrition, agglomeration, breakage, layering, segregation, funneling and channeling [54]. These effects occur to the multitude of different forces acting on the particles. Mass dependent forces include gravity, buoyancy and inertial force. Hydrodynamic forces are usually dependent on the particle surface and include the fluid drag force, the terminal sink velocity, lift force and Magnus force. The third group are the cohesive forces, which include capillary forces, van der Waals and electrostatic forces. Finally, for collisions between particles there is a distinction between friction and normal forces [35], [36], [55]–[57].

1.4 Purification of pharmaceuticals

Due to the many different process steps which are involved during the production of a pharmaceutical dosage form, the purity of the used substances is of great importance. The criteria from regulatory offices must be met throughout the entire production chain, therefore care must be taken to ensure that at no point in the different unit operations impurities are formed or integrated into the product stream. As impurity, generally every substance which is not part of the intended formulation (API or excipient) is meant [42]. The avoidance of these substances is critical, as they can interfere with the biological activity of the API, or in the worst case, have an adverse effect on the patients' health (e.g. being

carcinogenic or mutagenic)[58]. The impurities can be classified into different groups, being organic, inorganic, polymorphs, enantiomers or residual solvents[42]. Unreacted compounds during the API synthesis are an example for organic impurities. Inorganic impurities are for example catalysts or heavy metals that are used for the reaction design. Polymorphs and enantiomers are formed during the reaction, and often have different properties (solubility, biological function) than the intended API, therefore a thorough investigation of the reaction products has to be carried out. The API thalidomide serves as a terrifying example of why this is necessary, as the S-enantiomer caused severe malformation of the limbs of new-born infants in the early sixties [59].

For the removal of these impurities several methods can be used. The most commonly used processes are distillation, solvent exchange, extraction, adsorption-desorption, chromatography and crystallization [22]–[24]. The first part of this thesis focuses on solvent exchange. The traditional approach is to distillate the product from the crystallization, to evaporate solvents with different boiling points, requiring vast amounts of thermal energy and possibly destroying thermosensitive APIs.

The proposed process route presented in this work uses another approach, the addition of an anti-solvent to the product. By shifting the solubility of the compounds present in the slurry, the desired purification can be achieved. The obtained product can then be mechanically separated by filtration, which is favorable in terms of energy consumption. By dissolving the impurities and filtrating the liquid, the product is purified. These steps can be repeated several times, until the API is practically pure. A drawback of this technique is that the PSD and morphology of the product can change, due to the precipitating solids. This precipitation induces further problems, as process equipment can be subject to fouling or blockage due to solidification or plugging[24], [60]. Possible routes for this process are by using agitated filter dryers[35], [36] or implementing a continuous process, as described in this thesis. Thereby the mother liquor with solid content is continuously pumped through an ultrasonic process chamber, where it is mixed with a corresponding anti-solvent. By integrating a filter after the process and repeating this process step, a purification could easily be implemented, leaving API with residual solvent as a product [60]–[62].

1.5 Material characterization and rheology

In general, speaking of pharmaceutical powders, one refers to solids in the range of 0.5 to 1000 µm. To characterize these materials several parameters need to be investigated. As standard characterization one looks at the particle size, shape, porosity and specific surface area. Another aspect is the density, flowability and cohesion properties,

and compressibility. Additionally, the melting point, solubility, moisture content and hygroscopicity are important.

Particle size distributions can be computed number based (index 0), length based (1), area based (2) or based on volume or mass (3). Most commonly number or volume based distributions are used. For the depiction of particle size distributions, most commonly two distributions are computed, namely the cumulative (Figure 3a) and the density (Figure 3b) distribution. The cumulative distribution is the integral of density distribution and ranges between 0 and 1 (or 0 and 100 %), while the density distribution shows the relative amount of particles of a certain size. The smallest particle size visible during the measurement is x_{min}. Distinctive values of PSDs are the modal value ($x_{h,r}$), which is the particle size with the highest probability and the point of inflection (PI) of the cumulative distribution. PSDs with two or more maxima are called bimodal or multimodal. The median value ($x_{50,r}$) is the particle size which is greater than 50 % of the measured particles, and can easily be obtained from the cumulative distribution. Another characteristic value is the mean diameter, which is the average particle diameter of all measured particles. In case of a symmetric distribution those three values will be the same, for asymmetric distributions different.

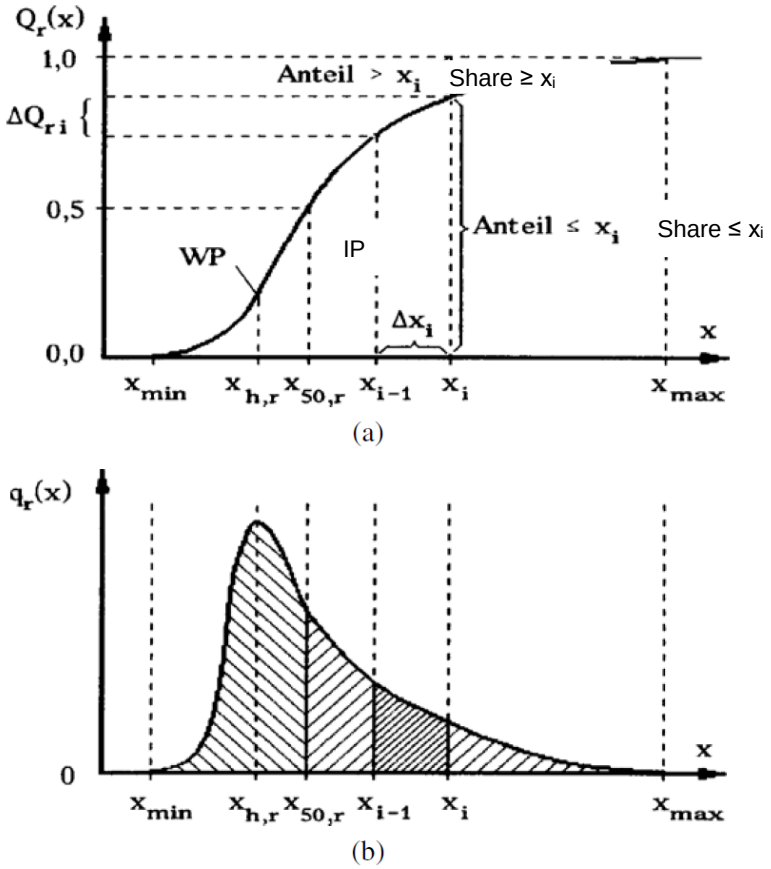

Figure 3. Typical cumulative (a) and density (b) distributions of particle size measurements [63].

For measuring the PSD of powders several considerations have to be made. It is hard to obtain relevant results, as already the sampling induces an error to the measurement. Depending on the used method the results will be different, and not all methods are suitable for all particle sizes. When the particle shape differs substantially from round, spherical particles, it has additionally to be decided which equivalent diameter is the best to use (e.g. Sauter mean diameter or sphere of same volume). Typical measurement systems work with image analysis, sieving, laser diffraction, sedimentation, dynamic light scattering or electric conduction. At the moment, laser diffraction becomes more and more important, due to its fast analysis time [64]. To get information about the particle shape, image analysis has to be performed. In general, smaller particle sizes are more cohesive [65] and also the particle shape considerably influences other flow properties, as compressibility [66].

The surface area of particles is usually measured by the Brunauer-Emmett and Teller (BET) method, which correlates the amount of adsorbed nitrogen to the surface area of the particles. Another method, which neglects the internal surface area, is the air permeability. In this method the resistance of a compacted powder plug towards an air flow is measured and correlated to the outer specific surface, which is inversely proportional to the pressure drop [63], [67].

Granular materials have several different densities which can be compared. The following densities are mentioned in increasing value. The unprocessed raw material has a certain bulk density, in which the entrapped air also contributes to the measured density value. After tapping the bulk material a defined number of times (i.e. 10, 500 and 1250 times) the solids move closer together and the density is measured again; the obtained values are referred to as tapped densities. However, still air is present between the particles. The apparent density is the value of the solids, with enclosed air between them (e.g. within agglomerates, but not between those agglomerates), and the true density is the density without enclosed air. The tapped and bulk densities are usually measured with a graduated 250 ml cylinder, in which 100 g of powder are weighed in and then tapped 10, 500 and 1250 times. The apparent density can be measured by a mercury porosimeter, which is able to measure all pores above 15 µm. The true density can be measured with a helium pycnometer [63].

Various methods can be used to determine the flowability of powders. Among those there is to measure the angle of repose, the Hausner ratio, Carr index, internal friction, wall friction and the powder rheometry. For the angle of repose 100 g of powder are placed in a funnel, and the steepness of the resulting cone below the funnel is measured. The larger

this angle is, the more cohesive the powder is. This method has the drawback that very cohesive materials will not move through the funnel at all. The Hausner ratio is the ratio between the tapped and bulk density. The closer it is to 1, the more flowable the powder is, whereas ratios above 1.5 are generally considered as poorly flowable. The Carr index is very similar, and computes the change in density in percent, where the closer to 0 the value is the better the flowability is. Percentages above 30 % indicate poor behavior [68]–[70].

To evaluate the internal and wall friction, shear cells can be used, such as the Jenike shear tester. For the internal friction, within such a shear cell the force to move particles against each other is measured, and the cohesive strength can be computed depending on the compaction of the powder. For the wall friction the force needed to displace the wall at several normal stresses is measured, which gives the yield locus [70]. Nowadays, automated rheometers exist, which enable the measuring of a multitude of parameters, such as the Freeman FT4 powder rheometer. This system has various blades and pistons, which are used to determine the torque and force acting on a powder sample. For the compressibility tests a powder bed is pre-conditioned by gentle mixing and afterwards compacted, while measuring the deformation. The aeration test uses a vented piston, and the resistance to the air flow is measured at various normal stresses. The easiest to obtain measure of the FT4 is the basic flowability energy (BFE) and the specific energy (SE), where the energy needed in several downward anti-clockwise and upward clockwise movements is collected. The trend of the needed energy gives an estimation about occurring segregation, attrition and agglomeration. For the shear cell test in the FT4, the powder bed is pre-sheared before each test run. A special shear head is mounted and increases the shear stress at constant normal forces, until the powder bed fails. Thereby the yield locus and the flow function ffc can be computed, which provides the ratio of the major principal stress and the unconfined yield strength. The higher this value is the better the flowability is; materials with a ffc below 4 are generally considered as poorly flowable [70]–[73].

A depiction of Mohr's circles of stress can be seen in Figure 4. The circles B1 to B3 are for the uniaxial stress test, hence σ_2 is 0. With increasing normal stress, the diameter of the circle increases. The consolidation stress circle is circle A, and as an example of a shear cell test, circle C is shown. The points where the material starts to flow are measured and connected, resulting in the yield limit line, giving the shear stress at any given normal force, where the granular material will start to flow [70].

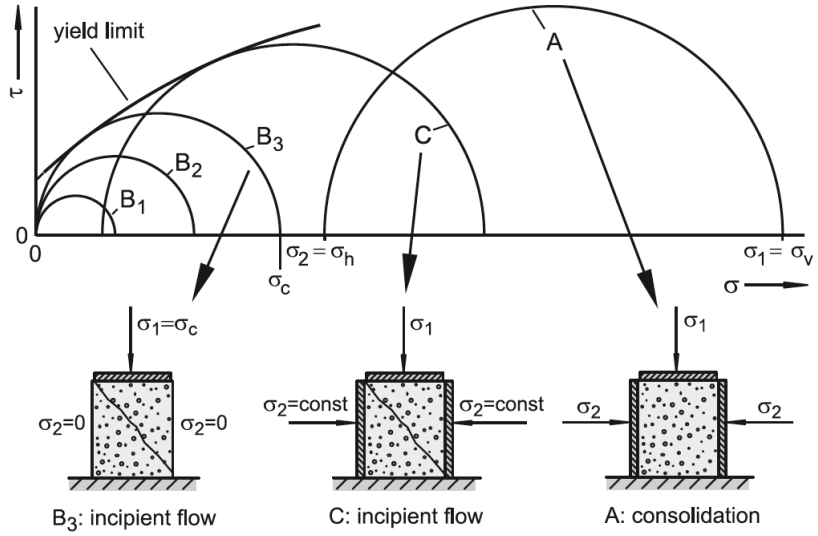

Figure 4. Schematic of the construction of Mohr's circles of stress and the yield limit [70].

1.6 Drying of pharmaceuticals

Drying is a critical process step in many different industries, as residual moisture or solvents can severely interfere with the quality attributes of the final product. By evaporating or sublimating a solvent, moisture is reduced to a minimal level of the to-be-dried substance. The driving force is usually the difference of the vapor pressure of the solvent in the gas phase to the vapor pressure at saturation. The two main, simultaneously occurring, processes during drying are the heat transfer to the to-be-dried material from the surroundings and the transfer of moisture towards the material surface. The moisture is transferred in four different modes, being the capillary flow of moisture inside the material, moisture diffusion due to concentration gradients, vapor diffusion due to partial pressure gradients and the diffusion in liquid layers, which are adsorbed at solid surfaces. The thermal energy from the surroundings transfers the vapor to the gas.

The drying process usually shows three different stages of drying rates, depicted in Figure 5. In the beginning, the material needs to heat up first and to find a state of equilibrium with the surrounding air, without significant changes in the moisture content (period A-B). This equilibrium is reached at the so-called wet-bulb temperature, which is lower than the air temperature (or dry-bulb temperature) due to the vaporization enthalpy. After this initiation phase, an almost linear drying rate can be observed at steady temperature, where the moisture is evaporated from the materials surface, as fast as it is transported from the inside of the material (period B-C). After a critical moisture content is reached, the drying rate declines, and the evaporation is mainly driven by diffusion, as the

water on the surface has already been evaporated. The temperature of the solid increases and approximates the dry-bulb temperature during this stage (period C-D) [74]–[76].

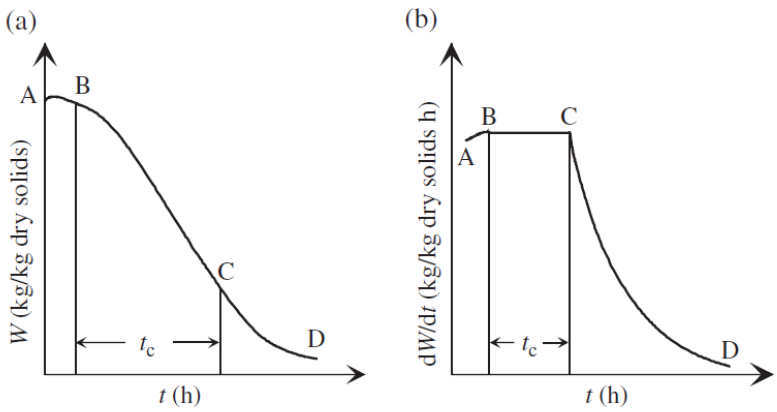

Figure 5. Drying periods for solid matter. Moisture content over time (a) and drying rate over time (b) [74].

It is especially challenging to estimate the efficacy of a drying process as not only are the thermal properties (conductivity, heat capacity, heat transfer coefficient) different at different moisture levels, but also the flow properties change [27], [75]–[77]. On top of that, air and material flow are usually very complex. This results in a very difficult modelling and predicting of drying processes, and experiments are needed to evaluate the applicability of a dryer [78]–[80].

Existing dryers in the pharmaceutical field can be classified into the three major classes of conductive, convective and radiative drying. Convective dryers supply the thermal energy via an induced gas, which is also the drying agent. Most common dryers in this class are spray dryers, flash dryers, fluidized bed dryers or belt dryers [76]. In conductive drying, the heat is supplied via hot surfaces, being in contact with the to-be-dried material. These dryers usually operate in batch mode. Examples of dryer types are drum dryers, vacuum dryers and freeze dryers. For radiative drying the energy is directly transported to the medium via electromagnetic fields. Therefore, heat is transduced on the surface as well as within the material, which is therefore simultaneously heated. Examples are microwave and infrared dryers. Numerous combinations of these classes exist, which makes the distinctive classification of drying systems complicated.

At the moment, no equipment is commercially available to continuously process poorly flowable materials in a small scale of up to 2 kg/h on a dry basis, while keeping the particle size and structure intact. To fill this gap, a novel drying technique is developed and characterized in the second part of this thesis. By altering the configurations of a paddle

dryer and implementing the design optimizations, a new, patented drying device was developed, working with a combination of conduction and convection principles [81]. It was possible to continuously process cohesive materials (i.e. di-calcium phosphate and Ibuprofen) at various moisture contents for up to 10 h, evaporating up to 680 g/h of water and reducing the moisture content to lower than 1 wt.%.

1.7 References

[1] FDA, “Guidance for Industry PAT: A Framework for Innovative Pharmaceutical Development, Manufacuring, and Quality Assurance,” 2004.

[2] FDA, “Pharmaceutical CGMPs for the 21s Century - A risk-based approach,” *FDA Off. Doc.*, no. September, p. 32, 2004.

[3] G. Allison, Y. T. Cain, C. Cooney, T. Garcia, and T. G. Bizjak, “Regulatory and Quality Considerations for Continuous Manufacturing,” 2017.

[4] L. X. Yu and J. Woodcock, “FDA pharmaceutical quality oversight,” *Int. J. Pharm.*, vol. 491, no. 1–2, pp. 2–7, 2015.

[5] A. C. Fisher *et al.*, “Advancing pharmaceutical quality: An overview of science and research in the U.S. FDA’s Office of Pharmaceutical Quality,” *Int. J. Pharm.*, vol. 515, no. 1–2, pp. 390–402, 2016.

[6] R. A. Lionberger, S. L. Lee, L. M. Lee, A. Raw, and L. X. Yu, “Quality by design: Concepts for ANDAs,” *AAPS J.*, vol. 10, no. 2, pp. 268–276, 2008.

[7] M. M. Nasr *et al.*, “Regulatory Perspectives on Continuous Pharmaceutical Manufacturing: Moving From Theory to Practice: September 26-27, 2016, International Symposium on the Continuous Manufacturing of Pharmaceuticals,” *J. Pharm. Sci.*, vol. 106, no. 11, pp. 3199–3206, 2017.

[8] C. Badman *et al.*, “Why We Need Continuous Pharmaceutical Manufacturing and How to Make It Happen,” *J. Pharm. Sci.*, vol. 108, no. 11, pp. 3521–3523, Nov. 2019.

[9] K. Plumb, “Continuous Processing in the Pharmaceutical Industry,” *Chem. Eng. Res. Des.*, vol. 83, no. 6, pp. 730–738, Jun. 2005.

[10] J. S. Srai, C. Badman, M. Krumme, M. Futran, and C. Johnston, “Future supply chains enabled by continuous processing-opportunities and challenges May 20-21, 2014 continuous manufacturing symposium,” *J. Pharm. Sci.*, vol. 104, no. 3, pp. 840–849, 2015.

[11] H. Leuenberger, “New trends in the production of pharmaceutical granules: Batch versus continuous processing,” *Eur. J. Pharm. Biopharm.*, vol. 52, no. 3, pp. 289–296, 2001.

[12] S. Mascia *et al.*, “End-to-end continuous manufacturing of pharmaceuticals: Integrated synthesis, purification, and final dosage formation,” *Angew. Chemie - Int. Ed.*, vol. 52, no. 47, pp. 12359–12363, 2013.

[13] M. Kumpugdee-Vollrath, *Easy Coating*, 1st ed. Vieweg+Teubner, 2011.

[14] L. L. Augsburger and S. W. Hoag, *Pharmaceutical Dosage Forms - Tablets*, vol. 2. CRC Press, 2008.

[15] M. Kreimer *et al.*, “Mechanical strength of microspheres produced by drying of acoustically levitated suspension droplets,” *Powder Technol.*, vol. 325, pp. 247–260, 2018.

[16] C. J. Welch, J. M. Hawkins, and J. Tom, “Precompetitive collaboration on enabling technologies for the pharmaceutical industry,” *Org. Process Res. Dev.*, vol. 18, no. 4, pp. 481–487, 2014.

[17] J. Vercruysse *et al.*, “Stability and repeatability of a continuous twin screw granulation and drying system,” *Eur. J. Pharm. Biopharm.*, vol. 85, no. 3 PART B, pp. 1031–1038, 2013.

[18] J. Khinast and M. Bresciani, “Continuous Manufacturing : Definitions and Engineering Principles.”

[19] C. Hroncich, “New Directions in Modular Manufacturing,” *Pharm. Technol.*, vol. 40, no. 9, pp. 62–66, 2016.

[20] A. Aigner *et al.*, *Die Pharmaindustrie - Einblick - Durchblick - Perspektiven*. Heidelberg: Spektrum Akademischer Verlag, 2009.

[21] M. Teżyk, B. Milanowski, A. Ernst, and J. Lulek, “Recent progress in continuous and semi-continuous processing of solid oral dosage forms: A review,” *Drug Dev. Ind. Pharm.*, vol. 42, no. 8, pp. 1195–1214, 2015.

[22] G. Székely, M. Gil, B. Sellergren, W. Heggie, and F. C. Ferreira, “Environmental and economic analysis for selection and engineering sustainable API degenotoxification processes,” *Green Chem.*, vol. 15, no. 1, pp. 210–225, 2013.

[23] W. E. Siew, A. G. Livingston, C. Ates, and A. Merschaert, “Continuous solute fractionation with membrane cascades - A high productivity alternative to diafiltration,” *Sep. Purif. Technol.*, vol. 102, pp. 1–14, 2013.

[24] M. Kreimer *et al.*, “Performance characterization of static mixers in precipitating environments,” *Org. Process Res. Dev.*, vol. 23, no. 7, pp. 1308–1320, 2019.

[25] X. Fu, D. Huck, L. Makein, B. Armstrong, U. Willen, and T. Freeman, “Effect of particle shape and size on flow properties of lactose powders,” *Particuology*, vol. 10, no. 2, pp. 203–208, 2012.

[26] L. X. Liu, I. Marziano, A. C. Bentham, J. D. Litster, E.T.White, and T. Howes, “Effect of particle properties on the flowability of ibuprofen powders,” *Int. J. Pharm.*, vol. 362, no. 1–2, pp. 109–117, Oct. 2008.

[27] A. Crouter and L. Briens, “The effect of moisture on the flowability of pharmaceutical excipients.,” *AAPS PharmSciTech*, vol. 15, no. 1, pp. 65–74, Feb. 2014.

[28] C. Hirschberg, C. C. Sun, J. Risbo, and J. Rantanen, “Effects of Water on Powder Flowability of Diverse Powders Assessed by Complimentary Techniques,” *J. Pharm. Sci.*, vol. 108, no. 8, pp. 2613–2620, Aug. 2019.

[29] G. Lumay *et al.*, “Effect of relative air humidity on the flowability of lactose powders,” *J. Drug Deliv. Sci. Technol.*, vol. 35, pp. 207–212, Oct. 2016.

[30] A. U. Neil and J. Bridgwater, “Attrition of particulate solids under shear,” *Powder Technol.*, vol. 80, no. 3, pp. 207–219, 1994.

[31] C. R. Bemrose and J. Bridgwater, “A review of attrition and attrition test methods,”

Powder Technology. 1987.

[32] M. Birch and I. Marziano, “Understanding and avoidance of agglomeration during drying processes: A case study,” *Org. Process Res. Dev.*, vol. 17, no. 10, pp. 1359–1366, 2013.

[33] S. Byrn *et al.*, “Achieving continuous manufacturing for final dosage formation: Challenges and how to meet them May 20-21, 2014 continuous manufacturing symposium,” *J. Pharm. Sci.*, vol. 104, no. 3, pp. 792–802, 2015.

[34] J. Burgbacher and J. Wiss, “Industrial Applications of Online Monitoring of Drying Processes of Drug Substances Using NIR,” *Org. Process Res. Dev.*, vol. 12, no. 2, pp. 235–242, 2008.

[35] A. Lekhal, K. P. Girard, M. A. Brown, S. Kiang, B. J. Glasser, and J. G. Khinast, “Impact of agitated drying on crystal morphology: KCl-water system,” *Powder Technol.*, vol. 132, no. 2–3, pp. 119–130, 2003.

[36] A. Lekhal, K. P. Girard, M. A. Brown, S. Kiang, J. G. Khinast, and B. J. Glasser, “The effect of agitated drying on the morphology of L-threonine (needle-like) crystals,” *Int. J. Pharm.*, vol. 270, no. 1–2, pp. 263–277, 2004.

[37] V. Warikoo *et al.*, “Integrated continuous production of recombinant therapeutic proteins,” *Biotechnol. Bioeng.*, vol. 109, no. 12, pp. 3018–3029, 2012.

[38] P. Poechlauer, J. Manley, R. Broxterman, B. Gregertsen, and M. Ridemark, “Continuous processing in the manufacture of active pharmaceutical ingredients and finished dosage forms: An industry perspective,” *Org. Process Res. Dev.*, vol. 16, no. 10, pp. 1586–1590, 2012.

[39] L. X. Yu and M. Kopcha, “The future of pharmaceutical quality and the path to get there,” *Int. J. Pharm.*, vol. 528, no. 1–2, pp. 354–359, 2017.

[40] A. S. Myerson, M. Krumme, M. Nasr, H. Thomas, and R. D. Braatz, “Control systems engineering in continuous pharmaceutical manufacturing may 20-21, 2014 continuous manufacturing symposium,” *J. Pharm. Sci.*, vol. 104, no. 3, pp. 832–839, 2015.

[41] D. Zhou, W. R. Porter, and G. G. Z. Zhang, “Drug Stability and Degradation Studies,” *Dev. Solid Oral Dos. Forms*, pp. 87–124, 2009.

[42] K. Pilaniya, H. K. Chandrawanshi, U. Pilaniya, P. Manchandani, P. Jain, and N. Singh, “Recent trends in the impurity profile of pharmaceuticals,” *J. Adv. Pharm. Technol. Res.*, vol. 1, no. 3, pp. 302–310, 2010.

[43] J. Kruisz, J. Rehrl, S. Sacher, I. Aigner, M. Horn, and J. G. Khinast, “RTD modeling of a continuous dry granulation process for process control and materials diversion,” *Int. J. Pharm.*, vol. 528, no. 1–2, pp. 334–344, 2017.

[44] M. Baumann and I. R. Baxendale, “The synthesis of active pharmaceutical ingredients (APIs) using continuous flow chemistry,” *Beilstein J. Org. Chem.*, vol. 11, pp. 1194–1219, 2015.

[45] S. Sacher and G. Krammer, “Investigation of different crystal habits without chemical additives in a three-phase reactor,” *Chem. Eng. Sci.*, vol. 60, no. 22, pp. 6307–6312, 2005.

[46] N. Rasenack and B. W. Müller, “Ibuprofen crystals with optimized properties,” *Int. J.*

Pharm., vol. 245, no. 1–2, pp. 9–24, 2002.

[47] B. P. Chekal *et al.*, “The challenges of developing an API crystallization process for a complex polymorphic and highly solvating system. Part I,” *Org. Process Res. Dev.*, vol. 13, no. 6, pp. 1327–1337, Nov. 2009.

[48] M. Kreimer, I. Aigner, D. Lepek, and J. Khinast, “Continuous Drying of Pharmaceutical Powders Using a Twin-Screw Extruder,” *Org. Process Res. Dev.*, vol. 22, no. 7, pp. 813–823, 2018.

[49] D. Suzzi *et al.*, “DEM simulation of continuous tablet coating: Effects of tablet shape and fill level on inter-tablet coating variability,” *Chem. Eng. Sci.*, vol. 69, no. 1, pp. 107–121, 2012.

[50] E. Stocker, G. Toschkoff, S. Sacher, and J. G. Khinast, “Use of mechanistic simulations as a quantitative risk-ranking tool within the quality by design framework,” *Int. J. Pharm.*, vol. 475, no. 1, pp. 245–255, 2014.

[51] C. Hare, M. Ghadiri, and R. Dennehy, “Prediction of attrition in agitated particle beds,” *Chem. Eng. Sci.*, vol. 66, no. 20, pp. 4757–4770, 2011.

[52] H. Didriksen, “Model based predictive control of a rotary dryer,” *Chem. Eng. J.*, vol. 86, no. 1–2, pp. 53–60, 2002.

[53] A. Eitzlmayr *et al.*, “Mechanistic modeling of modular co-rotating twin-screw extruders,” *Int. J. Pharm.*, vol. 474, no. 1–2, pp. 157–176, 2014.

[54] C. Wibowo and K. M. Ng, “Operational issues in solids processing plants: Systems view,” *AIChE J.*, vol. 47, no. 1, pp. 107–125, Jan. 2001.

[55] J. Seville, U. Tüzün, and R. Clift, “Particle mechanics,” in *Processing of Particulate Solids*, Dordrecht: Springer Netherlands, 1997, pp. 99–144.

[56] J. Seville, U. Tüzün, and R. Clift, “Particles in fluids,” in *Processing of Particulate Solids*, Dordrecht: Springer Netherlands, 1997, pp. 53–98.

[57] J. Seville, U. Tüzün, and R. Clift, “Storage and discharge of particulate bulk solids,” in *Processing of Particulate Solids*, Dordrecht: Springer Netherlands, 1997, pp. 298–367.

[58] N. Rama Rao, S. S. Mani Kiran, and N. L. Prasanthi, “Pharmaceutical impurities: An overview,” *Indian J. Pharm. Educ. Res.*, vol. 44, no. 3, pp. 301–310, 2010.

[59] T. Eriksson, S. Björkman, B. Roth, and P. Höglund, “Intravenous Formulations of the Enantiomers of Thalidomide: Pharmacokinetic and Initial Pharmacodynamic Characterization in Man,” *J. Pharm. Pharmacol.*, vol. 52, no. 7, pp. 807–817, Jul. 2000.

[60] M. Zettl *et al.*, “Runtime Maximization of Continuous Precipitation in an Ultrasonic Process Chamber,” *Org. Process Res. Dev.*, p. acs.oprd.9b00311, Mar. 2020.

[61] J. Gursch *et al.*, “Continuous Processing of Active Pharmaceutical Ingredients Suspensions via Dynamic Cross-Flow Filtration,” *J. Pharm. Sci.*, vol. 104, no. 10, pp. 3481–3489, 2015.

[62] J. Gursch *et al.*, “Dynamic cross-flow filtration: Enhanced continuous small-scale solid-liquid separation,” *Drug Dev. Ind. Pharm.*, vol. 42, no. 6, pp. 977–984, 2016.

[63] M. Stieß, *Mechanische Verfahrenstechnik - Partikeltechnologie 1*. Berlin, Heidelberg: Springer Berlin Heidelberg, 2009.

[64] B. Y. Shekunov, P. Chattopadhyay, H. H. Y. Tong, and A. H. L. Chow, "Particle size analysis in pharmaceutics: Principles, methods and applications," *Pharmaceutical Research*, vol. 24, no. 2. pp. 203–227, Feb-2007.

[65] I. G. Jolliffe and J. M. Newton, "An investigation of the relationship between particle size and compression during capsule filling with an instrumented mG2 simulator," *J. Pharm. Pharmacol.*, vol. 34, no. 7, pp. 415–419, Jul. 1982.

[66] L. X. Liu, I. Marziano, A. C. Bentham, J. D. Litster, E.T.White, and T. Howes, "Effect of particle properties on the flowability of ibuprofen powders," *Int. J. Pharm.*, vol. 362, no. 1–2, pp. 109–117, Oct. 2008.

[67] X. Fu, D. Huck, L. Makein, B. Armstrong, U. Willen, and T. Freeman, "Effect of particle shape and size on flow properties of lactose powders," *Particuology*, vol. 10, no. 2, pp. 203–208, Apr. 2012.

[68] F. Podczeck and Y. Miah, "The influence of particle size and shape on the angle of internal friction and the flow factor of unlubricated and lubricated powders," *Int. J. Pharm.*, vol. 144, no. 2, pp. 187–194, 1996.

[69] I. Tomasetta, D. Barletta, and M. Poletto, "Correlation of powder flow properties to interparticle interactions at ambient and high temperatures," *Particuology*, vol. 12, no. 1, pp. 90–99, 2014.

[70] D. Schulze, *Powders and Bulk Solids*, 1st ed. Berlin, Heidelberg: Springer Berlin Heidelberg, 2007.

[71] A. W. Jenike, "Gravity Flow of Bulk Solids," in *Bulletin of the University of Utah No. 108*, vol. 52, no. 29, 1961, p. 322.

[72] R. Freeman, "Measuring the flow properties of consolidated, conditioned and aerated powders — A comparative study using a powder rheometer and a rotational shear cell," *Powder Technol.*, vol. 174, no. 1–2, pp. 25–33, May 2007.

[73] T. M. Chitu, D. Oulahna, and M. Hemati, "Rheology, granule growth and granule strength: Application to the wet granulation of lactose-MCC mixtures," *Powder Technol.*, vol. 208, no. 2, pp. 441–453, 2011.

[74] İ. Dinçer and C. Zamfirescu, *Drying Phenomena*. Chichester, UK: John Wiley & Sons, Ltd, 2015.

[75] A. Bejan and A. D. Kraus, *Heat Transfer Handbook*. Hoboken, NJ: John Wiley & Sons, 2003.

[76] A. S. Mujumdar, *Handbook of Industrial Drying*. CRC Press, 2014.

[77] M. C. Coelho and N. Harnby, "The effect of humidity on the form of water retention in a powder," *Powder Technol.*, vol. 20, no. 2, pp. 197–200, Jul. 1978.

[78] A. Aubin, R. Ansart, M. Hemati, T. Lasuye, and M. Branly, "Determination of PVC powder drying kinetics at particle scale: Experimental study and modeling," *Dry. Technol.*, vol. 34, no. 16, pp. 2000–2023, 2016.

[79] A. Aubin, R. Ansart, M. Hemati, T. Lasuye, and M. Branly, "Modeling and simulation of drying operations in PVC powder production line: Experimental and theoretical

study of drying kinetics on particle scale," *Powder Technol.*, vol. 255, pp. 120–133, 2014.

[80] M. Kohout, A. P. Collier, and F. Stepanek, "Vacuum Contact Drying of Crystals: Multi-scale Modelling and Experiments," *Comput. Aided Chem. Eng.*, vol. 18, pp. 1075–1080, 2004.

[81] P. van der Wel *et al.*, "Drying device, rotary valve and drying method," NL2020740B1, 16-Oct-2019.

„To study and not think is a waste. To think and not study is dangerous."
Confucius (551 B.C. – 479 B.C.)

2 Runtime Maximization of Continuous Precipitation in an Ultrasonic Process Chamber

Manuel Zettl[1], Manuel Kreimer[1], Isabella Aigner[1], Thomas Mannschott[2], Peter van der Wel[3], Johannes Khinast[1,4], Markus Krumme[2]*

[1] Research Center Pharmaceutical Engineering (RCPE) GmbH, 8010 Graz, Austria

[2] Novartis Pharma AG, 4056 Basel, Switzerland

[3] Hosokawa Micron B.V., Gildenstraat 26, 7005 BL Doetinchem, Netherlands

[4] Graz University of Technology, Institute for Process and Particle Engineering, 8010 Graz, Austria

*Corresponding author: Markus Krumme

Published in Organic Process Research and Development: https://pubs.acs.org/doi/10.1021/acs.oprd.9b00311

TOC-Graphic

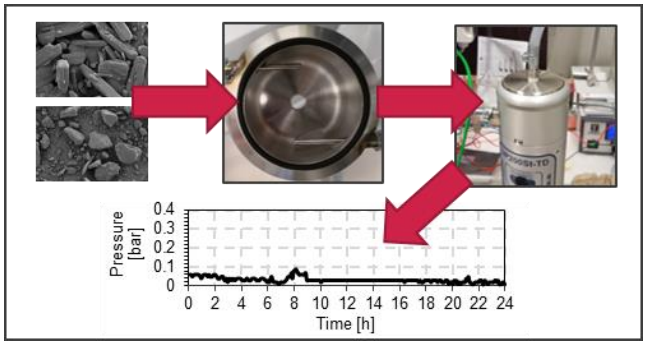

2.1 Abstract

The goal of this investigation was to develop a continuous process for producing as much dry material as possible, at stable operating conditions in an intentionally or unintentionally precipitating environment. Despite the challenge of solids formation, the risk of fouling, and as a result clogging of the system, the goal was achieved by maximizing uninterrupted runtime. The novel approach of excitement of the mixing zone by ultrasound (US), in a specially configured process chamber, was used. The main focus was the investigation on how to avoid fouling and solids build-up in the process chamber, which is an undesired effect in continuous manufacturing. Often these are unavoidable side effects in a precipitating environment, which in the worst case can lead to a process shutdown. In this work, two model substance combinations were used (lactose/water/isopropanol and ibuprofen/ethanol/water) to demonstrate a hydrophilic and a lipophilic case. A feed suspension was mixed with an anti-solvent in an ultrasonic process chamber, with a persisting helical flow pattern and perpendicular introduction of ultrasound. Solids are precipitated during mixing and blockage of the system can occur, due to the introduced fouling and accumulation. Critical process parameters (product temperature, US-input and solid loading) were analyzed with respect to their influence on process stability and duration. As this process could also be applied to produce or purify particles, the particle size distribution (PSD) of the two substances was evaluated with regard to agglomeration and attrition. The described precipitating environment can be applied to pharmaceutical manufacturing.

Key words: precipitation, mixing, ultrasound application, suspensions, crystallization

2.2 Introduction

As the pharmaceutical industry is shifting from batch manufacturing to continuous operations[1,2], special considerations have to be made with regard to the last two process steps in primary manufacturing: the washing and drying of crystals which have been produced in the final crystallization step of an active pharmaceutical ingredient (API). Continuous washing is challenging and only a few processes have been developed so far[3,4]. In the continuous processing of API suspensions, equipment fouling as well as the quality of the finished product are issues. Physical properties (e.g., size and shape) of a crystalline API strongly influence the dissolution and disintegration behavior of the drug product[5,6], as well as the flowability[7], segregation[8,9] and performance of downstream operations (i.e., filtration[4,11-12], drying[12], blending[11], tabletting[13] and capsule filling[14]). Therefore, the final steps following crystallization (which is usually carefully controlled) are important since

changes in the particle morphology and the physical properties can occur. Thus, in the context of this work, changes in the particle properties during processing were carefully examined as a function of process conditions.

Preventing fouling on the surface of process equipment during operation is quite challenging in continuous manufacturing, especially when processing liquids or pastes. The main causes of fouling are powder sticking, precipitation, corrosion, solidification, biofouling, chemical reactions and composite fouling[15–21]. While fouling can easily be addressed in batch processing by cleaning the equipment, it can change the process conditions significantly in continuous processing and, in the worst case, even lead to a complete shut-down of the process. Fouling is very difficult to predict, prevent and control since it can occur for many reasons, meaning there are a multitude of variables to consider. Moreover, fouling kinetics depend on a multitude of parameters and conditions, occurring mostly in places where non-ideal mixing or other non-ideal conditions occur.

Fouling occurs in consecutive stages: initiation, transport, attachment, removal and aging[22]. In the beginning of a process the equipment is new or cleaned. Depending on the process, the **initiation** phase can last from a few seconds (e.g., in the case of fast chemical reactions and rough surface materials[23]) to a few days (e.g.,. for scaling or other mineral fouling processes[22]). During the **transport** phase, solids with the tendency to create fouling are introduced to the solid-fluid interface between the equipment and the process fluid via diffusion, thermophoresis or sedimentation[20]. Subsequently, in the **attachment** phase, the fouling deposits attach to each other and the surface material. In this context the important parameters are the particle size, particle concentration, fluid density, fluid velocity and stickiness, as well as attraction and repulsion forces between the particles[24]. The deposition of fouling material occurs simultaneously with its **removal** and mainly depends on the velocity gradients on the surface, the surface roughness and the fluid viscosity[23]. During the final phase, **aging**, the amount of deposited material can steadily increase or decrease over time[17]. These accumulations can severely disrupt the process and, in the worst case, lead to a forced shut-down due to system blockage[18].

Ultrasound (US) has been widely applied in various industries. For example, in the food industry it has been used for the stabilizing, de-fattening and emulsifying of dairy products[25–27], as well as for influencing fermentation processes[28]. Applications in the petrochemical industry also include emulsification[29] and reaction enhancement[30]. Ultrasound penetration also shows promising effects in terms of reaction intensification[31–33]. It was also shown that ultrasound prolongs the feasible process duration in harsh chemical environments[18]. Harsh chemical environments outside reactions which

intentionally produce solids are e.g. reactions during which excessive precipitation may occur as an undesired side effect of a reaction or as part of a solvent exchange process. As mentioned above, in the manufacturing of APIs such steps are often part of a process. Even during such steps product properties should not be changed unintentionally. Moreover, the process should also be stable and effective. Therefore, it was decided to investigate this effect further.

In our work we are interested in continuous purification (i.e., the removal of mother liquor by cake washing) of a crystal suspension coming from the crystallizer. This continuous washing occurs by mixing the crystal suspension with an anti-solvent. Subsequently, the washed suspension is continuously filtered to reach a higher solid content (15 wt. %). The two process steps, mixing and filtration, are repeated multiple times until the desired residual dissolved solid content in the liquid is reached[34–36]. Based on the findings of Kreimer et al.[18], a novel process for continuous precipitation in precipitating chemical environments was developed and optimized in terms of blockage and fouling behavior. Several screening test runs were performed for two material combinations and the effect of various process parameters was analyzed. Using the results, a process configuration was obtained that could process the slurry for at least 24 hours for both surrogate substances.

2.3 Materials and methods

2.3.1 Process equipment

The setup used in this work is illustrated in Figure 6. To avoid sedimentation of the solids in the feed suspension, a Heidolph stirrer RZR 200 was used (Heidolph Instruments GmbH & CO. KG, Schwabach, Germany). Two eccentric screw pumps MX10S-10/20 (Knoll Maschinenbau GmbH, Bad Salgau, Germany) were used for feeding the liquids. To compensate the ultrasound induced temperature increase of the liquids in the ultrasonic cell[37] the anti-solvent was cooled prior to entering the process chamber. For cooling, the anti-solvent was pumped through a 15 m PVC-pipe coil, which was placed inside a LAUDA Alpha RA 12 (Lauda Dr. R. Wobser GmbH & Co. KG, Lauda-Königshofen, Germany) cooling bath set to 5 or 10 °C. The ultrasonic cell and the pumps were placed on a table and the product was collected on a scale on the ground. The suspension tank was placed next to the table on the ground and the cooler and the anti-solvent tank above the table on a platform, due to limited available space.

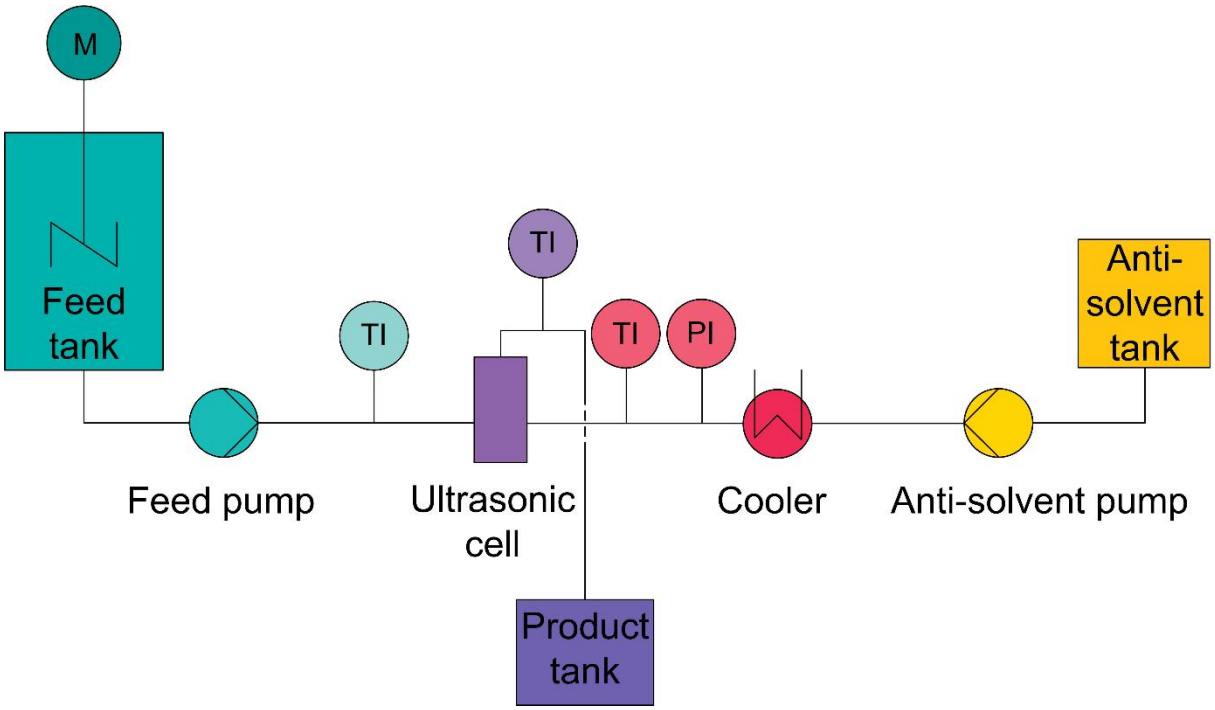

Figure 6. Flow sheet of the experimental setup

The two liquid feeds, suspension and anti-solvent, were fed into the ultrasonic chamber (see Figure 7). Mixing of the two liquids occurs in the ultrasound cell under constant US-input. The US transducer was placed at the bottom of the US cell and served as the bottom plate of the process chamber (Figure 7d). Thereby, the US-penetration of liquid in the US chamber was optimized, with respect to the efficiency of the energy input. The ultrasound was generated and transduced by an UP200St-TD_CupHorn (Hielscher Ultrasonics GmbH, Teltow, Germany) unit (Figure 7c).

The cell had an inner diameter of 54 mm and a chamber height of 36 mm, resulting in a filling volume of roughly 82 ml. It operates at a frequency of 26 kHz, with a maximum energy input of 200 W, resulting in a maximum energy density of 2.44 W/cm³ in water, based on the filling volume of the ultrasound transducer, and a maximum amplitude of 10 µm, adjustable in 1 % steps. The maximum process pressure was limited to 0.4 bar over-pressure since the process chamber seals could not withstand higher pressures. The liquid feeds were introduced through steel pipes with an outer diameter of 3 mm and an inner diameter of 2.4 mm, reaching inside the process chamber 1 or 2 cm away from the wall, as depicted in Figure 7 (bottom view and closed process chamber).

The feed suspension and the anti-solvent entered the process chamber of the ultrasonic flow cell, as described above, from different sides. The two fluids were mixed in the ultrasonic process chamber and the product was released on the top to avoid gas

accumulations in the system. Due to the design specifics of the inlet positioning and the design orientation, the hydrodynamics of the mixing pattern is likely helical. This was not explicitly confirmed in this specific setup, but in similar ones. The product was collected in a container placed on a ML 4002 M scale (Mettler Toledo GmbH, Vienna, Austria), thereby fluctuations of the product flow, due to process irregularities, could be investigated.

The pressure in the system was measured on the anti-solvent side using an Optibar P 3050 C pressure sensor (KROHNE Messtechnik GmbH, Duisburg, Germany). The temperature was measured via stainless steel type K thermocouples suitable for a temperature range between -100 °C and 1100 °C (RS Components Handelsges.m.b.H., Gmünd, Austria) and logged with a testo 176, a 4-channel temperature logger (Testo GmbH, Vienna, Austria).

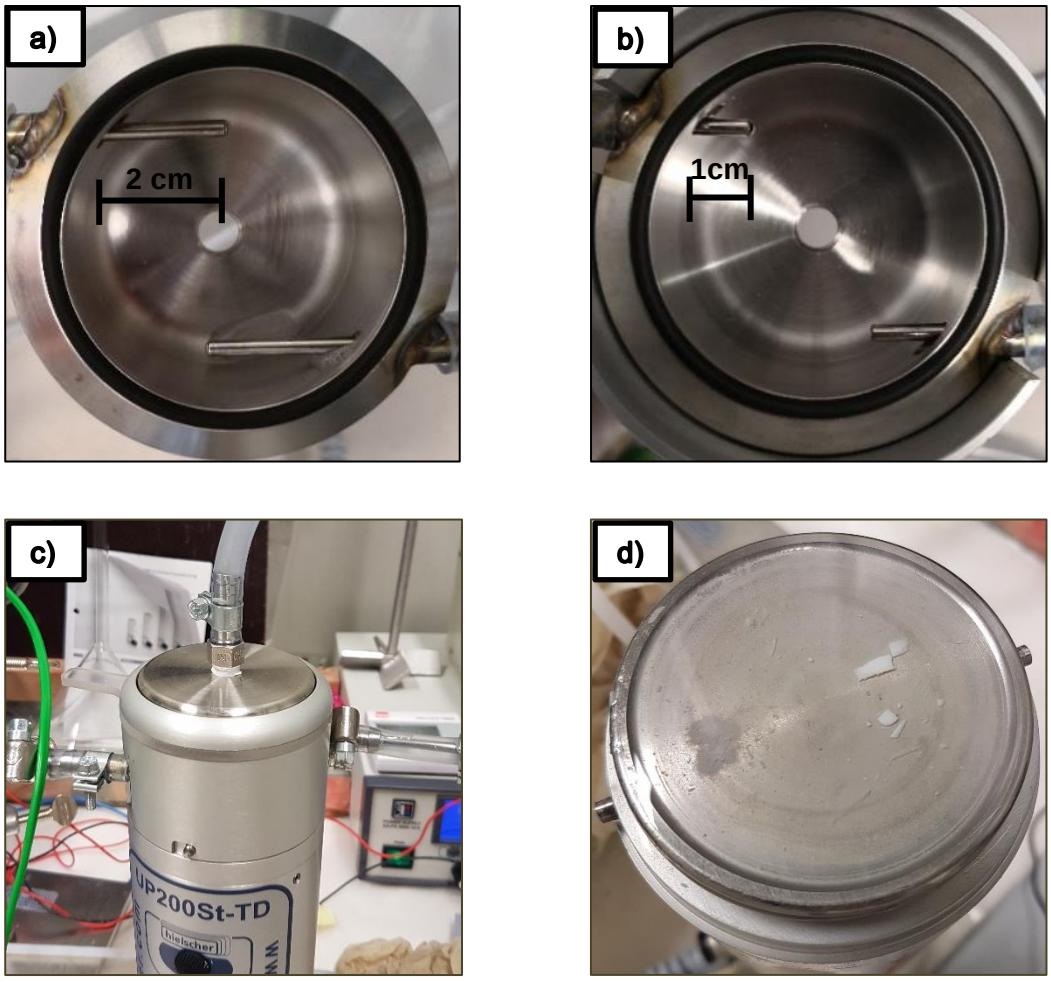

Figure 7. View of the equipment and process chamber configurations: a) test runs 1-10, b) test runs 11 and 12, c) view of the closed process chamber, with the addition of the feed suspension from the left, the anti-solvent from the right and the product outlet on the top, d) the transducing plate, placed below the process chamber, after a test run with lactose flakes on it.

2.3.2 **Materials**

Ibuprofen 25 (BASF SE, Ludwigshafen, Germany) and α -Lactose (GranuLac 230, Meggle AG, Wasserburg am Inn, Germany) were used as model substances to represent typical APIs. Ibuprofen 25 is a non-steroidal, anti-inflammatory drug. The rod-shaped ibuprofen particles are shown in Figure 8a. The second substance, α-Lactose - monohydrate is a common excipient in pharmaceutical formulations. The irregular, rock-like shape is shown in Figure 8b. The pictures of particle shape were generated using a scanning electron microscope (SEM), Zeiss Ultra 55 (Carl Zeiss AG, Oberkochen, Germany) with an Everhart-Thornley detector, at an acceleration voltage of 5 keV. The samples were prepared in an EM ACE 600 sputter coater (Leica Camera AG, Wetzlar, Germany), which sputtered a 15 nm gold platinum (80 %-20 %) coating onto the particles (See Kreimer et al.[18]).

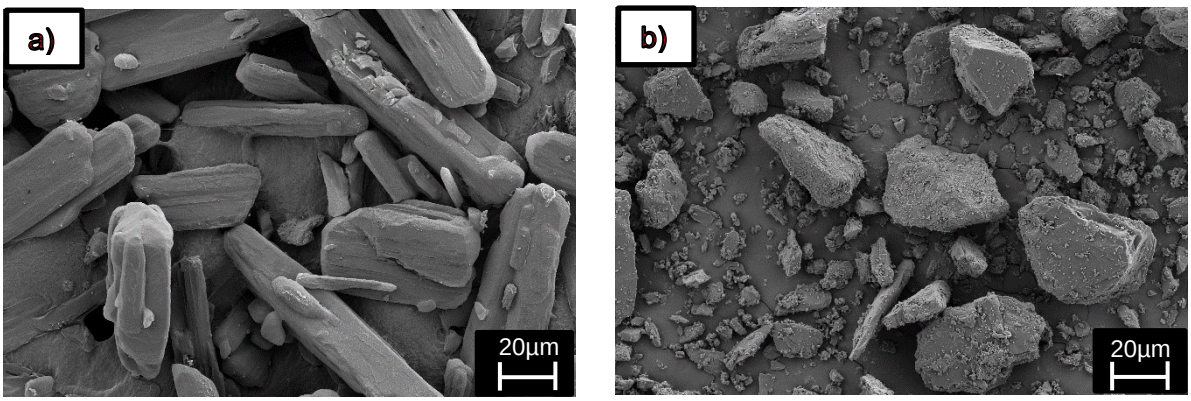

Figure 8. SEM pictures of the particle shapes of materials used: a) Ibuprofen 25; b) the used α -Lactose

2.3.3 **Suspension preparation**

The feed suspensions were prepared by dissolving the precise amount of solid required for a saturated solution at the operating temperature. The solvent mixture was prepared at a temperature of 50 °C to ensure complete dissolution of the added solids in the saturated solution. For the aqueous lactose suspension 233 g α-Lactose were added per 1000 g of water and were stirred until the material was fully dissolved. Afterwards, the solution was allowed to cool down to 25 °C in order to obtain a saturated solution. Figure 9 and Figure 10 show the solubility of lactose in aqueous isopropanol mixtures and of ibuprofen crystals in ethanol-water mixtures, respectively.

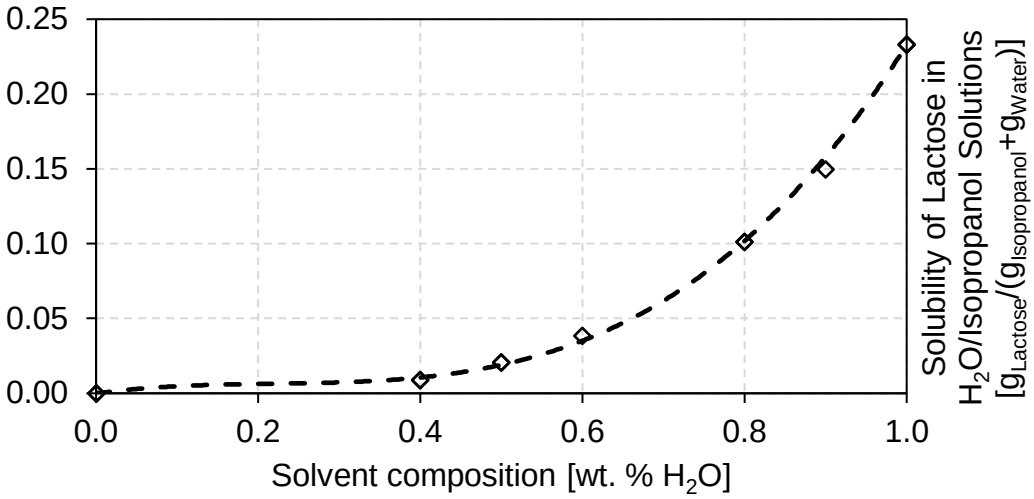

Figure 9. Solubility of lactose in aqueous isopropanol solutions at 25 °C[34,35]

Next, additional solids were added until the solid phase of the suspension reached the desired percentage of the suspension's weight. In all runs, except run 6 with the solid concentration of 55 wt. %, the weight fraction of solids was set to 15 wt. % according to Kreimer et al.[18], who reported this to be the optimal solid loading for the process, based on the total amount of processed solids. At all times, the suspension was stirred to avoid sedimentation. In the lactose experiments, isopropanol (IPA) with a purity ≥ 98 % (VWR Chemicals, Radnor, PA, USA) was used as an anti-solvent.

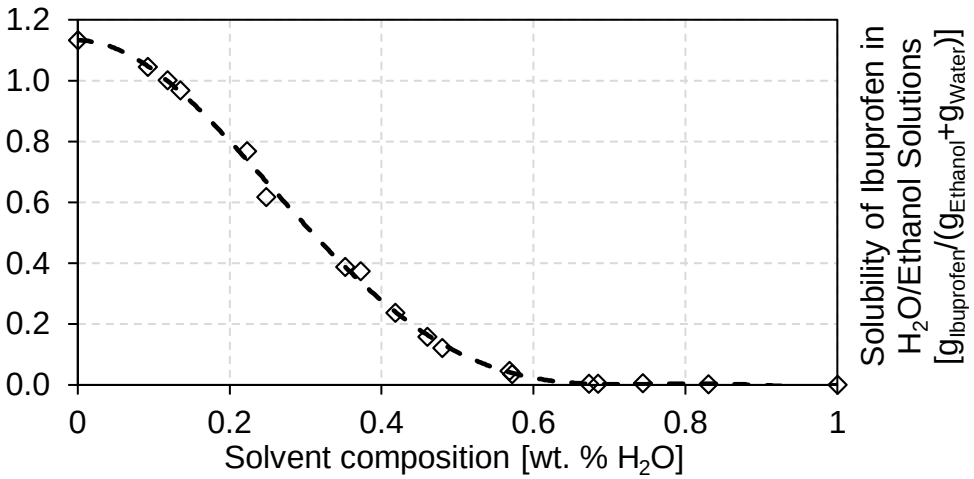

Figure 10. Solubility of ibuprofen in aqueous ethanol solutions at 25 °C[36]

For the ibuprofen suspension, 80 g solids were added per 1000 g 50 °C warm solvent mixture. The solvent mixture consisted of 50 weight percent water and 50 weight percent ethanol. The ethanol (EtOH) was 96 % denatured alcohol (Carl Roth GmbH + Co.

KG, Karlsruhe, Germany), to which water was added to reduce the solubility and achieve a similar amount of dissolved solids in the liquid, as with saturated lactose solutions (shown in Table 1). The alcohol was de-natured by the addition of 1 l IPA, 1 l butanone and 1 g denatonium benzoate per 100 l of pure ethanol, the rest of the solution being water. In non-diluted ethanol, the solubility of ibuprofen is about 1.18 g/g at 25 °C, which would have caused excessive material precipitation. By adding water, the solubility was reduced to 0.08 g/g at 25 °C. Afterwards, the suspension was prepared in the same manner as it was done for the lactose runs. Table 2 summarizes the mass fractions of the different suspensions. Tap water was used for the test runs, because a total of roughly 290 l of water was needed and therefore, the use of distilled water was not feasible. Table 3 shows the product suspensions compositions. The composition of the product was already known from and described in a previous work (Kreimer et al.[18]). The obtained product composition has proven to be suitable to compare the processability of the system to a real process in terms of possible precipitation and agglomeration of material.

Solubility is temperature dependent for both the lactose and the ibuprofen system. Therefore, an increase in temperature will lead to dissolution of solid material[34,36]. The number of fines is particularly sensitive to temperature, because smaller particles with higher surface area are usually dissolved first. A decrease in product temperature would lead to more precipitation and can therefore facilitate the formation of agglomerates. For this reason, process temperature should be kept as constant as possible to obtain comparable results. As US-input, heat of crystallization and heat of mixing different solvents impact the product temperature, deviations of product temperature will occur with different process settings, as explained in section 3.

Table 1. Composition of saturated solutions with the dissolved solid mass fraction in the saturated solution ($w_{d,sat.sol.}$), water mass fraction in saturated solution ($w_{H_2O,sat.sol.}$) and ethanol mass fraction in the saturated solution ($w_{EtOH,sat.sol.}$)

Solid	$w_{d,sat.sol.}$	$w_{H_2O,sat.sol.}$	$w_{EtOH,sat.sol}$
[-]	[wt.%]	[wt.%]	[wt.%]
α -Lactose	18.9	81.1	-
Ibuprofen 25	7.4	46.3	46.3

Table 2. Composition of feed suspensions with the suspended solid mass fraction in the feed ($w_{s,f}$), dissolved solid mass fraction in the feed ($w_{d,f}$), water mass fraction in the feed ($w_{H_2O,f}$) and ethanol mass fraction in the feed ($w_{EtOH,f}$)

Solid	$w_{s,f}$	$w_{d,f}$	$w_{H_2O,f}$	$w_{EtOH,f}$
[-]	[wt.%]	[wt.%]	[wt.%]	[wt.%]
α -Lactose	15	16.1	68.9	-
α -Lactose	55	8.5	36.5	-
Ibuprofen 25	15	6.3	39.35	39.35

Table 3. Composition of product suspensions with suspended solid mass fraction in the feed ($w_{s,f}$), suspended solid mass fraction in the product ($w_{s,p}$), dissolved solid mass fraction in the product ($w_{d,p}$), water mass fraction in the product ($w_{H_2O,p}$), isopropanol mass fraction in the product ($w_{IPA,p}$) and ethanol mass fraction in the product ($w_{EtOH,p}$)

Solid	$\boldsymbol{w_{s,f}}$	$\boldsymbol{w_{s,p}}$	$\boldsymbol{w_{d,p}}$	$\boldsymbol{w_{H_2O,p}}$	$\boldsymbol{w_{IPA,p}}$	$\boldsymbol{w_{EtOH,p}}$
[-]	**[wt.%]**	**[wt.%]**	**[wt.%]**	**[wt.%]**	**[wt.%]**	**[wt.%]**
α –Lactose	15	14.6	0.9	34.5	50	-
α –Lactose	55	31.3	0.5	18.2	50	-
Ibuprofen 25	15	10.4	0.2	69.7	-	19.7

2.3.4 **Particle size distribution measurement**

The particle size distribution (PSD) of the solids in the suspension was measured with a HELOS KR laser diffractometer and a CUVETTE dispersion system (Model 3047, Sympatec GmbH, Clausthal-Zellerfeld, Germany). For the PSD measurements, two samples of about 300 ml and 50 ml were taken. The larger sample was filtered to serve as the background medium for the wet dispersion measurements in the laser diffractometer. The sample for the PSD measurement was continuously stirred with a magnetic stirrer at 1000 rpm to minimize segregation effects. After drawing the sample from the sample

beaker, a small sample was pipetted directly into the liquid until the solid concentration was in the ideal measurement range of the device (10 % absorbance). The magnetic stirrer was operated at 1000 rpm. This sample preparation method ensured that each sample had the exact composition of the liquid phase at the same process time as a background medium and saturation of the liquid was guaranteed. This also ensured that no precipitation or dissolving occurred, as long as the sample temperature did not change. The temperature of the samples for all measurements was set to 25 °C in order to avoid the influence of solubility on the particle size. Figure 11 shows the PSD of ibuprofen in a 1:1 water-ethanol mixture, corresponding to a volumetric mean diameter (VMD) of 110 µm. For the lactose system, the PSD with a measured VMD of 30 µm is shown in Figure 12.

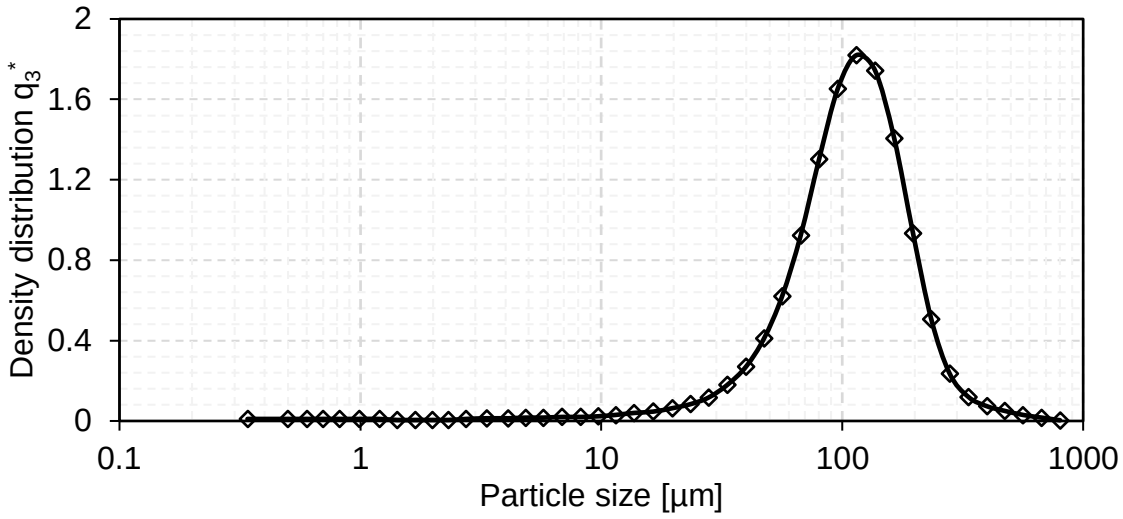

Figure 11. PSD of Ibuprofen 25

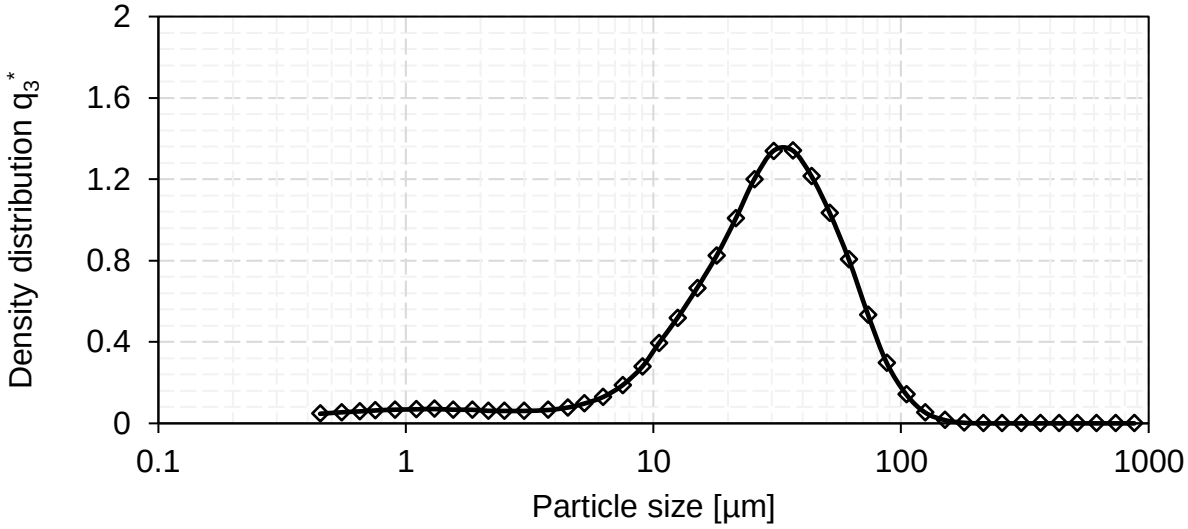

Figure 12. PSD of the used α –lactose monohydrate.

2.3.5 **Experimental procedure**

This section describes the experimental procedures. In total, 11 experiments with two material combinations (lactose in water and ibuprofen in 1:1 ratio ethanol:water) were performed to investigate the influence of the following process parameters: the process temperature (adjusted by pre-cooling the anti-solvent), the US power and the solid loading. The experimental runs were concluded with two long-term runs of 24 h, one for each material combination. An overview of the configurations is provided in Table 4.

Table 4. Experimental procedure and setup for the evaluation of process behavior

No.	Material [-]	Solid Content [wt. %]	Cooling Bath [°C]	US-input [W]	Process Duration [hh:mm]
1	α -Lactose	15	10	15-100	00:30 for each setting
2	α -Lactose	15	-	50	05:00
3	α -Lactose	15	5	50	02:00
4	α -Lactose	15	5	50	05:16
5	α -Lactose	15	5	100	08:00
6	α -Lactose	15	5	100	08:00
7	α -Lactose	55	5	100	03:00
8	Ibuprofen	15	5	20-110	00:20 for each setting
9	Ibuprofen	15	5	110	05:00
10	Ibuprofen	15	5	110	08:00
11	α -Lactose	15	5	100	24:00
12	Ibuprofen	15	5	110	24:00

In all experiments, a feed mass flow rate and anti-solvent mass flow rate of 100 g/min were chosen, resulting in a total mass flow of 200 g/min. Experiments 1-10 were carried out using the configuration shown in Figure 7a, with the steel pipes reaching into the process chamber 2 cm from the wall. Before performing the 24-h runs 11-12, the steel pipes were shortened by 1 cm as illustrated in Figure 7b, to maximize the distance between the wall and the mixing point.

2.3.5.1 Influence of the US-input on the PSD and temperature

To evaluate the effect of US-input and the applicability of the process to both systems, the US power was varied in the experiments. The experiments with α-Lactose were conducted using the 15 wt. % suspension as follows: In the first test run, the US-input was varied between 15-120 W to establish its influence on the product temperature, particle size distribution and process. First, 100 % amplitude was set in the US transducer, resulting in a power intake of around 100 W. Next, the US amplitude was reduced in 20 % steps to 80 %, 60 %, 40 % and 20 %, corresponding to net powers of 85 W, 50 W, 30 W and 15 W, respectively. The anti-solvent was pre-cooled by being pumped through a 15 m PVC-pipe coil (6 mm outer diameter) placed in a 10 °C cooling bath. The samples were taken after 15 minutes and 30 minutes at each power level to determine if the PSD changes over time at the same power level. Furthermore, the system was allowed to return to the stationary state after the power change.

In the ibuprofen experiments, a 15 wt. % solid concentration in a 1:1 water/ethanol mixture was processed with water as an anti-solvent. The cooling bath temperature was chosen to be 5 °C for the ibuprofen test runs. As it was determined that time does not affect the PSD of the particles, a slightly different approach was chosen for the PSD experiment. The PSD of ibuprofen at different US-inputs was measured in experiment 8. Therefore, the US-input was set to 100 %, 67 % and 33 %, corresponding to 110 W, 60 W and 22 W, and the samples were collected after 20 minutes at each power level.

2.3.5.2 Evaluation of the temperature influence on the process and particles

To evaluate the temperature influence on the process and the particle properties, the process parameters were chosen so they could directly be compared to the results previously obtained by Kreimer et al.[18]. A standard configuration was chosen: a flow rate of 100 g/min of 15 wt. % lactose suspension. Precipitation was induced by adding 100 g/min of isopropanol, resulting in a total flow rate of 200 g/min. In these three experiments (2-4),

the US power was chosen to be half of the maximum for the equipment (approximately 50 W).

In the first experiment no additional cooling bath was installed so that the experiment could be used as a reference for the other experiments. In the second test run, the anti-solvent (IPA) was fed through a 15 m PVC-pipe coil with an outer diameter of 6 mm, which was placed into the cooling bath set to 5 °C to further reduce the product's temperature and thereby reduce the amount of solids that re-dissolve, due to the temperature increase in the suspension. This way, an even more challenging chemical environment can be created[35]. In the third test run, the cooling bath was set again to 5 °C and the power input to 50 W in order to establish the long-term effect of such low temperatures at this power level. The planned duration of this experiment was 8 h.

Since a similar trend was expected for both surrogate substances, this investigation was only carried out for the lactose suspensions.

2.3.5.3 Evaluation of the long-term US influence on the process

To evaluate the US effect in longer experiments with the lactose material combination, the cooling bath configuration was kept constant at 5 °C, as it was in experiment 4. In experiment 5, the US was set to 100 %, resulting in a mean power input of 100 W. The duration of this run was also intended to last for 8 h so that the two US configurations could be compared directly. This experiment was repeated (test run 6) to evaluate the reproducibility of the process. After the processes, the chamber was opened and visually inspected to determine if material accumulation was present on the equipment.

To assess this effect in the ibuprofen experiments, the US was set to the maximum power input, resulting in a power consumption of approximately 110 W. Experiment 9, which lasted for 5 h, examined the various educts and the long-term process stability. The last experiment in this group (10), which ran for 8 h in the same settings as experiment 9, was performed to establish the reproducibility of the processes and the effect of an even longer process time.

2.3.5.4 Effect of solid loading on the process

To evaluate the influence of the solid concentration on the process and to test the system boundaries, the feed suspension was altered in experiment 7. A 3 h experiment with a solid concentration of 55 wt. % was performed and compared to the findings of the other test runs. The total solid mass processed was approximately doubled by increasing the solid load from 15 to 55 wt. % for the lactose configuration (Table 10).

As ibuprofen showed no wall adhesion and processability issues in previous runs, the investigation was performed only for lactose as a surrogate substance.

2.3.5.5 Long-term stability of the process setup

To evaluate the applicability of the system for continuous operations, a 24 h test run was performed for each material combination (experiments 11-12). The only adaption to the system was a reduction in the length of the steel pipes. This was done because it was observed in previous test runs that agglomeration of material happens on the wall opposing the material entrance. By reducing the length of the pipes, the material entering point was moved further away from the wall (compare Figure 7a to Figure 7b). The cooling bath was set to 5 °C and the mass flow was kept constant at 100 g/min for the suspension and anti-solvent, as the previous runs indicated that this configuration was promising.

2.4 Results and discussion

In this section the results of the experiments described in section 2.5 are presented. The evaluation was based on the pressure curve during the test runs, the temperature profiles of the feed and the product stream, and the visual observations of the deposits within the flow cell after the test runs. The product compositions obtained are shown in Table 3.

2.4.1 Influence of the US-input on the PSD and temperature

Figure 8 shows the particle size density distribution at 100 W after 15 minutes and 30 minutes for all measurements in test run 1, in comparison to the initial density distribution of the feed suspension. The significant increase in the particle size is due to the precipitation of solids on the previously-suspended particles[18]. However, as can be seen, the particle size distribution does not change significantly over time.

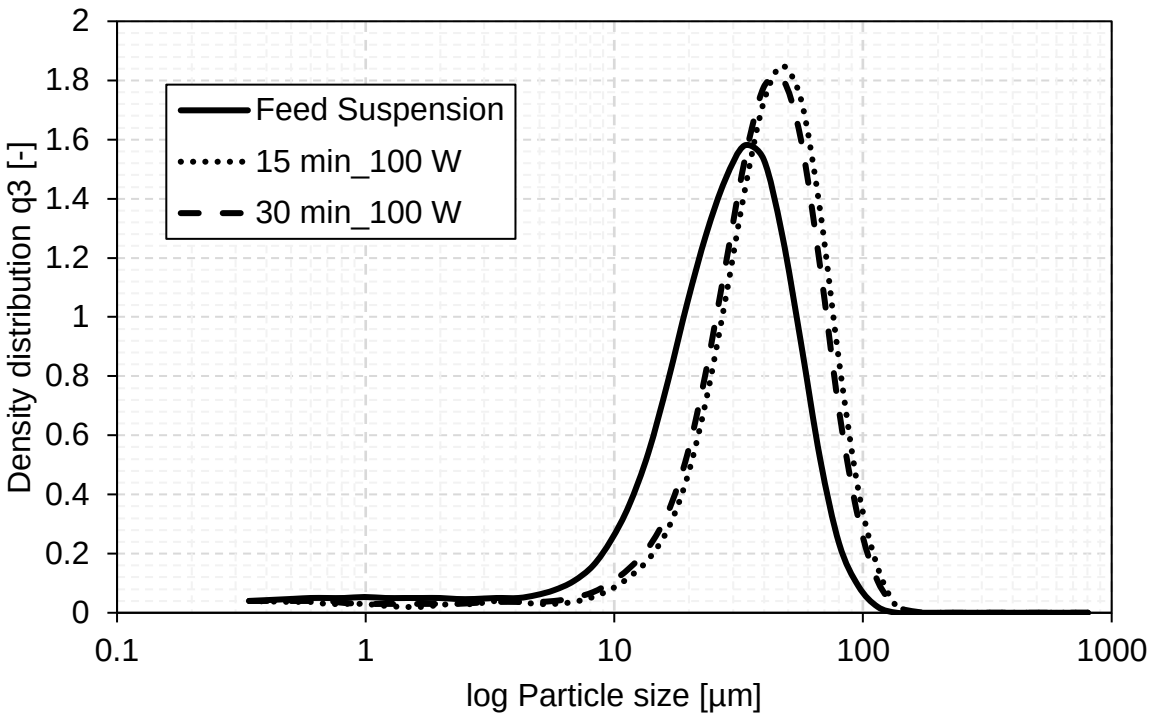

Figure 13. Results of the PSD measurements in run 1 of the lactose test: density distributions of the feed suspension (solid line), after 15 minutes (dotted line) and after 30 minutes (dashed line) at 100 W US-input.

Figure 14 shows the characteristic diameters (x50, SMD, VMD) of the particles as functions of the US energy input. It can be observed that the particle size is only minimally reduced by the increasing energy input, indicating that it is almost unaffected by the US. However, particles are slightly larger at low energy intakes. A possible explanation for this effect is that the low energy input is not sufficient to break up the agglomerates in the system. The de-agglomerating effect of US is illustrated in the figures below. Figure 15a shows that with the lowest US-input significantly more agglomerates are formed in the process chamber, than during tests with the highest US-input (see Figure 15b). Comparing the material agglomeration at 15 W and 100 W to the values at 50 W, it can be seen that once a power of 50 W is exceeded, only the amount of surface adhesion influences the process stability. This amount can be altered by changing the temperature, as will be discussed later in this section.

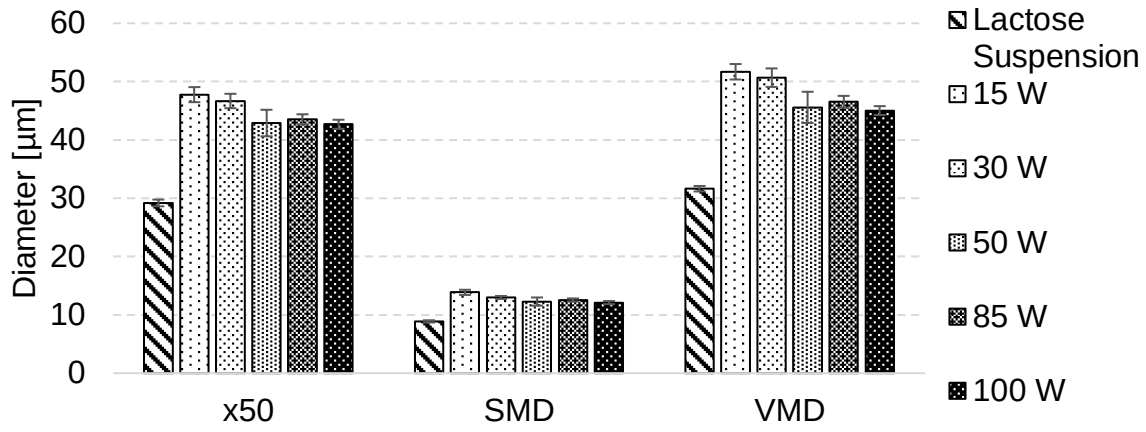

Figure 14. Results of the PSD measurements in the lactose test run: x50 diameter, Sauter mean diameter (SMD) and volumetric mean diameter (VMD).

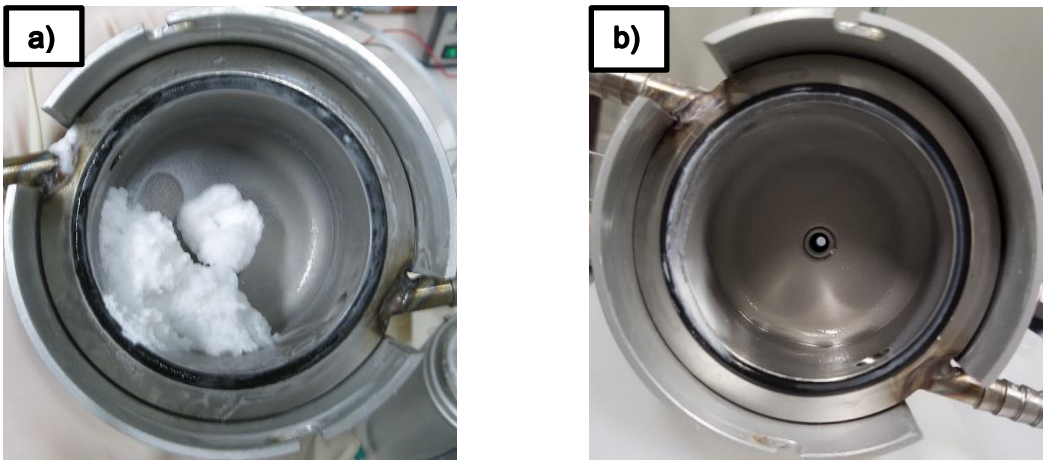

Figure 15. Influence of the US-input in the lactose system. a) 15 W US-input (test run 1). b) 100 W US-input (test run 5)

The results of these experiments indicate that US can be used to de-agglomerate particles in this system. The smallest accumulation and build-up in the process chamber is achieved at the highest US-input. However, particles were not destroyed when increasing the net US power (as seen in Figure 14). However, the higher the net power intake is, the higher the product temperature is. As such, a compromise must be made between the negative effect of heating the product suspension via the US-input and the positive effect of high US-input on the de-agglomeration.

To examine the versatility of the process equipment, a different material combination was tested. The system contained ibuprofen suspended in a 1:1 ratio EtOH:H_2O mixture that had been saturated as described in section 2. Results with this system are shown in Figure 16. In contrast to the lactose runs, foaming occurs in the process chamber. Additionally, there is almost no adhesion of the precipitated material to the walls. Figure 16 shows the process chamber after the PSD experiment. At the lowest US setting (22 W net

power) leakage occurred, because the pressure increased above the critical value of 0.4 bar. No sample could be collected for this setting. A comparison between Figure 16a and Figure 16b indicates that less and thinner foam accumulates at a higher US-input.

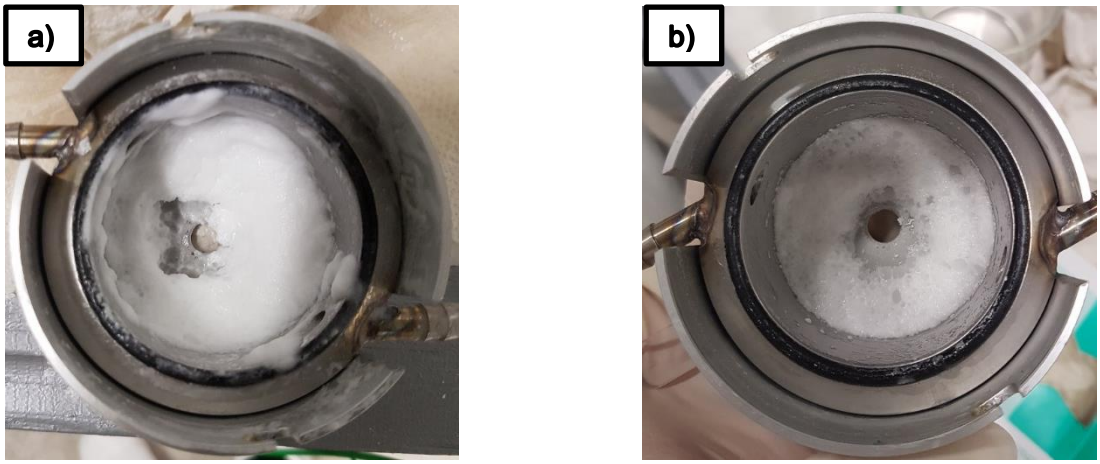

Figure 16. Comparison of the US-input effect on the foam accumulation in the ibuprofen test runs. a) 22 W US-input for ibuprofen (run 8). b) 5-h experiment at 110 W US-input, cooling bath set to 5 °C (run 9)

Figure 17 shows the PSD of the initial suspension and the product's PSD at a US-input of 110 W and 60 W after 20 minutes of process time. The respective mean diameters (x50, Sauter mean diameter and volumetric mean diameter) are depicted in Figure 18. The PSD for all measurements is practically the same and hence not affected by US in this setting.

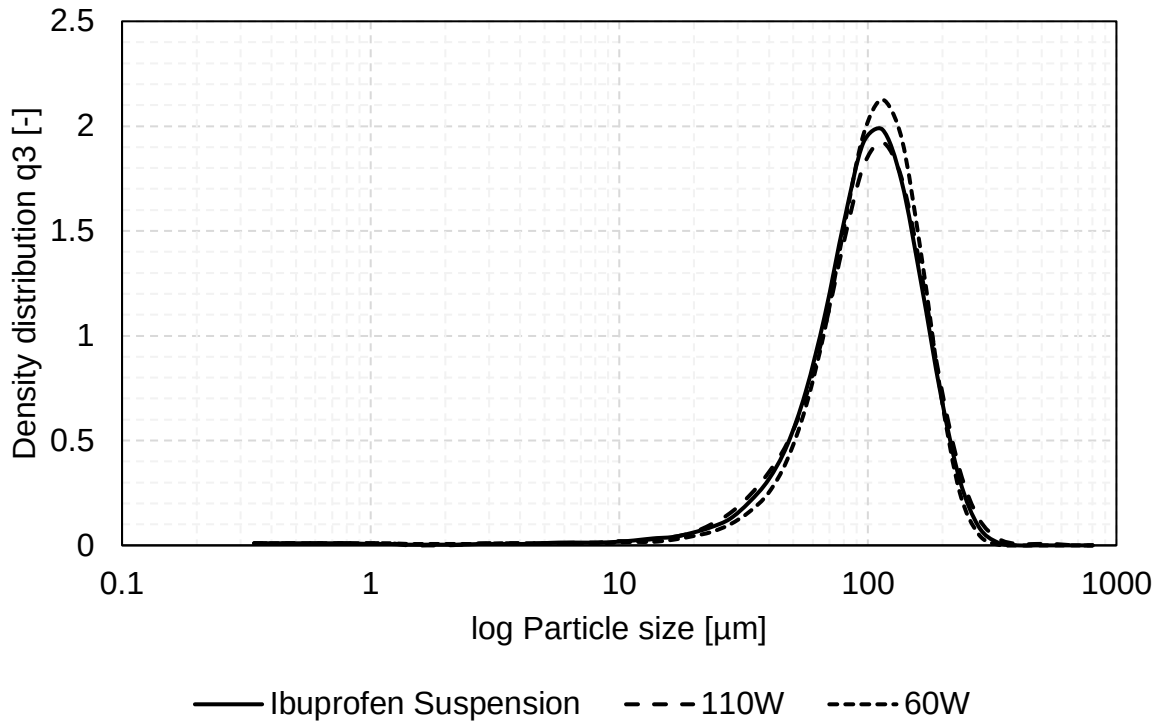

Figure 17. Results for the PSD measurements in the ibuprofen test run 8: density distributions of the feed suspension (Solid line) and at 110 W (Dashed line) and 60 W (Dotted line) US-input.

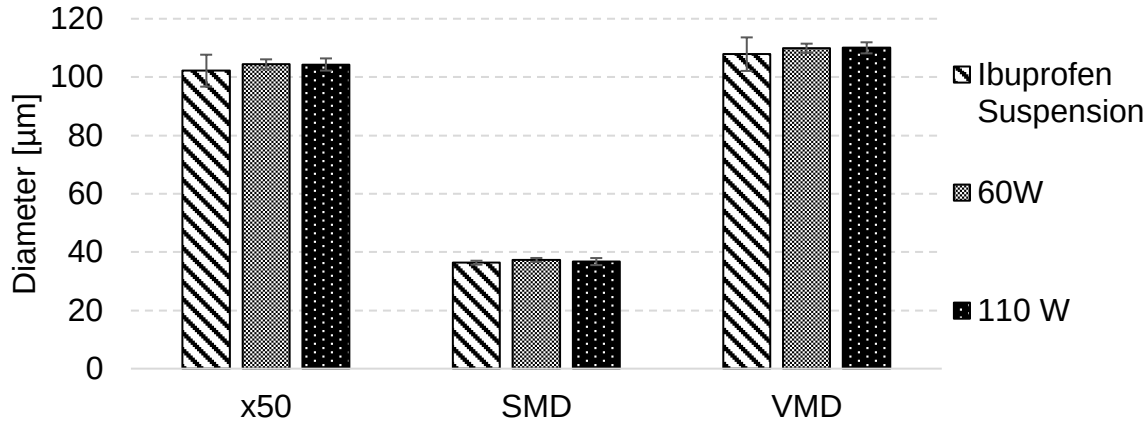

Figure 18. Results of the PSD-measurements in the ibuprofen test run 8: x50, SMD and VMD.

The results of the PSD-measurements show that the precipitation of the dissolved solids has no measurable influence on the particle size in the setup used in our work. The non-linearity of the net power intake at varying ultrasound levels can be explained by the different material distributions in the process chamber, as linearity was visible when using water as a test substance (data not shown). The varying amount of sedimented and agglomerated particles, as well as foam, are interfering with the propagation of the ultrasound through the chamber. The foam is likely produced by the degassing of the anti-

solvents. Therefore, the foam consists of more gas, and is thus thinner at higher US-input, as more gas is degassed from the liquid phase.

Table 5 shows that higher US-input leads to higher product temperatures. For the lactose system, a product temperature of 22 °C is reached for 15 W US-input, which increases to 28°C at the maximum power level of 100 W. The IPA, which served as an anti-solvent, was pre-cooled to 12 °C in the cooling bath set to 10 °C. For the ibuprofen test run, the cooling bath was set to 5 °C, resulting in an anti-solvent (water) temperature of 8 °C. A higher energy intake of the ibuprofen system may be attributed to a lower US propagation velocity at an increasing ethanol concentration. The US attenuation is higher and more energy is consumed[38].The amount of processed material is stated in Table 2 and Table 3.

Table 5. Resulting temperatures of all US-inputs for both material combinations

Material [-]	**Cooling Bath** [°C]	**US-input** [%]	**US-input** [W]	**Anti-Solvent Temperature** [°C]	**Product Temperature** [°C]
α-Lactose	10	20	15	12	22
α-Lactose	10	40	30	12	23.5
α-Lactose	10	60	50	12	25
α-Lactose	10	80	85	12	26.8
α-Lactose	10	100	100	12	28
Ibuprofen 25	5	100	110	8	28
Ibuprofen 25	5	67	60	8	25
Ibuprofen 25	5	33	22	8	22

In addition to the energy input of the ultrasound, the temperate of the solution (Table 6) as well as the temperature of the different mixed solvents (Table 7) contribute to the temperature increase. The typical temperature of the solution for crystalline alpha-lactose monohydrate is 56.2 J/g at 25 °C[39]. It is assumed that the same amount of energy is released during the precipitation of the solids. This corresponds to roughly 803.7 J/min for

this process. Another factor is the temperature of the different mixed solvents. For water and 2-propanol the mixing enthalpy is around -6.5 J/g based on the mass of 2-propanol[40], and therefore around -650 J/min, which are released from the mixture exothermically. The mixing enthalpies were calculated by interpolating the data of Lama et Lu[40] to fit the used fractions of materials. This energy heats up the mixture and the surrounding parts, resulting in an elevated temperature of the process over time. Ibuprofen shows a higher temperature of solvation of around 135.8 J/g in the solvent mixture used in this study, resulting in approximately 801.5 J/min in our process[41]. For this calculation the data from Manrique et Martínez[41] was interpolated. The phase separation that was described in their study did not occur during our experiments, probably due to the US-input or the solids present. For ethanol-water mixtures, the mixing enthalpy is calculated differently, as most of the heat provided by mixing is already released during the preparation of the saturated solution. The data from Lama et Lu[40] was interpolated for both mass fractions used (the 1:1 mixture and the final dilution) and the mixing enthalpy was computed as the difference between the two values, resulting in very slight exothermic behavior[40]. The energy amount which is exothermically released by precipitation and mixing is therefore around 1457.7 J/min for the 15 wt. % lactose system, and around 805.7 J/min for the ibuprofen system. It must be mentioned that the provided mixing enthalpies are for pure, binary mixtures and therefore cannot be considered as exact for saturated solutions. The energy amounts are based on the precipitated amount of solids (14.3 g/min of lactose, 5.9 g/min of ibuprofen) and of the amount of anti-solvent (100 g/min for 2-propanol and 42.5 g/min for ethanol).

Table 6. Crystallization temperatures of the used material combinations[39,41]. The used molecular weight of ibuprofen was 230.26 g/mol[41]

Substance [-]	**Rate of precipitation [g/min]**	**Enthalpy of solution [J/g]**	**Released Energy [J/min]**
Alpha-Lactose monohydrate[39]	14.3	56.2	803.7
Ibuprofen[41]	5.9	135.8	801.5

Table 7. Mixing enthalpies of the used material combinations[40]

Mixture [-]	**Mass flow (1) [g/min]**	**Mass flow (2) [g/min]**	**Mixing enthalpy [J/g]**	**Mixing enthalpy [J/min]**
H_2O (1) – IPA (2)	85	100	-6.5	-654
1:1 H_2O-EtOH (1) – H_2O (2)	85	100	-0.1	-4.2

2.4.2 Evaluation of the anti-solvent temperature influence on the process and particles

Table 8 illustrates that the product temperature is reduced by 3 °C if the anti-solvent temperature is lowered by 11 °C (from 23 °C to 12 °C). Cooling the anti-solvent down to 8 °C reduces the product temperature from 25 °C to 24 °C. This can be explained by additional heat of crystallisation[42], as at lower temperature more solids are precipitated, and the released mixing enthalpy (See section 3.1.1). Depending on the temperature levels, the different enthalpy contributions are changing and, therefore, the correlation is not linear. Regarding the process chambers after the test runs (Figure 19a and b) it can be seen that lower temperatures lead to more accumulations.

Table 8. Resulting temperatures for the various cooling bath configurations

Cooling Bath [°C]	US-input [W]	Anti-Solvent Temperature [°C]	Product Temperature [°C]
-	50	23	28
10	50	12	25
5	50	8	24

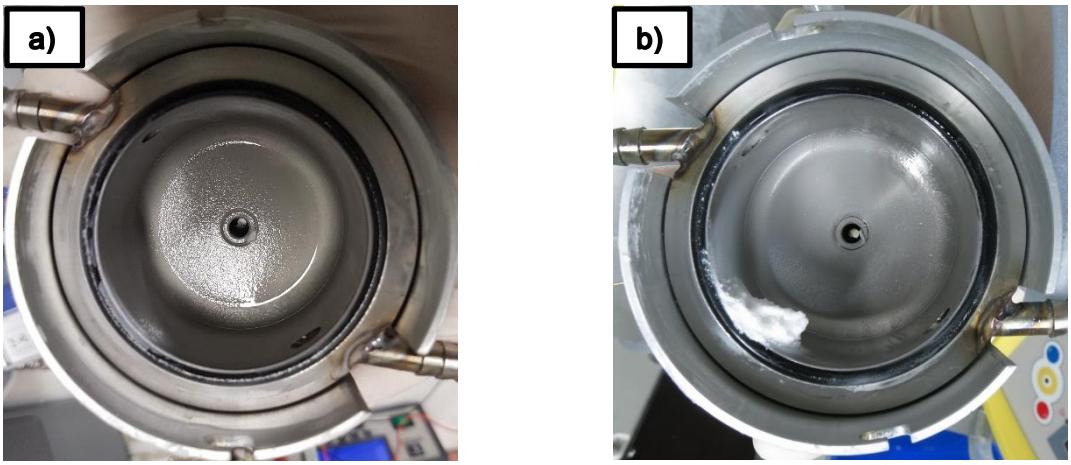

Figure 19. Comparison of the influence of pre-cooling the anti-solvent on the accumulation in the process chamber. a) Process chamber after the uncooled test run 2, 50 W US-input. b) Process chamber after adding pre-cooled anti-solvent, 50 W US-input, test run 3, after 2 h

The resulting temperatures in test runs 2-4 for the different US-configurations are shown in Table 8. At a product temperature of 25 °C, 8.76 kg of lactose were processed in the uncooled test run shown in Figure 19a (neglecting the residual dissolved lactose in the product), while in the first pre-cooling test run (Figure 19b) only 3.54 kg were processed, but more accumulation occurred in the chamber.

In the process stability test runs, the highest US power and the lowest cooling bath temperature were applied. This was the best combination in terms of system accumulations and amount of precipitated solid.

2.4.3 Evaluation of the influence of US on long-term process stability

The effect of various US levels on the long-term process performance was investigated in test runs 4-6. The fourth run was performed to evaluate whether there is a maximum amount of accumulation in the system and whether the US is powerful enough to break up the agglomerates at some point. The run had to be stopped due to leakage caused by flakes breaking off from the accumulations and blocking the outlet of the process chamber, leading to a pressure rise. Figure 20a shows the corresponding process chamber. When comparing the outcome of this test run to test run 3 (Figure 19b), it is clearly visible that the amount of accumulated lactose increases over time.

The next test run was performed using the same process parameters, but at the maximum possible US-input. Only a small amount of material accumulated in the process chamber (Figure 20b). Experiment 6, which was performed to evaluate the reproducibility of this result, had a very similar outcome (Figure 20b and c). In run 4 (Figure 19a) 9.23 kg of lactose on a dry basis were processed, while in runs 5 and 6 (Figure 19b and c) 14.02 kg of lactose were processed with less accumulation.

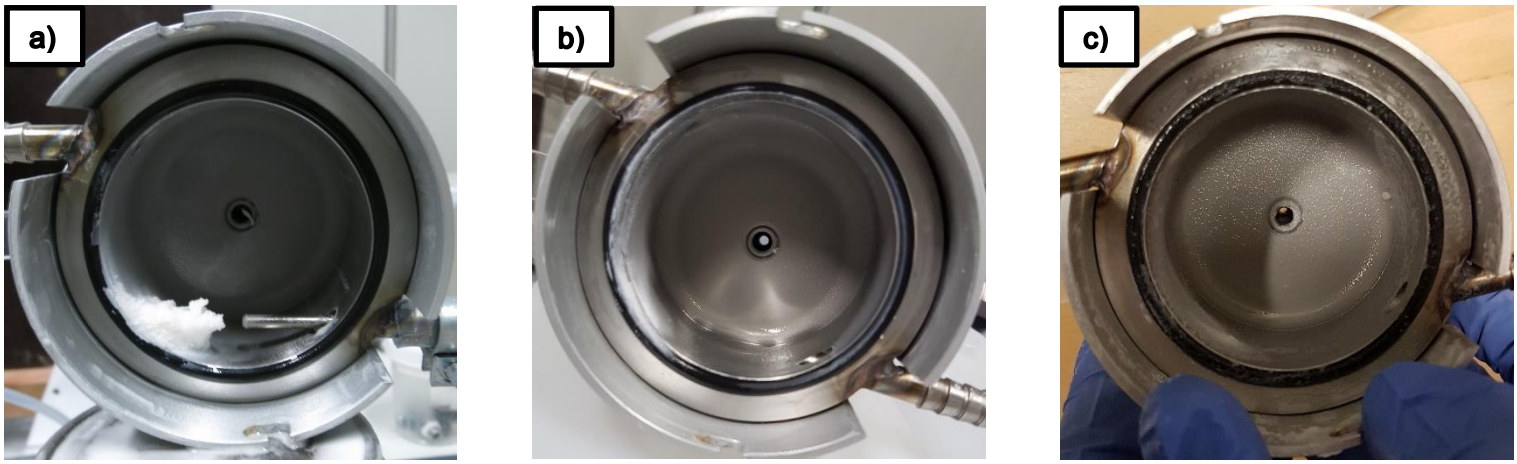

Figure 20. Influence of the US-input on the accumulations in the process chamber in the lactose experiments. a) Process chamber run 4, after 5 h 16 min. b) Process chamber; 8 h experiment (5); 15 wt. % lactose-suspension; 100 % US-input; cooling bath 5 °C. c) Accumulations in the process chamber after the repetition of the 8 h experiment (6) with a 15 wt. % lactose-suspension with full US-input and the cooling bath set to 5 °C.

To evaluate the long-term applicability of the ibuprofen setup, the 5-h (run 9, previously shown in Figure 16b) and 8-h run (run 10), tests were performed at the maximum US-input and with the cooling bath at 5 °C. Figure 21a and b show the accumulations after the 8-h run. The difference between Figure 21a and Figure 21b is that the foam was rinsed off with water so that the adhesion to the surface could be seen. Only a very small amount adhered to the wall, close to the outlet.

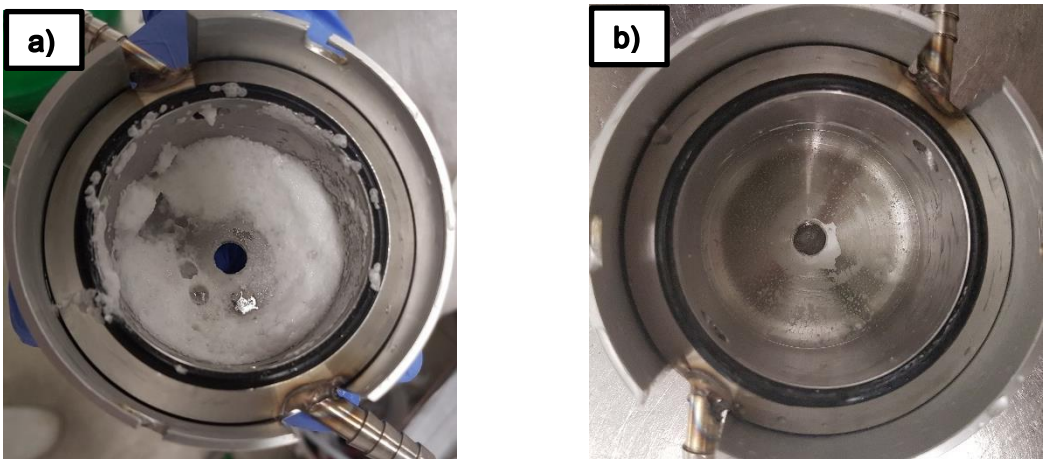

Figure 21. Accumulation in the process chamber after an 8-h experiment with a 15 wt. % ibuprofen suspension, a full US-input and the cooling bath set to 5 °C (run 10). a) Accumulations in the process chamber after an 8-h experiment with a 15 wt. % ibuprofen suspension, a full US-input and the cooling bath set to 5 °C (run 10). b) Accumulations in the process chamber after an 8-h experiment with a 15 wt. % ibuprofen suspension, a full US-input and the cooling bath set to 5 °C, after rinsing the equipment with water (run 10).

The results of the ibuprofen experiments show that the process is also stable for hydrophobic materials. However, other effects prevail in terms of accumulation in the system. In contrast to the lactose experiments, foaming occurs, while the solidification of material on the process chamber surface is negligible. Comparing Figure 16b to Figure 21a indicates that the amount of foam is not time-dependent. The weights of processed material on a dry basis were 6.24 kg and 9.98 kg in the 5 h and 8 h experiments.

2.4.4 **Effect of solid loading on the process behaviour**

To test the system's boundaries, a test run with a solid loading of 55 wt. % was performed and compared to the findings of experiments with a lower solid content (i.e. 15 wt. %). The resulting US configurations and temperatures are shown in Table 9. A lower solid loading leads to a higher product temperature, which can be explained by a higher rate of precipitation and heat of crystallization. To illustrate this, the amounts of processed solids for the two configurations are shown in Table 10. In total, approximately twice the

amount of solids are processed, while only about half of the solids are precipitated compared to the lower solid loading.

Table 9. Resulting temperatures for the two solid loadings

Solid loading [wt.%]	Cooling Bath [°C]	US-input [W]	Anti-Solvent Temperature [°C]	Product Temperature [°C]
15	5	100	8	27
55	5	100	8	26

Table 10. Processed solids for the two solid loadings

Solid loading [wt.%]	Processed solids [g/min]	Solids in feed [g/min]	Precipitated solids [g/min]	Solids remaining dissolved [g/min]	Total amount of processed solids in run time [kg]	Duration [h]
15	31.1	15	14.3	1.8	14.9	8
55	62.6	55	6.6	1.0	11.3	3

Figure 22a and b show that the accumulations in the process chamber increase at a higher solid loading. Despite the process being 5 h shorter than in the 15 wt. % case, the amount of material adhering to the walls is significantly higher. The process time was reduced since a similar amount of processed solids enabled a visual comparison of the depositions on the wall.

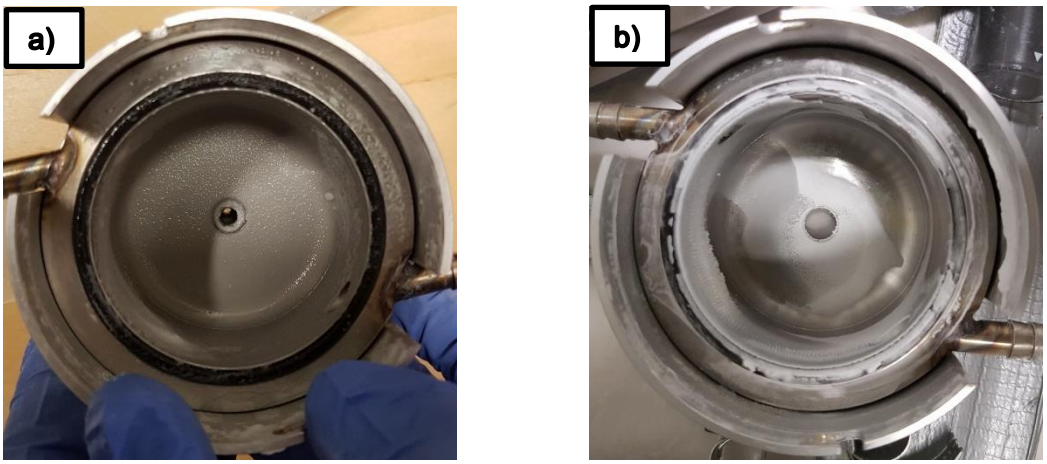

Figure 22. Influence of solid loading on the accumulation in the process chamber. a) Accumulations in the process chamber after 8 h for a 15 wt. % lactose suspension with 100 W US-input and the cooling bath set to 5 °C (run 6). b) Accumulations in the process chamber after 3 h for a 55 wt. % lactose suspension with 100 W US-input and the cooling bath set to 5 °C (run 7)

To reduce the negative effect of higher solid loadings on the accumulation in the system, the solid mass fraction should be as low as possible. However, as this reduces the amount of processed solids even further, we maintained a 15 wt. % mass fraction of solids as minimum loading. While in the 8-h experiment with 15 wt. % a total of 14.02 kg of lactose were processed, in the 55 wt. % run 11.27 kg were processed after 3 h. If the 55 wt. % process had been run for 8 h, 30.05 kg lactose would have been processed, which sums up to more than twice the amount of solids. Nonetheless it can be seen that in terms of accumulated material the lower loading is favorable because less accumulation is built after the same amount of material has been processed. It is the goal of this optimization to run the process with the highest product yield between cleaning cycles. Therefore, the optimal setup will be the one with the lowest material adhesion per kg of processed product.

2.4.5 **Long-term stability of the process setup**

To evaluate the potential of this process setup for continuous operations, two 24-h experiments were performed: one with lactose and the other one with ibuprofen. For both surrogate substances, a solid loading of 15 wt. %, the maximum US-input and a cooling bath temperature of 5 °C were chosen.

The entrance and mixing points of the material streams were moved 1 cm away from the wall in streaming direction. The geometry is of critical importance for the success of the process, as the flow pattern inside the process chamber determines where precipitation occurs and how it distributes. The moving of the entrance points did not harm the process, but kept the outcome similar to the 8 h experiments, indicating that excessive agglomeration

and surface adhesion after mixing can be avoided with this setup. Both runs were successfully completed. The resulting pressure curve for the lactose run is shown at the top of Figure 23. Throughout the experiment, the relative pressure never exceeded 0.1 bar, indicating a very stable process. Especially when comparing this data to the findings of Kreimer et al.[18] who reported a pressure increase of over 4 bar in every experiment with the same material combinations, the advantages of this process setup are obvious. In total, 44.8 kg of α-Lactose were processed. Out of these, in the feed suspension 21.6 kg were initially suspended, an additional 20.6 kg were precipitated and only 2.6 kg remained dissolved in the product. Figure 24a presents a comparison to the accumulations in the shorter experiments, indicating that the material accumulation inside the process chamber increases with prolonged process times (these may reach a critical level after some time in a real continuous application).

The pressure curve for the ibuprofen experiment looked very similar, as shown at the bottom of Figure 23. In this experiment the relative pressure never exceeded 0.1 bar. The negative pressure values can be explained by the calibration of the system with the water-filled system, which has a higher density than the product, therefore applying a higher static pressure on the sensor. The total amount of processed solid material was 30.5 kg of Ibuprofen 25, with 21.6 kg being suspended in the feed. The precipitated amount of solid was 8.4 kg and 0.5 kg remained dissolved in the product. Figure 24b and c show that in this system the accumulation of foam is time-independent since the amount is comparable to the accumulation after the 8-h experiments. Furthermore, adhesion to the surface at the outlet did not increase considerably.

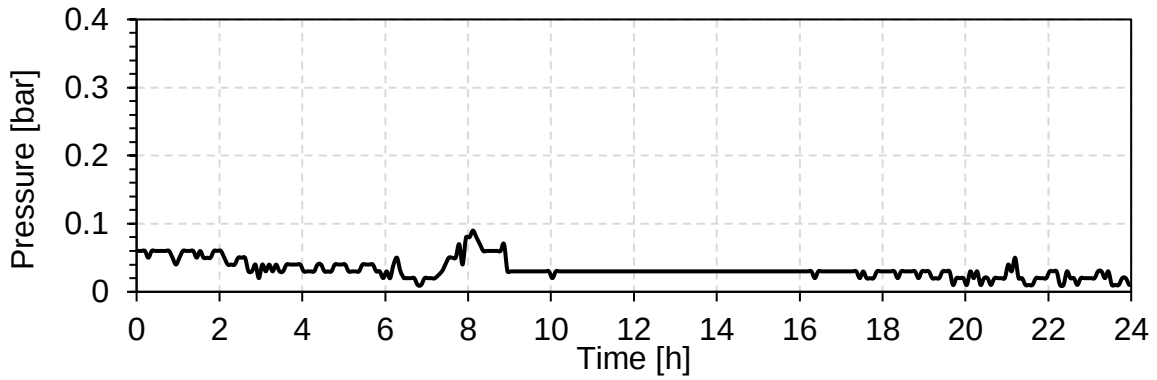

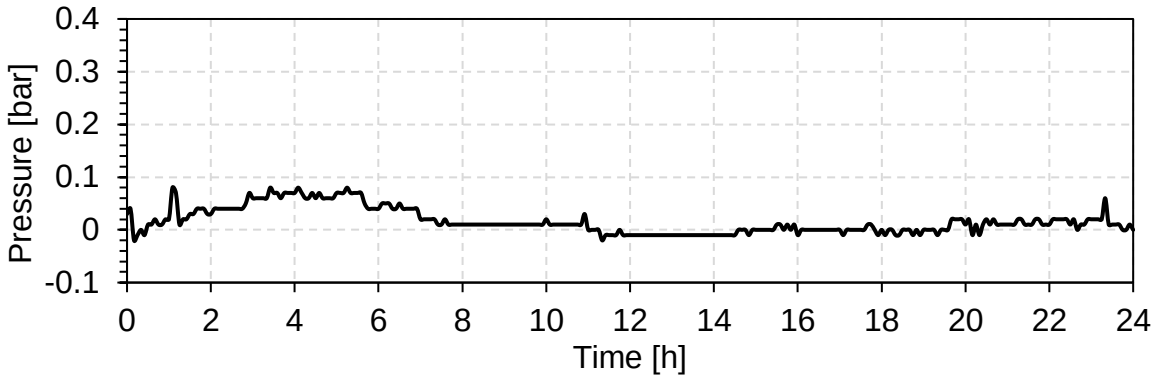

Figure 23. Relative pressure for the 24-h test runs (lactose run 11 on the top, ibuprofen run 12 at bottom)

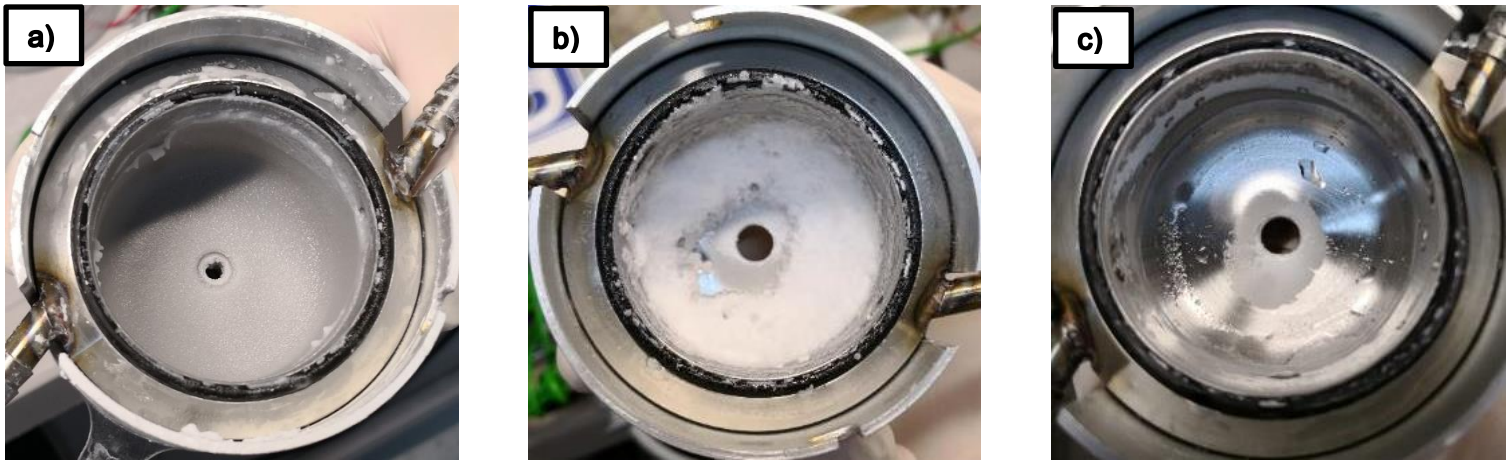

Figure 24. Process chamber after the 24-h test run with lactose. a) Process chamber after a 24-h test run with lactose, b) Process chamber after a 24-h test run with ibuprofen, c) Process chamber after a 24-h test run with ibuprofen, foam rinsed away to assess the surface adhesion

The two test runs were very stable and no blockage was observed during the operation. Considering that precipitation tended to block the system in another setup[18], this setup is a significant improvement, as it made it possible to run the process for 24 h without interruptions.

2.5 Conclusion

This work focused on the applicability of an ultrasonic process chamber in precipitating environments. Two model substances were used: lactose suspended in a saturated lactose- water solution and ibuprofen suspended in a saturated solution of ibuprofen in an aqueous ethanol mixture.

It was observed that ibuprofen and lactose behave differently during processing. Lactose forms stable and crystalline appearing deposits, while ibuprofen forms a foam. The amount of deposits formed by lactose is process time dependent, as more accumulations are formed after longer process times. The foam formed by ibuprofen is independent of process time. In both cases, application of further ultrasound leads to enhanced process performance, because the amount of agglomerates and the amount of formed foam is reduced.

The temperature of the process and additional cooling of the anti-solvent flow leads to additional agglomeration in the system, because the solubility in the product is reduced. The amount of processed material also influences the amount of agglomerations. Two key factors must be considered. These are the solid loading of the flow and the maximum process duration. Higher solid loading results in more material processed per hour. Lower loading results in a longer process duration. It was found that lower solid loading leads to a more stable process and therefore to a higher amount of total produced material between cleaning cycles. Hence a compromise between these influencing factors must be found, in terms of processed materials and process stability.

Based on the results of the screening tests, it was possible to operate the system for both substances without problems for 24 hours. However, since surface adhesion, which may eventually block the system, occurred in the lactose test run, a recurrent washing procedure could be necessary to enable a multiple day continuous operation. The 24 hour experiment was quite stable for ibuprofen, with its outcome being very similar to the 16 hour shorter experiment. The particle size distribution of both material combinations was not influenced by the application of ultrasound. In summary, a positive effect of direct US application in a process chamber with a circular or helical flow pattern has clearly been established.

In order to prepare this technology for production, the equipment must be optimized and adapted to meet pharmaceutical production/cleaning standards. To support a fully continuous operation, a second process chamber needs to be implemented, with a washing strategy to clean the first chamber, when its solid loading becomes too high. Especially in

the pharmaceutical industry, where the search for suitable continuous processes is important[1–4], an optimized system based on these findings could be used for continuous crystallization and mixing in primary manufacturing. Through this, linking drug substance and drug product manufacturing can be achieved, with the associated production time and costs tremendously reduced.

2.6 Acknowledgements

This work has been funded within the Austrian COMET Program under the auspices of the Austrian Federal Ministry of Transport, Innovation and Technology (BMVIT), the Austrian Federal Ministry of Economy, Family and Youth (BMWFJ) and by the State of Styria (Styrian Funding Agency SFG). COMET is managed by the Austrian Research Promotion Agency FFG. We acknowledge the support of Sarah Koller (RCPE), Daniel Wiegele (RCPE) and Heidrun Gruber-Wölfler (TU Graz).

2.7 Nomenclature

x_{50}	Median mean diameter / µm
H_2O	Water
SMD	Sauter mean diameter / µm
VMD	Volume mean diameter / µm
$w_{d,sat.sol.}$	Dissolved solid mass fraction in the saturated solution / wt.%
$w_{H_2O,sat.sol.}$	Water mass fraction in saturated solution / wt.%
$w_{EtOH,sat.sol.}$	Ethanol mass fraction in saturated solution / wt.%
$w_{s,f}$	Suspended solid mass fraction in feed / wt.%
$w_{d,f}$	Dissolved solid mass fraction in feed / wt.%
$w_{H_2O,f}$	Water mass fraction in feed / wt.%
$w_{EtOH,f}$	Ethanol mass fraction in feed / wt.%
$w_{s,p}$	Suspended solid mass fraction in product / wt.%
$w_{d,p}$	Dissolved solid mass fraction in product / wt.%
$w_{H_2O,p}$	Water mass fraction in product / wt.%
$w_{IPA,p}$	Isopropanol mass fraction in product / wt.%
$w_{EtOH,p}$	Ethanol mass fraction in product / wt.%

2.8 Abbreviations

API	Active pharmaceutical ingredient
BASF	Badische Anilin- & Soda-Fabrik
EtOH	Ethanol
IPA	Isopropanol
PSD	Particle size distribution
M	Motor mixer
PI	Pressure indicator
PVC	Polyvinyl chloride
SEM	Scanning electron microscope
TI	Temperature indicator
US	Ultrasound
VWR	Van Water and Rogers

2.9 References

(1) FDA. Guidance for Industry PAT: A Framework for Innovative Pharmaceutical Development, Manufacuring, and Quality Assurance; 2004.

(2) Badman, C.; Cooney, C. L.; Florence, A.; Konstantinov, K.; Krumme, M.; Mascia, S.; Nasr, M.; Trout, B. L. Why We Need Continuous Pharmaceutical Manufacturing and How to Make It Happen. J. Pharm. Sci. 2019, 108, 3521–3523.

(3) Jolliffe, H. G.; Gerogiorgis, D. I. Process Modelling and Simulation for Continuous Pharmaceutical Manufacturing of Ibuprofen. Chem. Eng. Res. Des. 2015, 97, 175–191.

(4) Ottoboni, S.; Price, C. J.; Steven, C.; Meehan, E.; Barton, A.; Firth, P.; Mitchell, A.; Tahir, F. Development of a Novel Continuous Filtration Unit for Pharmaceutical Process Development and Manufacturing. J. Pharm. Sci. 2019, 108, 372–381.

(5) Nokhodchi, A.; Amire, O.; Jelvehgari, M. Physico-Mechanical and Dissolution Behaviours of Ibuprofen Crystals Crystallized in the Presence of Various Additives. DARU J. Pharm. Sci. 2010, 18, 74–83.

(6) Besenhard, M. Continuous Crystallization of Active Pharmaceutical Ingredients via a Tubular Reactor : Simulation and Process Design, Graz University of Technology, 2014.

(7) Liu, L. X.; Marziano, I.; Bentham, A. C.; Litster, J. D.; E.T.White; Howes, T. Effect of Particle Properties on the Flowability of Ibuprofen Powders. Int. J. Pharm. 2008, 362, 109–117.

(8) Combarros, M.; Feise, H. J.; Zetzener, H.; Kwade, A. Segregation of Particulate

Solids: Experiments and DEM Simulations. Particuology 2014, 12, 25–32.

(9) Adam, S.; Suzzi, D.; Radeke, C.; Khinast, J. G. An Integrated Quality by Design (QbD) Approach towards Design Space Definition of a Blending Unit Operation by Discrete Element Method (DEM) Simulation. Eur. J. Pharm. Sci. 2011, 42, 106–115.

(10) Wakeman, R. The Influence of Particle Properties on Filtration. Sep. Purif. Technol. 2007, 58, 234–241.

(11) Sen, M.; Rogers, A.; Singh, R.; Chaudhury, A.; John, J.; Ierapetritou, M. G.; Ramachandran, R. Flowsheet Optimization of an Integrated Continuous Purification-Processing Pharmaceutical Manufacturing Operation. Chem. Eng. Sci. 2013, 102, 56–66.

(12) Kreimer, M.; Aigner, I.; Lepek, D.; Khinast, J. Continuous Drying of Pharmaceutical Powders Using a Twin-Screw Extruder. Org. Process Res. Dev. 2018, 22, 813–823.

(13) Mirza, S.; Miroshnyk, I.; Heinämäki, J.; Antikainen, O.; Rantanen, J.; Vuorela, P.; Vuorela, H.; Yliruusi, J. Crystal Morphology Engineering of Pharmaceutical Solids: Tabletting Performance Enhancement. AAPS PharmSciTech 2009, 10, 113–119.

(14) Faulhammer, E.; Llusa, M.; Radeke, C.; Scheibelhofer, O.; Lawrence, S.; Biserni, S.; Calzolari, V.; Khinast, J. G. The Effects of Material Attributes on Capsule Fill Weight and Weight Variability in Dosator Nozzle Machines. Int. J. Pharm. 2014, 471, 332–338.

(15) Watkinson, A. P.; Wilson, D. I. Chemical Reaction Fouling: A Review. Exp. Therm. Fluid Sci. 1997, 14, 361–374.

(16) Hochstrasser, M.; Jussen, D.; Riedlberger, P. Towards Process Intensification: Remediation of Fouling in Continuous Microscale Synthesis of Phosphated TiO2. Chem. Eng. Process. Process Intensif. 2017, 121, 15–23.

(17) Awad, M. M. Fouling of Heat Transfer Surfaces. In *Heat Transfer - Theoretical Analysis, Experimental Investigations and Industrial Systems*; Belmiloudi, A., Ed.; InTech, 2011; Vol. 10, pp 505–542.

(18) Kreimer, M.; Zettl, M.; Aigner, I.; Mannschott, T.; Van der Wel, P.; Khinast, J. G.; Krumme, M. Performance Characterization of Static Mixers in Precipitating Environments. Org. Process Res. Dev. 2019, 23, 1308–1320.

(19) Deshannavar, U. B.; Ramasamy, M. A Model to Determine Maximum Heat Flux under Forced Convective Heat Transfer Regime for Crude Oil Fouling Studies. Appl. Therm. Eng. 2019, 156, 485–493.

(20) Epstein, N. Elements of Particle Deposition onto Nonporous Solid Surfaces Parallel to Suspension Flows. Exp. Therm. Fluid Sci. 1997, 14, 323–334.

(21) Schoenitz, M.; Grundemann, L.; Augustin, W.; Scholl, S. Fouling in Microstructured Devices: A Review. Chem. Commun. 2015, 51, 8213–8228.

(22) Kazi, S. N. Fouling and Fouling Mitigation on Heat Exchanger Surfaces. In *Heat*

Exchangers - Basics Design Applications; Mitrovic, J., Ed.; InTechOpen, 2012; pp 507–532.

(23) Mitrovic, J. Heat Exchangers - Basics Design Applications; Mitrovic, J., Ed.; InTech, 2012.

(24) Müller-Steinhagen, H.; Reif, F.; Epstein, N.; Watkinson, A. P. Influence of Operating Conditions on Particulate Fouling. Can. J. Chem. Eng. 1988, 66, 42–50.

(25) Ashokkumar, M. Applications of Ultrasound in Food and Bioprocessing. Ultrason. Sonochem. 2015, 25, 17–23.

(26) Heffernan, S. P.; Kelly, A. L.; Mulvihill, D. M.; Lambrich, U.; Schuchmann, H. P. Efficiency of a Range of Homogenisation Technologies in the Emulsification and Stabilization of Cream Liqueurs. Innov. Food Sci. Emerg. Technol. 2011, 12, 628–634.

(27) Leong, T. S. H.; Zhou, M.; Zhou, D.; Ashokkumar, M.; Martin, G. J. O. The Formation of Double Emulsions in Skim Milk Using Minimal Food-Grade Emulsifiers – A Comparison between Ultrasonic and High Pressure Homogenisation Efficiencies. J. Food Eng. 2018, 219, 81–92.

(28) Ojha, K. S.; Mason, T. J.; O'Donnell, C. P.; Kerry, J. P.; Tiwari, B. K. Ultrasound Technology for Food Fermentation Applications. Ultrason. Sonochem. 2017, 34, 410–417.

(29) Zhang, M.; Yewe-Siang Lee Shee We, M.; Wu, H. Direct Emulsification of Crude Glycerol and Bio-Oil without Addition of Surfactant via Ultrasound and Mechanical Agitation. Fuel 2018, 227, 183–189.

(30) Ho, W. W. S.; Ng, H. K.; Gan, S. Advances in Ultrasound-Assisted Transesterification for Biodiesel Production. Appl. Therm. Eng. 2016, 100, 553–563.

(31) Sancheti, S. V.; Gogate, P. R. Intensification of Heterogeneously Catalyzed Suzuki-Miyaura Cross-Coupling Reaction Using Ultrasound: Understanding Effect of Operating Parameters. Ultrason. Sonochem. 2018, 40, 30–39.

(32) Ajmal, M.; Fieg, G.; Keil, F. Analysis of Process Intensification in Enzyme Catalyzed Reactions Using Ultrasound. Chem. Eng. Process. Process Intensif. 2016, 110, 106–113.

(33) Mane, S. N.; Gadalkar, S. M.; Rathod, V. K. Intensification of Paracetamol (Acetaminophen) Synthesis from Hydroquinone Using Ultrasound. Ultrason. Sonochem. 2018, 49, 106–110.

(34) Kreimer, M.; Aigner, I.; Sacher, S.; Krumme, M.; Mannschott, T.; van der Wel, P.; Kaptein, A.; Schroettner, H.; Brenn, G.; Khinast, J. G. Mechanical Strength of Microspheres Produced by Drying of Acoustically Levitated Suspension Droplets. Powder Technol. 2018, 325, 247–260.

(35) Machado, J. J. .; Coutinho, J. A.; Macedo, E. A. Solid–Liquid Equilibrium of α-Lactose in Ethanol/Water. Fluid Phase Equilib. 2000, 173, 121–134.

(36) Rashid, A.; White, E. T.; Howes, T.; Litster, J. D.; Marziano, I. Effect of Solvent Composition and Temperature on the Solubility of Ibuprofen in Aqueous Ethanol. J. Chem. Eng. Data 2014, 59, 2699–2703.

(37) Potoroko, I.; Kalinina, I.; Botvinnikova, V.; Krasulya, O.; Fatkullin, R.; Bagale, U.; Sonawane, S. H. Ultrasound Effects Based on Simulation of Milk Processing Properties. Ultrason. Sonochem. 2018, 48, 463–472.

(38) Figueiredo, M. K.-K.; Costa-Felix, R. P. B.; Maggi, L. E.; Alvarenga, A. V.; Romeiro, G. A. Biofuel Ethanol Adulteration Detection Using an Ultrasonic Measurement Method. Fuel 2012, 91, 209–212.

(39) Hogan, S. E.; Buckton, G. The Quantification of Small Degrees of Disorder in Lactose Using Solution Calorimetry. Int. J. Pharm. 2000, 207, 57–64.

(40) Lama, R. F.; Lu, B. C. Y. Excess Thermodynamic Properties of Aqueous Alcohol Solutions. J. Chem. Eng. Data 1965, 10, 216–219.

(41) Manrique, J.; Martínez, F. Solubility of Ibuprofen in Some Ethanol + Water Cosolvent Mixtures at Several Temperatures. Lat. Am. J. Pharm. 2007, 26, 344–354.

(42) Bhugra, C.; Pikal, M. J. Role of Thermodynamic, Molecular, and Kinetic Factors in Crystallization from the Amorphous State. J. Pharm. Sci. 2008, 97, 1329–1349.

„There's real poetry in the real world. Science is the poetry of reality"
*Richard Dawkins (*1941)*

3 Establishing the Missing Link: the Development of a Dryer Suitable for Continuous Processing of Cohesive Materials

Manuel Zettl[1], Isabella Aigner[1], Craig Hauser[1,6], Thomas Mannschott[2], Peter van der Wel[3], Hartmuth Schröttner[4,5], Johannes Khinast[1,6], Markus Krumme[2,*]

[1] Research Center Pharmaceutical Engineering (RCPE) GmbH, 8010 Graz, Austria

[2] Novartis Pharma AG, 4056 Basel, Switzerland

[3] Hosokawa Micron B.V., 7005 BL Doetinchem, Netherlands

[4] Graz University of Technology, Institute for Electron Microscopy and Nanoanalysis, 8010 Graz, Austria

[5] Austrian Centre for Electron Microscopy and Nanoanalysis (FELMI-ZFE), 8010 Graz, Austria

[6] Graz University of Technology, Institute for Process and Particle Engineering, 8010 Graz, Austria

*Corresponding author: Markus Krumme

Adapted and submitted to the Journal of Pharmaceutical Innovation

3.1 Abstract

In recent years, there has been a growing interest in linking primary and secondary drug manufacturing due to a shift towards continuous manufacturing in the pharmaceutical industry. A dryer proposed in this study can run continuously with poorly flowable materials, establishing the missing link between primary (drug substance) and secondary (drug product) manufacturing. A paddle dryer was tested and, based on the results, an optimized prototype was designed and constructed. As a test substance, ibuprofen was used since it is difficult to process due to its poor flowability and very low melting point. This makes it well-suited for simulating other active pharmaceutical ingredients (API).

In the first test setup it was possible to dry ibuprofen to a residual water content below 1 wt. %. Much accumulation occurred inside the dryer, leading to an unstable residence time distribution (RTD), which is unsuitable for pharmaceutical products. However, since the product properties where very promising (i.e., little to no attrition and almost no agglomeration), to overcome the issues of product accumulation a new dryer was developed, and preliminarily tested using wet di-calcium phosphate and ibuprofen. As a result, the unwanted accumulation of material in the dryer was reduced significantly, making it possible to run the dryer continuously for extended periods of time (5.5 hours) with a stable hold-up. The dryer has an evaporation capacity of up to 640 g/h in the configurations tested.

Key words: Continuous manufacturing, drying, cohesive materials, temperature sensitive, agglomeration, equipment development

3.2 Introduction

Throughout the 20th century, the main production route in the pharmaceutical industry was batch-wise manufacturing, whereas other industries (e.g., oil and chemical) implemented continuous processes decades ago. The transition towards continuous manufacturing (CM) in the pharmaceutical industry only began in the early 21st century after the U.S. Food and Drug Administration (FDA) published a new set of guidelines[1,2]. The relatively slow transition towards CM on the part of pharmaceutical companies is primarily due to high initial costs, lack of trained personnel, regulatory insecurity and non-existing or unreliable equipment[3–5]. Furthermore, a variety of products can be manufactured using batch equipment, while continuous processes are

often tailored to suit a certain purpose. The main advantages of continuous production are increased mechanistic process understanding, automation, energy and material efficiency, as well as a shorter production time. Another advantage of CM is the reduced storage time of intermediate products. In batch production, the material is stored between process steps, increasing the amount of material in stock and the stored capital.

Since the throughput in a typical pharmaceutical manufacturing process is orders of magnitude smaller than in other industries, it is often a challenge to find suitable processing equipment that can handle continuous material flow rates in the range of a few grams to a few kilograms per hour. The scaling down of such processes is often impossible for geometry reasons[5]. Existing continuous equipment is often only available on a scale beginning at 10 kg/h (corresponding to 60 t/a. with a 6000 h operation time), which may be way too much for modern highly potent active pharmaceutical ingredients (APIs). For example, a medication of two tablets a day with 5 mg of API for 1 million patients would require an annual production of roughly 3.65 t/a of API substance. Increasing the throughput via continuous processes can easily be implemented by numbering up the units. Moreover, CM offers the flexibility of processing various products since multi-purpose plants can yield an annual demand within a few weeks, before switching to another product. Another advantage of CM is that residence times are shorter, lowering the risk of degeneration[6].

In primary pharmaceutical manufacturing the API is produced, while in secondary manufacturing the actual dosage form (e.g., tablets, suppositories, infusions, etc.) is created. API's are generally tailored to meet a certain biological function in the patient and are thus crystallized to have a certain morphology and size. During downstream processing there is a high risk of altering these properties. Therefore, special care must be taken when processing such substances. Today, primary and secondary manufacturing take place in different locations [5,7]. A technology linking the two production sequences (i.e., connecting primary and secondary manufacturing) would be beneficial. Continuous crystallization and continuous drying are therefore critical processes to create a continuous manufacturing environment.

In this study the focus is on continuous drying. Drying involves heat and mass transfer, whereby a solvent is removed via evaporation or sublimation. During the process, thermal properties, such as thermal conductivity, specific heat capacity and heat transfer coefficient, are a function of time and position in the drying processes and may vary depending on the water content. Flowability can change tremendously depending on the moisture content[8–10], electrostatics, agglomeration, attrition and heat. Moreover, the air and material flows inside dryers

are generally very complicated. These constraints make modelling and predicting of the dryer performance difficult, and experiments must be performed to evaluate the efficacy of a certain drying technique[11–13].

Existing drying systems can be classified in numerous ways according to the drying agent (e.g., air, steam etc.), the continuity of process (batch or continuous), the heat transfer method (direct, indirect, via electromagnetic fields) and the handling characteristics (e.g., tray, tunnel, through)[13]. In the food or chemical industries, large continuous dryers are typically used, while in pharmaceutical manufacturing mainly fluid-bed dryers, filter-bed dryers or plate dryers are implemented in batch models. Continuous spray dryers are mainly used for particle generation, i.e., to make amorphous particles, and are not used to dry crystallized powders.

In general, drying has the potential to massively change the particle size distribution due to agglomeration and attrition, which is a typical problem in crystal drying [14,15]. Since high temperatures are typically required during drying, thermal decomposition can occur[16–20]. To address these issues, we developed a dryer prototype for the continuous drying of cohesive materials on small-to-intermediate production scales between 0.5 kg/h and 2 kg/h on a dry basis, with the main goal of avoiding agglomeration and attrition. The novel dryer should process materials with moisture levels typical for a product after mechanical filtration (50 wt. % to 35 .wt. %[21]), as well as at lower moisture levels. Ideally, the residual moisture of the product should be below 1 wt. % for further processing.

To minimize the risk of thermal API degradation, the residence time should be narrow and short and the hold-up in the system should be as low as possible. To achieve these goals a completely new dryer was developed. The new dryer was subsequently tested and improved to limit the amount of material accumulation within the system. To be able to process thermosensitive materials, the use of a vacuum was considered in the design.

3.3 Materials

3.3.1 Model Substances

As a main model substance, Ibuprofen 25 (BASF SE, Ludwigshafen, Germany) was used. Due to its poor flowability, its cohesive nature[22] and its sensitivity to heat, it is ideally suited to represent a typical API. Its low solubility in water (21 mg/l at 25 °C[23]) made it possible to dry it without producing strong agglomerates[7], making it a perfect compound for analyzing the robustness of the conveying mechanisms involved in a drying process. After optimizing the

equipment, anhydrous di-calcium phosphate DICAFOS A150 (Chemische Fabrik Budenheim KG, Budenheim, Germany) was used to assess the applicability of the drying technology to other materials. In comparison to ibuprofen, dry DICAFOS has a rather good flowability, which decreases with the increasing moisture content (See Chapter 2.1.2). It is practically insoluble in water[24].

3.3.1.1 Particle Size Distribution and Morphology

The particle size distribution (PSD) was measured via a HELOS KR laser diffractometer (Sympatec GmbH, Clausthal-Zellerfeld, Germany) within a CUVETTE dispersion system. As a background medium, distilled water was used, mixed with one droplet (~0.015 ml) of Tween 80 (Sigma-Aldrich, Vienna, Austria) as a surfactant for the ibuprofen measurements. The mixture was continuously stirred at 1000 rpm and the solids were added until the optical concentration was at about 10 % absorbance, which is an ideal measurement range for the instrument being used. The obtained PSDs are shown in Figure (a volumetric mean diameter (VMD) of 50 µm and 174 µm for Ibuprofen 25 and DICAFOS A150, respectively).

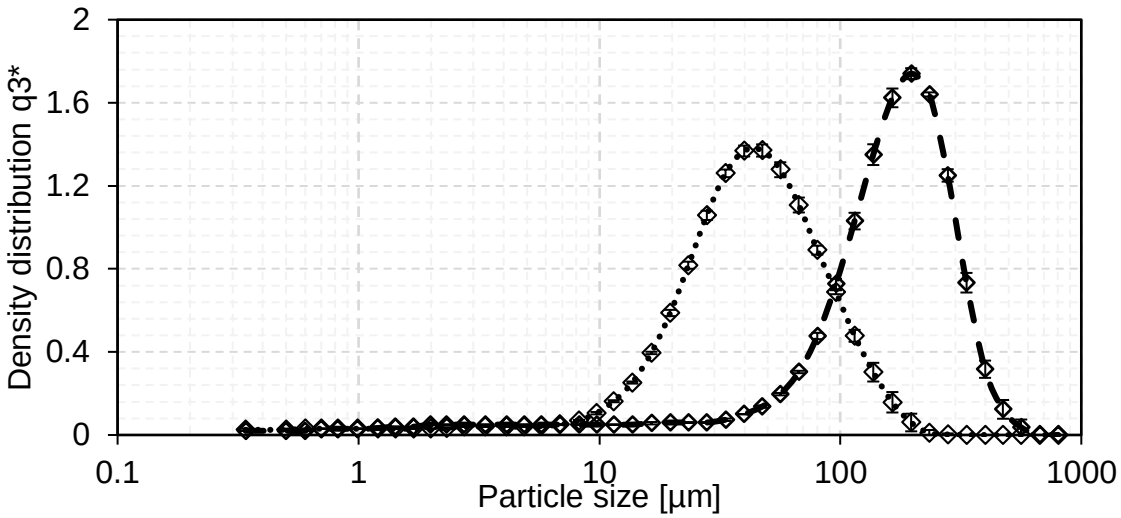

Figure 25. PSD of Ibuprofen 25 (dotted line) and DICAFOS A150 (dashed line). Estimated standard deviation based on three measurements.

The di-calcium phosphate particles are bigger by a magnitude of 3, and the morphology of single particles differs substantially. Figure 26 indicates that the ibuprofen particles have a rod-like shape while the DICAFOS ones look similar to agglomerated clumps. The scanning electron microscope (SEM) used was a Zeiss Ultra 55 (Carl Zeiss AG, Oberkochen, Germany), combined with an Everhart-Thornley detector, at an acceleration voltage of 5 keV. Sample preparation was

performed in an EM ACE 600 sputter coater (Leica Camera AG, Wetzlar, Germany), which covered the samples with 15 nm of gold and platinum (80 %-20 %) coating (see Kreimer et al.[25]).

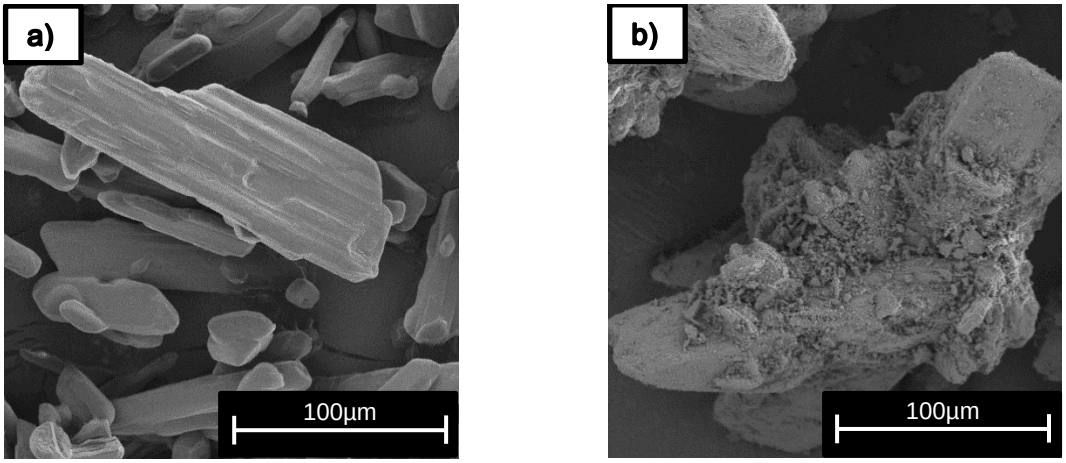

Figure 26. SEM-Pictures of a) Ibuprofen 25 and b) DICAFOS A150.

3.3.1.2 Basic Flow Properties

The flow properties were measured using an FT4 powder rheometer (Freeman Technology, Tewkesbury, United Kingdom). Several tests were used to characterize the flowability of the test substances[26]. The dry substances and the feed substances were analyzed with regard to their flowability, compressibility and shear stress. Additionally, the tapped density of the substances was measured as a dry material, with 10, 20 and 30 wt. % water content. The results shown below are based on triplicate measurements.

The basic flowability energy (BFE) was assessed by measuring the specific energy (SE), the stability index (SI) and the flow rate index (FRI) of the “stability and variable flow rate” program of the FT4 in a 50 mm vessel. A 90 ml sample of the powder preconditioned in the FT4 was tested seven times in a row, using conditioning before each test. During the test, a blade was moved counterclockwise in a downward motion at a tip speed of 100 mm/s to generate a compressing, high-stress flow pattern in the bed. The BFE is calculated according to equation (3.1) based on the effort required to move the blade through the entire sample. Subsequently, the blade was moved upward clockwise, in a gentle lifting and low stress inducing manner. The work from this cycle is related to the SE, as shown in equation (3.2). The SI was computed by dividing the necessary energy of the first test by the seventh test energy (BFE, equation (3.3)) to establish how much the behavior of the powder changed over time. Finally, four more cycles at various tip

speeds (i.e., 100, 70, 40 and 10 mm/s) were run to estimate how sensitive the powder is to the flow rate changes. The FRI was calculated according to equation (3.4).

$$BFE = E_7 \quad \textbf{(3.1)}$$

$$SE = \frac{(E_{6,up} + E_{7,up})/2}{m} \quad \textbf{(3.2)}$$

$$SI = \frac{E_7}{E_1} \quad \textbf{(3.3)}$$

$$FRI = \frac{E_{11}}{E_8} \quad \textbf{(3.4)}$$

The measured material properties are summarized in Table 11. With the increasing moisture levels, the energy required to make the materials flow increases, with the exception of ibuprofen mixed with 10 wt.% water, which interestingly has a higher flowability than the dry one. The SI indicates that for ibuprofen the flowability increases with the number of measurements, while for raw di-calcium phosphate it decreases and remains more or less the same for a 30 wt.% water mixture. The FRI indicates that all materials except for raw DICAFOS A150 are more or less unaffected by the flow rate changes. The SE is in relatively good accordance with the BFE. The more cohesive a powder is, the more energy is required to move it upward through the sample.

Table 11. Material flow properties of Ibuprofen 25 (raw, 10 and 30 wt.% water) and DICAFOS A150 (raw, 30 wt.% water) obtained via the “stability and variable flow rate” program of Freeman FT4.

Material [-]	BFE [mJ]	SI [-]	FRI [-]	SE [mJ/g]
Ibuprofen 25 raw	1176.13	0.70	0.97	10.29
Ibuprofen 25; 10 wt.% water	1020.53	0.91	1.06	10.35

Ibuprofen 25; 30 wt.% water	2096.31	0.93	0.94	11.57
DICAFOS A150 raw	891.61	1.19	2.29	9.21
DICAFOS A150 30 wt.% water	1973.27	1.01	1.04	12.55

In the compressibility test run, three conditioning cycles were performed to homogenize the powder bed before reducing the sample to 90 ml. Subsequently, a vented piston compressed the powder bed with an increasing pressure of up to 15 kPa. The compressibility was subsequently calculated according to equation (3.5). To compare the samples at various moisture levels, the compressibility without water was computed via equations (3.6) to (3.10). To that end, the volume was split into dry and wet volume and, since the liquid phase is incompressible, the compressibility was corrected by factor f.

$$C = \frac{V_{start,t} - V_{end,t}}{V_{start,t}} \tag{3.5}$$

$$C = \frac{(V_{start,p} + V_{start,l}) - (V_{end,p} + V_{end,l})}{(V_{start,p} + V_{start,l})} = \frac{V_{start,p} - V_{end,p}}{V_{start,p} + V_{start,l}} \tag{3.6}$$

$$\frac{V_{start,p} - V_{end,p}}{V_{start,p} + V_{start,l}} = \frac{V_{start,p} - V_{end,p}}{V_{start,p}} * \frac{1}{1 + \frac{V_{start,l}}{V_{start,p}}} = C^* * f \tag{3.7}$$

$$V_{start,l} = \frac{m_t * w_l}{\rho_l} \tag{3.8}$$

$$V_{start,p} = \frac{m_t * (1 - w_l)}{\rho_p} \tag{3.9}$$

$$f = \frac{1}{1 + \frac{V_{start,l}}{V_{start,p}}} = \frac{1}{1 + \frac{w_l * \rho_p}{(1 - w_l) * \rho_l}} \tag{3.10}$$

The moisture-corrected results are shown in Figure 27. While the very free-flowing raw DICAFOS A150 has the lowest compressibility of only up to 20 % for 15 kPa, the compressibility

and standard deviations grow significantly when 30 wt.% of the mixture is water, increasing the compressibility to 53 %. Ibuprofen behaves differently. Even the dry powder has a compressibility of around 30 %. Adding 10 wt. % of water decreases it by approximately 2 %. When increasing the amount of water in the mixture to 30 wt.%, the compressibility increases to around 39 %.

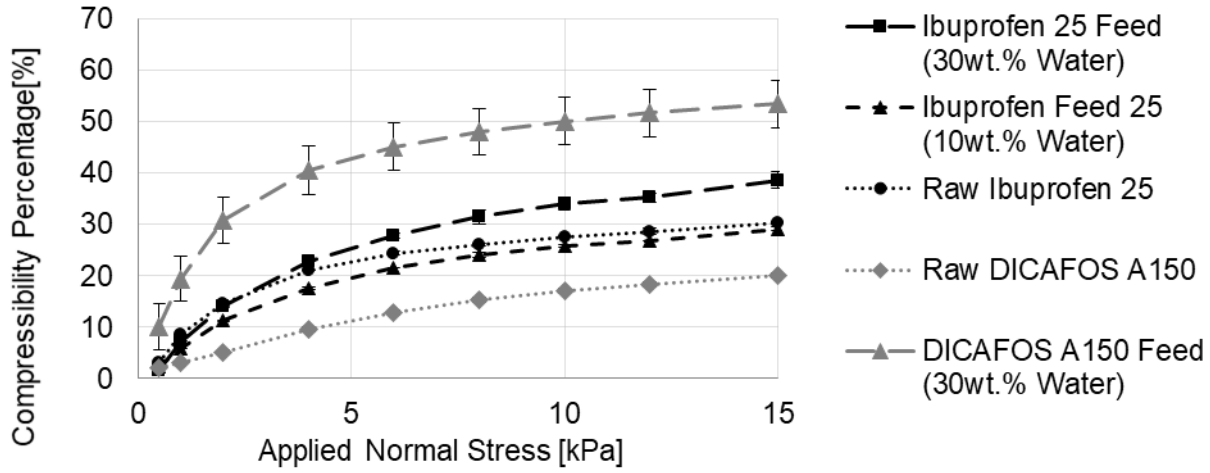

Figure 27. Compressibility of the raw materials and feed substances studied. Standard deviation is estimated via triplicate measurements.

For the shear cell test, the powder in the 90 ml 50 mm vessels was again conditioned and pre-sheared with a vented piston at 9 kPa. Afterwards, the shear head was mounted and the sample was pre-sheared at the same normal stress until it remained constant for 20 s. Afterwards the powder bed was put under lower normal stress (7, 6, 5, 4 and 3 kPa, respectively) and sheared again until a beginning failure (i.e., breakage) in the powder bed was detected. This pre-shearing and shearing method was used at each stress level. Next, the obtained values for each normal stress/shear stress pair were automatically evaluated to obtain the flow function, ffc, which is computed according to equation (3.11) by dividing the major principal stress by the unconfined yield strength. The higher the ffc value is, the more flowable the granular material is. The results for the material are shown in Table 12.

According to Schulze[27], all of the feed materials used are either very cohesive (ibuprofen with water) or cohesive (raw ibuprofen and di-calcium phosphate mixtures). Raw DICAFOS A150, however, had the best flowability according to this calculation. Another aspect is, that Ibuprofen with 10 wt. % moisture content contradicts the behavior measured in Table 11, as the flow function states a worse flowability than raw Ibuprofen.

$$ffc = \frac{\sigma_1}{\sigma_c} \quad \textbf{(3.11)}$$

Table 12. Major principal stress ($\boldsymbol{\sigma_c}$), unconfined yield strength ($\boldsymbol{\sigma_1}$) and flow function coefficient ($\boldsymbol{ffc}$) of Ibuprofen 25 (raw, 10 and 30 wt.% water) and DICAFOS A150 (raw and 30 wt% water) and classification according to Schulze[27].

Material [-]	σ_c **[kPa]**	σ_1 **[kPa]**	ffc **[-]**	**Classification**[27] **[-]**
Ibuprofen 25 raw	5.13	15.15	2.96	Cohesive
Ibuprofen 25; 10 wt.% water	9.18	13.51	1.48	Very cohesive
Ibuprofen 25; 30 wt.% water	8.07	15.32	1.89	Very cohesive
DICAFOS A150 raw	4.73	16.20	3.43	Cohesive
DICAFOS A150 30 wt.% water	8.02	16.95	2.12	Cohesive

To analyze the bulk and tapped densities, a Pharma-Test PT-TD200 (Pharma Test Apparatebau AG, Hainburg, Germany) was applied. The test cylinder was filled to 250 ml, noting the mass required. The volume after 500, 750 and 1250 strokes was measured three times for each material. The resulting densities and standard deviations are shown in Table 13.

As expected, the bulk and tapped densities increase with higher water content for ibuprofen, while the 20 and 30 wt. % samples of di-calcium phosphate show a different behavior. This was possibly due to encapsulated air bubbles at the higher moisture content of DICAFOS A150 that did not always escape during the tapping. These difficulties in measuring the feed material manually illustrate how challenging it is to continuously handle cohesive materials.

Table 13. Bulk and tapped densities of Ibuprofen 25 and DICAFOS A150 as raw materials and with 10, 20 and 30 wt. % of water added, with the respective standard deviations. Tapped density is given after 1250 strokes.

Material [-]	Moisture content [wt. %]	Bulk Density [g/cm³]	Standard Deviation [g/cm³]	Tapped Density [g/cm³]	Standard Deviation [g/cm³]
Ibuprofen 25	-	0.337	0.001	0.540	0.007
Ibuprofen 25	10	0.382	0.011	0.597	0.005
Ibuprofen 25	20	0.433	0.009	0.668	0.008
Ibuprofen 25	30	0.469	0.020	0.759	0.008
DICAFOS A150	-	0.719	0.004	0.904	0.003
DICAFOS A150	10	0.806	0.003	0.997	0.003
DICAFOS A150	20	0.618	0.009	0.927	0.01
DICAFOS A150	30	0.641	0.032	1.036	0.012

3.3.2 **Process Description and Experimental Procedure**

Two dryer systems were used in this work. The first one, a paddle dryer, was used to investigate the general flow behavior of the material in the dryer and the effect of the process on the particle size distribution. Based on these findings, the second dryer, a continuous vacuum dryer, was developed and tested. Both dryers and their respective experimental operation are described in this section.

3.3.2.1 Paddle Dryer

The preliminary test runs to classify the problems were carried out in a small-scale paddle dryer provided by Hosokawa Micron B.V. (Doetinchem, The Netherlands). The flow sheet of the system is shown in Figure 28.

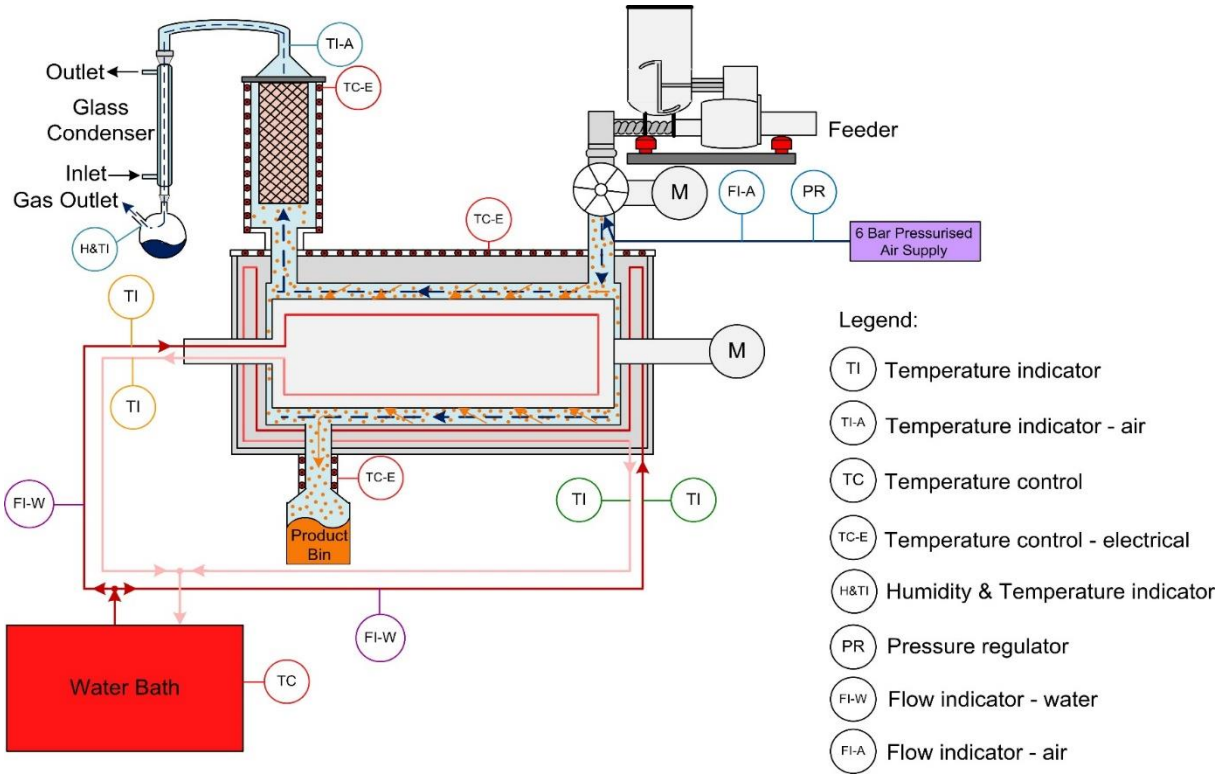

Figure 28. Flow sheet of the experimental setup with a small-scale paddle dryer.

Wet ibuprofen was introduced into the rotary valve at the inlet by a KT20 feeder (Coperion GmbH, Stuttgart, Germany). After the rotary valve, the powder fell into the drying chamber and was fluidized via various conveying mechanism towards the end of the dryer, where the dried material was discharged into a product bin. As a drying medium, pressurized air was used. The pressure was reduced and the air flow was regulated using a DK800 PV (Krohne, Duisburg, Germany). The air was inserted from below into the rotary valve chambers to force the material out. This way, the air flow was co-current with the material flow. The exhaust vapor and gas left the dryer via a filter at its end, on top of the product outlet. The water vapor was condensed in a water-cooled condenser, and the residual moisture and temperature of the air were measured at the condenser outlet using a Vaisala MI70 measurement indicator with an HMP75 probe (Vantaa, Finland) in order to calculate the mass and energy balances of the drying step. Additionally, the

temperature of the air right after the filter was measured with a type K thermocouple and logged via a PCE-T390 thermometer (Meschede, Germany). A Thermo Haake ® C10 heating bath was used to heat up and circulate the water to the housing and shaft of the dryer. The water temperature was measured at the inlet and outlet as close as possible to the dryer with thermocouples of type K connected to a testo 176-T4 logger (Lenzkirch, Germany). The complete experimental setup is shown in Figure 29.

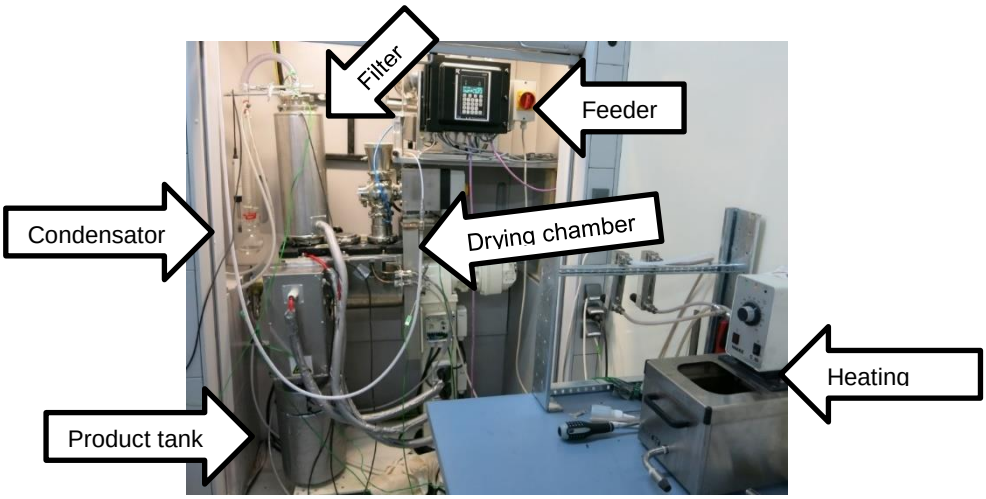

Figure 29. Experimental setup of the preliminary test runs in the paddle dryer.

3.3.2.2 Experimental Procedure

In each experiment with the paddle dryer, the water baths were set to the desired temperature and the air flow was turned on before starting the powder flow. The equipment was heated until the temperatures of the in- and outgoing water and the exiting air were constant. Subsequently, the rotor and rotary valve were started and the gravimetric feeder was turned on at the relevant mass flow. During the experiment, the system was stopped and opened at least once every hour to weigh the product bin and condensate mass for the holdup calculation (see calculations 2.12 to 2.14 below). After the experiment, the dryer was stopped and opened and the interior was photographed before the equipment was cleaned. The calculation of hold-up within the system was based on the mass of dried powder moving in and out. This method proved to be advantageous, since the moisture contributions did not have to be considered, making it easier to compare experiments with different materials and moisture levels. Based on that, the cumulative sum of the difference between the dry material entering and leaving the system is computed (equation (2.12)). The evaporated water is then computed by calculating the difference between the in- and outgoing water, as shown in equation (2.13). The weight percentage of water in the

powder is computed via equation (2.14). The dry mass (m_dry) of samples in the paddle dryer is obtained by drying the respective samples for at least 24 h at 60 °C and 200 mbar in a vacuum drying chamber.

$$Hold-up_{dry} = \sum_{i=1}^{N}((\dot{m}_{wet,in,i} * (1 - w_{feed}) - \dot{m}_{dried,out,i} * (1 - w_{product})) \quad \textbf{(3.12)}$$

$$\dot{m}_{evap} = \dot{m}_{wet,in} * w_{feed} - \dot{m}_{dried,out} * w_{product} \quad \textbf{(3.13)}$$

$$w = \frac{m_{wet} - m_{dry}}{m_{wet}} \quad \textbf{(3.14)}$$

All experiments in this paddle dryer were performed using ibuprofen with various moisture levels. The improvement measures are described in each section.

3.3.2.3 Continuous Vacuum Dryer

With the optimization possibilities determined based on the paddle drying system's analysis, a new prototype was designed and constructed (Figure 30 and Figure 31). The wet powder is fed into the system via a KT20 feeder (Coperion GmbH, Stuttgart, Germany). The interlocking screw design (described in Section 3.1 below) moves the powder through the inlet rotary valve (Section 3.3) and the dryer, groove by groove. Subsequently, it is discarded through an interlocking outlet rotary valve (Section 3.4). The powder is collected either in a bucket on a scale (ML 4001, Mettler Toledo GmbH, Vienna, Austria) or is moved over the conveyor belt prior to the scale to evaluate product's morphology, mass flow stability and/or residence time distribution inside the dryer when using the colored material. To preheat the process air, a Julabo F25 (Julabo GmbH, Seelbach, Germany) heating circulator has been installed, with water as a heating medium. The air passes through the liquid in a copper coil and is heated up before entering the drying chamber. The air temperature and the ambient temperature are recorded during the final process via a 4-channel temperature logger T176-T4 (Testo GmbH, Vienna, Austria) and measured using thermocouples of type K. Next, the air is passed in the counter-current direction over the powder that is dried and is released through the filter. Pressure sensors before and after the filter are implemented to evaluate the pressure drop over the filter and to detect blockage of the filter. In subsequent experiments, the temperature and relative humidity of outgoing gas were measured using a Vaisala HMT337 Humicap (Vaisala, Vantaa, Finland). The system has two

separate heating circuits: one for the filter and one for the shaft and housing of the dryer. The heating baths used for these circuits are Julabo HL-4 (Julabo GmbH, Seelbach, Germany) heating circulators, filled with tap water.

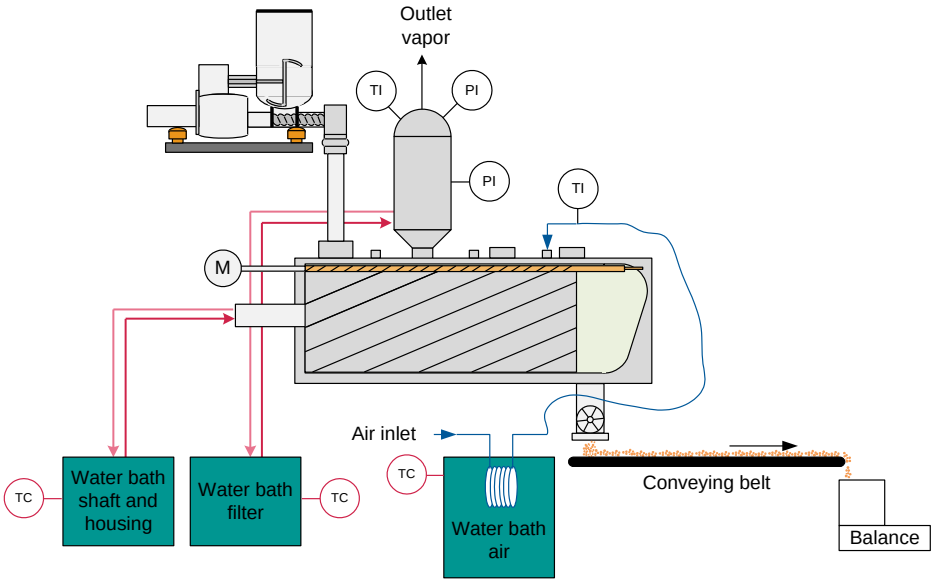

Figure 30. Flow sheet of the final setup of the new contact-convective dryer.

3.3.2.4 Experimental Procedure

At the beginning of each experiment, data logging began. To that end, a LabView routine was created. It integrated the process data of the feeder and dryer (via OPC servers and of the scale via an RS232 serial connection), recording and visualizing the values every second. Before introducing the material into the dryer, the heating baths were heated to the desired temperature and the air flow was turned on. The equipment was heated until constant temperatures of the in- and outgoing water and of the exiting air were achieved (i.e., temperature increase below 0.1 °C in 5 minutes). To guide the process air through the filter and avoid its loss through small gaps at the in- and outlets, a suction unit was installed after the filter, ensuring that a small amount of air is sucked into the system. This was tested by simultaneously sealing the in- and outlets with rubber gloves and checking if they deflated. Next, the rotor with the inlet and the outlet were started and the gravimetric feeder was turned on. Finally, we waited until the process reached a steady state, i.e., when the outgoing mass flow of powder matched the ingoing mass flow ±5 % on a dry basis for at least 10 minutes. Due to the data logging, it was not necessary to stop the equipment, and only samples for the residual moisture measurement (at least 3 per hour) and the particle size distribution (at least 3 per process) were collected. The moisture measurements were made at-

line with a moisture analyzer HC103 (Mettler Toledo GmbH, Vienna, Austria) set to a heating temperature of 60 °C with the stopping criteria of the mass change being less than 1 mg per 90 s. After the experiment, pictures of all parts were taken before the cleaning procedure was started. The hold-up calculation of these test runs was based on the dry mass of powder according to equation (2.12). This approach allowed a better comparison between the various moisture levels and materials, since it does not depend on the residual moisture of the respective product. For assessing the effect of changing flowabilities on the process and the conveying mechanism, di-calcium phosphate was used as test substance.

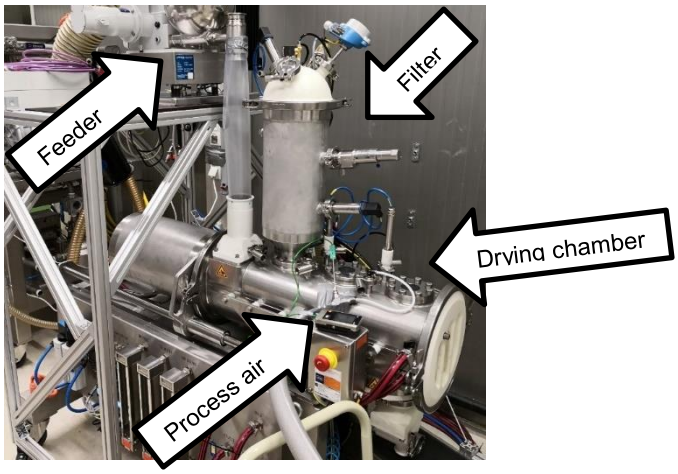

Figure 31. Final experimental setup of the new contact-convective dryer prototype.

3.4 Development of the Dryer

3.4.1 Dryer Conveying Mechanism and Screening Test Runs

In order to move the material through the dryer in an effective and gentle manner, several paddle configurations (Figure 32) were tested. Both the geometry and the orientation of the inserts were altered numerous times to determine a suitable process behavior in terms of accumulation within the system, residence time distribution (RTD), tendency towards agglomeration and attrition (by evaluating the PSD) and drying efficacy.

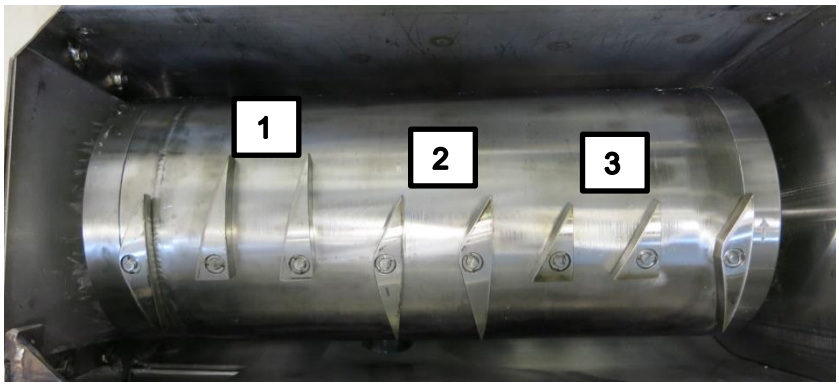

Figure 32. Shaft of the dryer with the paddles that were tested. The picture was taken from above, with the dryer lid open. The types were: (1) single-peaked with a long triangular shape; (2) double-peaked with a long and a short side; and (3) single-peaked with a short triangular shape.

These investigations demonstrated that 180° 2-rows of paddle arrangements failed to yield a desired outcome, and the flow through the dryer was very poor. The behavior was improved by changing the setup to a 3-row setup with a 120° offset. In these test runs, the double-peaked paddles (1) were applied. Information for the performed test runs with the 3-row arrangement is provided in Table 14. The conveying principle was tested with three rows pointing from the inlet to the outlet in the forward direction (3F). At first, the configuration was tested without air holes. Since this resulted in blockage and unreproducible test runs, we attempted to improve the powder flow by drilling holes into the top cover below the filter to achieve a gentler air flow over the powder. To assess their effectiveness, the old material with a residual moisture of around 7 wt. % was used at different mass flows and shaft speeds. Subsequently, the configuration was tested at different shaft speeds and air flows (120 rpm and 3.7 Nm^3/h and 60 rpm and 1.8 Nm^3/h) to determine the effect on the process performance. To establish the influence of various material properties, refeeding test runs were executed, starting with an initial moisture of approximately 30 wt. %, where the product was collected and re-fed twice under standard operating conditions (60 rpm

shaft speed, 55°C water temperature, 3.7 Nm³/h air flow). Afterwards, the paddle configuration was changed, with one row pointing to the inlet in order to increase the residence time and improve the drying performance. The air flow was reduced as a countermeasure since in the previous test runs the material was undesirably transported to the filter. To compensate for this, the temperature was elevated. Since this test run was unsatisfactory, the holes were replaced by a large hole to give the material more space to fall down into the process chamber. This configuration was tested twice at 65 and 75 °C water temperature to establish the influence of the temperature on the drying performance. Since the large air hole resulted in an even worse process performance, it was eliminated. This setting was tested at the even higher water temperature of 85 °C. After the first test run, the second one was performed with the paddle arrangement all forward (3F) again. The typical results of these test runs are shown in Figure 33b. The inlet and outlet zones had a lot of accumulated material, while a relatively small amount of the material was conveyed through the middle section of the dryer. Since this behavior leads to an uncontrollable residence time, a large hold-up and an unstable product flow, other mechanisms for moving the powder had to be identified.

Table 14. Test run configurations for the 3 row, 120° test runs with the double-peaked paddles.

Setup [-]	**Moisture content [wt. %]**	**Mass flow [kg/h]**	**Shaft speed [rpm]**	**Water temperature [°C]**	**Air flow [Nm³/h]**
3F, no air holes	8.8	2.5	60	60	3.7
3F, no air holes	16.0	2.5	60	60	3.7
3F, no air holes	8.4	2.5	60	60	3.7
3F, no air holes	22.9	2.5	60	60	3.7
3F, small air holes	7.06	1.25	60	55	3.7
3F, small air holes	7.73	2.5	120	55	3.7
3F, small air holes	9.38	1.25	120	55	3.7

3F, small air holes	9.49	1.25	60	55	1.8
3F, small air holes	29.67	1.25	60	55	3.7
3F, small air holes	19.32	1.25	60	55	3.7
3F, small air holes	10.16	1.19	60	55	3.7
2F+1B, small air holes	8.86	1.25	60	65	1.8
2F+1B, air hole open	9.46	1.25	60	65	3.7
2F+1B, air hole open	10	1.25	60	75	3.7
2F+1B, air hole closed	9.8	1.25	60	85	3.7
3F, air hole closed	9.82	1.25	60	85	3.7

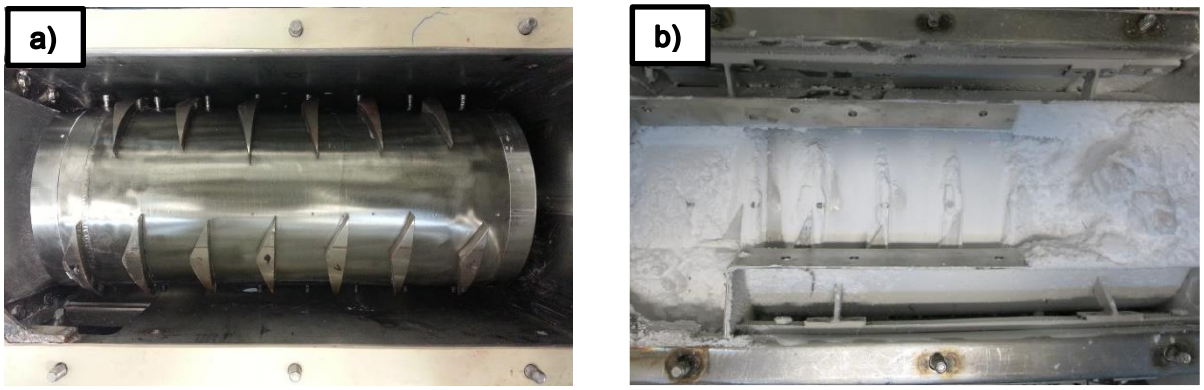

Figure 33. Ibuprofen accumulations (a) before and (b) after a test run with three rows of double-peaked paddles, all pointing in the forward direction, glued to the shaft in three spiral rows with an offset of 120°, half-shells still mounted. The pictures were taken from above, with the dryer lid open.

To eliminate the stagnating areas, a screw was inserted on top of the shaft in order to avoid the accumulation in the beginning and at the end of the dryer (Figure 34). The top part of the dryer was not completely filled up anymore, and the powder was conveyed more smoothly along the dryer, enabling a more stable process.

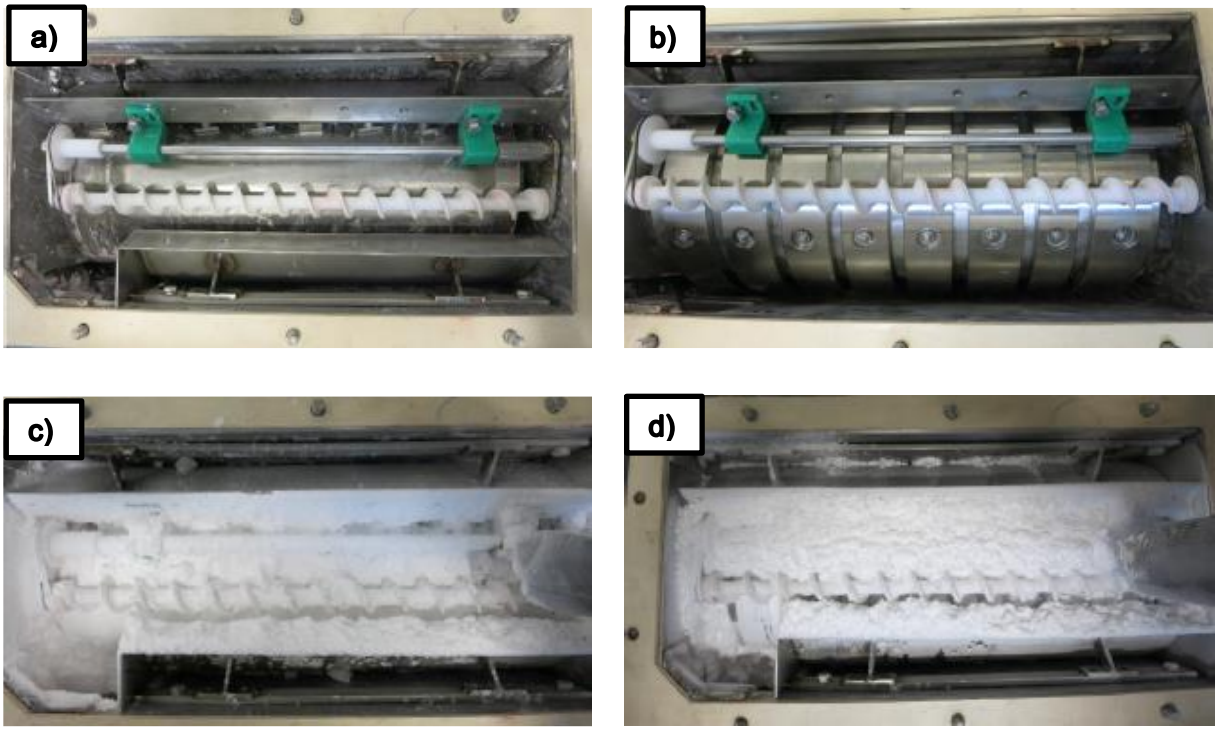

Figure 34. The two screw configurations tested in the paddle dryer and their respective outcomes. In a) and c) the screw with a paddle arrangement was installed and in b) and d) half shells were mounted to the shaft to reduce the available dryer volume. The pictures were taken from above, with the dryer lid open.

Based on these findings, a completely new conveying mechanism was developed (Figure 35). Conveying was achieved via an interlocking screw design, with a 3D-printed small screw driving the larger rotor. The material is now gently forced from one groove to the next, enabling a steady flow of powder towards the end of the dryer, without excessive compaction or friction, which prevents agglomeration or attrition.

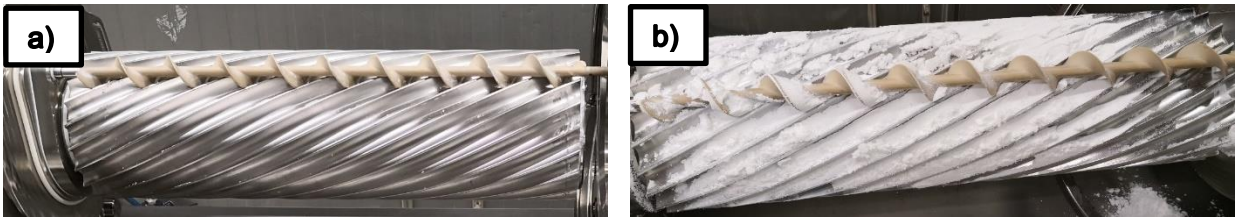

Figure 35. A conveying mechanism of the new prototype. In a) the clean system and b) the system previously tested using di-calcium phosphate. This new conveying mechanism was implemented in the continuous vacuum dryer since a complete redesign of the dryer was necessary. The pictures were taken from the side, with the rotor pulled out.

3.4.2 **Dead-Zone Reduction and Process Gas Optimization**

During the first test runs ibuprofen was accumulating all around the drying chamber, possibly due to the high speed of the rotor resulting in high compaction, tribocharging and dusting. To reduce the volume in which the material could accumulate, metal plates were mounted above the rotor to keep the material down (Figure 36a). Despite these efforts, the material was found all over the free space above. Typical accumulations after the process are shown in Figure 36b. The inlet zone was not covered by a metal plate since this would result in blockage. The dryer was not filled up with the material in the test runs.

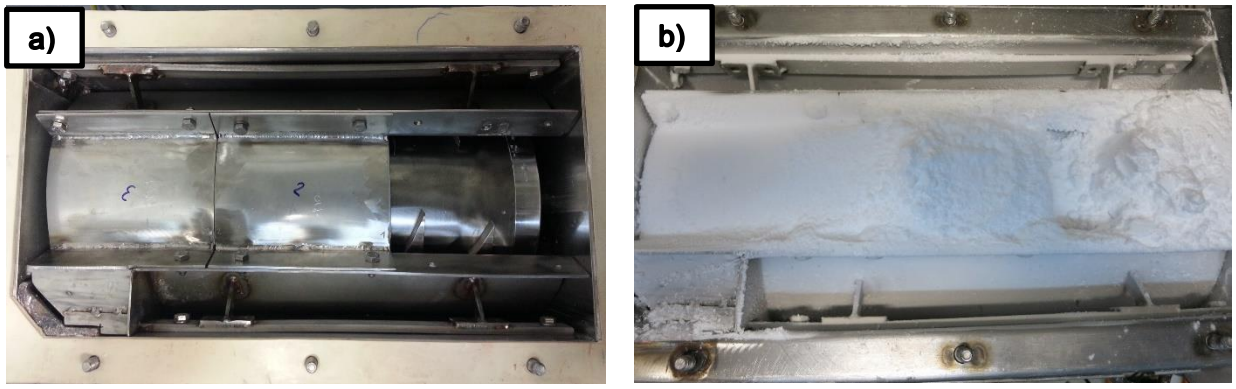

Figure 36. (a) dead zone reduction configuration without the air holes and (b) respective accumulations after the process. The pictures were taken from above, with the dryer lid open.

To improve this situation, air-holes were drilled beneath the filter and the top area was additionally blocked with foam rubber since the material was probably driven up by the process air moving towards the filter. The configuration is shown in Figure 37a). Figure 37b) indicates that the ibuprofen strands pressed through the holes would eventually fill up the filter above. Therefore, we investigated if enlarging the hole would improve the flowability in the process chamber by enabling the air flow that would break up the solid bridges.

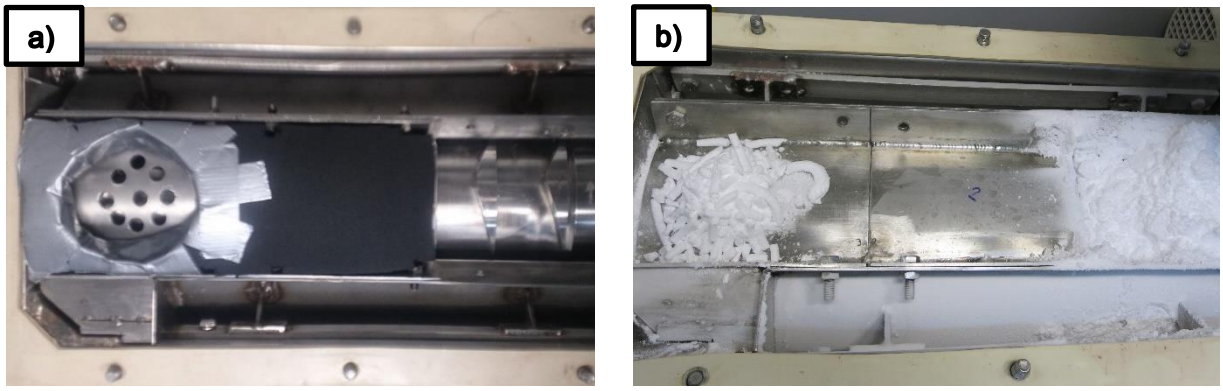

Figure 37. Dead zone reduction configuration with air holes (a) before and (b) after the drying process, without the foam rubber. The pictures were taken from above, with the dryer lid open.

The configuration and outcome for the larger air hole are depicted in Figure 38a-c. An increase in the free surface did not improve the process at all and rather led to blockage before the filter, since material was pressed up against instead of into the product container.

Figure 38. Dead zone reduction configuration with one large air hole (a) before and (b) after the drying process. (c) blocked filter on top of the opening visible in (b). The pictures were taken with the dryer lid closed, at the filter opening from (a, b) above and (c) from below of the filter.

Since no suitable configuration was found to reduce the dead zones and guide the airflow in a gentle way without conveying the powder, several adjustments were made to the design of the new prototype. The powder transport from groove to groove was moved towards the side rather than the top to avoid accumulations. In addition, a large area for the air to bypass the powder was created, with tight contours of less than 2 mm on the sides and bottom of the rotor. The top part of the new housing did not follow the contour of the rotor in order to make enough space for the conveying screw and the bypassing air. The final design of the drying prototype is shown in Figure 39a-b. In the cases of both free-flowing (a) and cohesive (b) feed materials no accumulation on top of the dryer or in front of the filter occurred. In the case of relatively free-flowing, dry di-

calcium phosphate (Figure 39a), only the bottom of the process chamber was covered with the material, while the cohesive, wet material in Figure 39b accumulated at the sides. Optimization of the void zone at the outlet of the new prototype is discussed in Section 3.4.

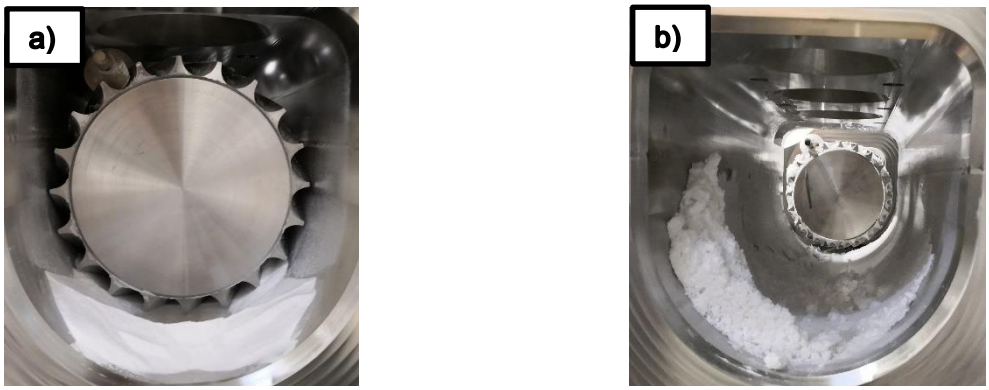

Figure 39. The final design of the dryer (front view). a) processing dry di-calcium phosphate (rotor inside process chamber). b) processing di-calcium phosphate with 30 wt. % water (rotor pulled out of process chamber). The pictures were taken from the end of the dryer into the process chamber, with the dryer lid open.

Initially, the process air was introduced unheated in the co-current mode and exited the dryer through a filter above the outlet. To enhance the drying capacity of the process air, the preheating system was installed. To achieve the highest possible drying rate the filter position and the air flow were changed to counter the current mode.

3.4.3 **Inlet Optimization**

Since feeding the ibuprofen into the system proved to be very complicated, efforts were made to improve the inlet zone. The problems and adaptions are depicted in Figure 40a-d. In Figure 40a, the inlet zone after the rotary valve is shown. On the left side, to force the material out, the air is blown upwards towards the rotary valve. In addition, air channeling through the powder into the dryer occurred, and there was a lot of stagnant material on the sides of the connecting pipe. In Figure 40b, the material that accumulated inside the rotary valve is depicted, which remains inside despite the air blowing upward in the direction of the valve. To further improve the material transport, a Teflon foil was placed on the metal surface to reduce the surface adhesion (Figure 40c). The result of this configuration is depicted in Figure 40d. Even though the accumulation is significantly reduced, the air removes the material in places where it is directly inserted, resulting in a high hold-up in the rotary valve. Placing Teflon foil underneath the rotary

valve did not have much impact on the accumulations inside the connection piece. Based on these findings, it was concluded that a gentle, mechanically forced flow inside the dryer was the optimal strategy for introducing cohesive materials into the system.

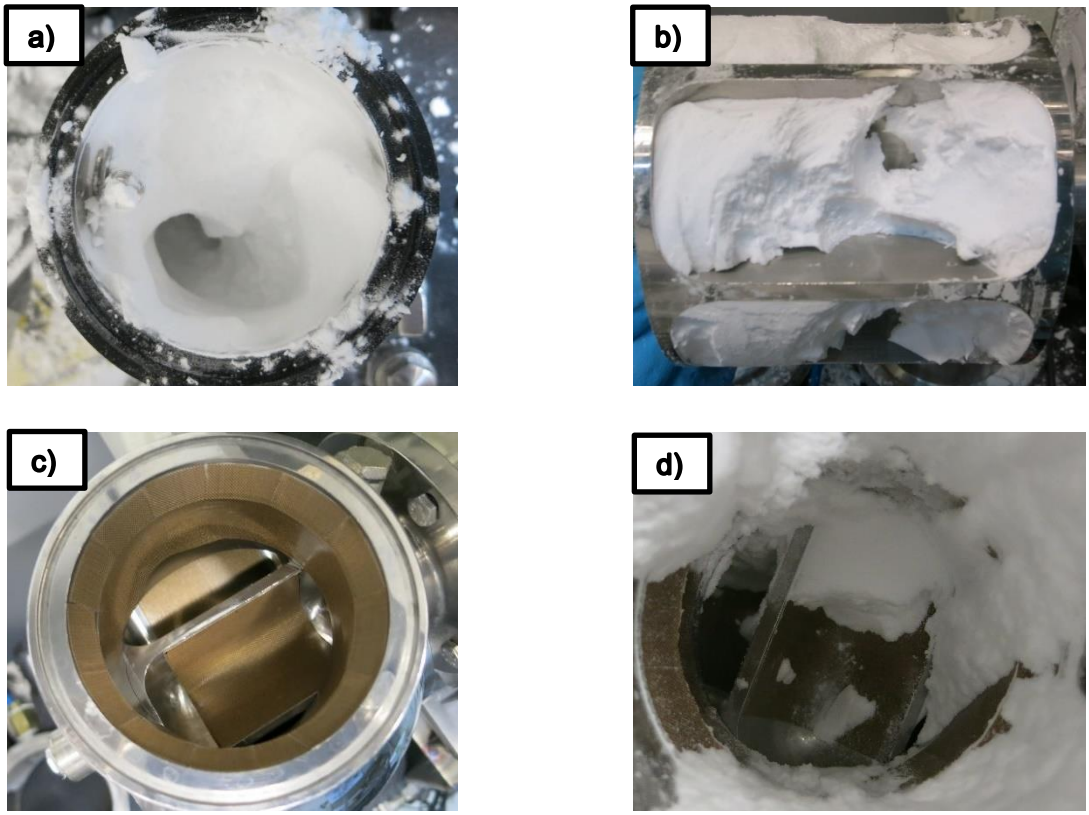

Figure 40. Inlet zone of the paddle dryer: a) inlet of the process air at the left side and the resulting channeling; b) accumulations after the process with no surface treatment; c) the configuration with the Teflon tape; and d) the accumulation with the Teflon tape after the process (view from above). The pictures were taken (a) below the rotary valve to the dryer inlet zone; (b) from the side into the dismounted rotor of the rotary valve; and (c, d) from the top into the mounted rotary valve.

A new rotary valve was developed (Figure 41) based on the conveying mechanism described in Section 3.1. The powder is now introduced from the top into the grooves and then conveyed into the dryer via the rotation of the interlocking parts. The small intermeshing driving screw specified in Section 3.1 is driving the rotor of the valve, removing the material from the pockets of the rotor. This way, hold-up and accumulation are minimized and a stable mass-flow is achieved.

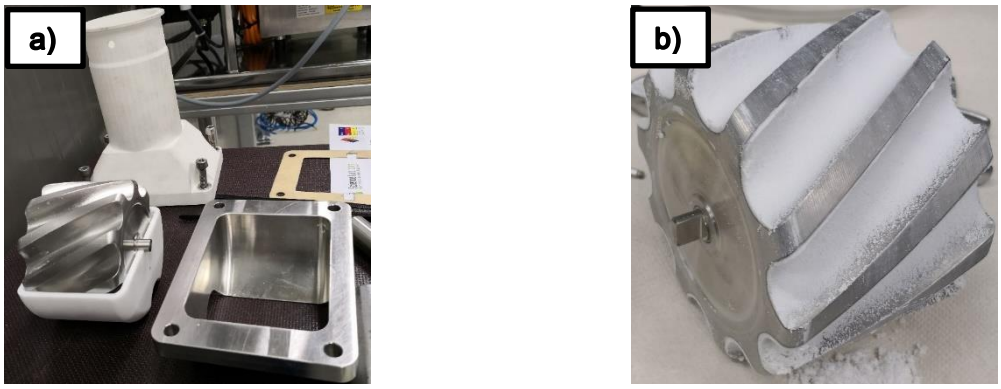

Figure 41. (a) Parts of the rotary valve of the new dryer prototype and (b) hold-up in the rotary valve after a test run.

3.4.4 **Outlet Optimization**

As mentioned in Section 3.1, accumulations before the outlet of the paddle dryer had a negative impact on the hold-up and process stability during the test runs. Therefore, when designing the new continuous vacuum dryer, the ejection hole was placed centrally below the rotor to ensure a better material flow out of the dryer. For initial testing of the equipment, the space behind the rotor was left void and the closing lid had no additional inserts mounted on it (Figure 42a1). This configuration resulted in a lot of material conveyed past the ejection pipe, as shown in Figure 42a2. To address this issue, a PTFE-plate was attached to the closing lid, reaching towards the product hole diagonally so that the material would be able to roll back (Figure 42b1). The outcome was better than before, but not completely satisfactory (Figure 42b2). As such, a new, more complex design was created. A PTFE-plate was formed to a half-chute, and silicon stripes were attached to the sides to connect them smoothly to the surrounding metal walls (Figure 42c1). This resulted in the least accumulations (Figure 42c2) and was used in the final design.

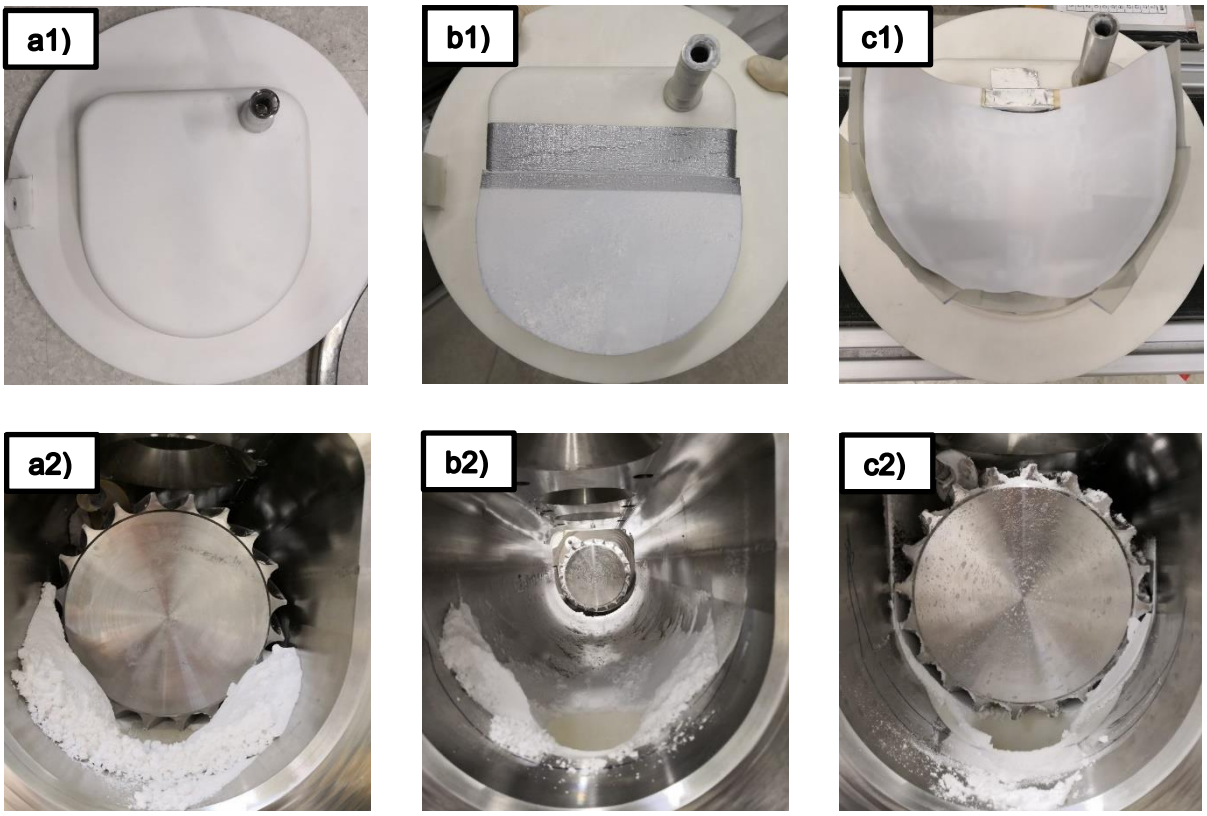

Figure 42. Outlet configurations tested (a1, b1, and c1) and their respective outcomes (a2, b2 and c2).

An outlet rotary valve had to be developed in order to seal the process chamber from the surroundings. Based on the previous findings for the inlet rotary valve (Section 3.4), a design was chosen using the same principle of interlocking rotating parts, with a screw scraping the powder out of the grooves of the metal rotor. The valve and its parts are shown in Figure 43a-d.

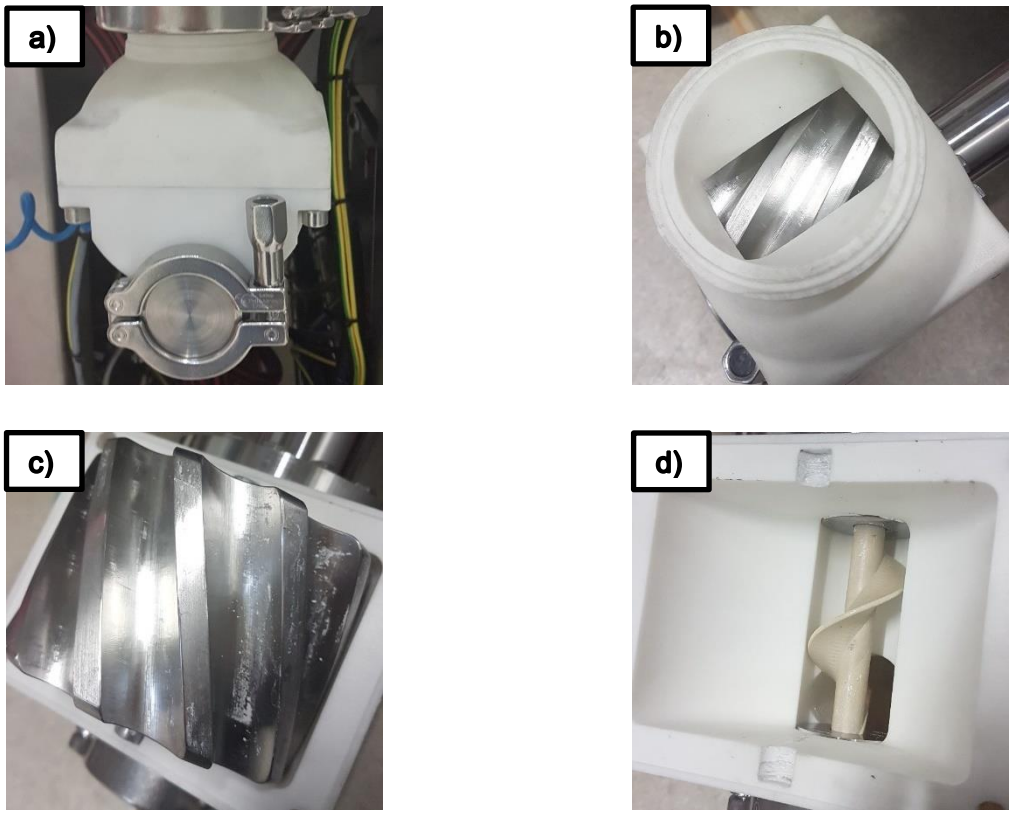

Figure 43. Outlet rotary valve mounted (a), disconnected from the dryer (b), without top part (c) and without metal rotor (d).

3.4.5 **Final Design and Initial Testing**

Figure 44 (the CAD-model of the dryer) shows a complete overview of the system. The rotor and the small conveying screw are depicted out of the housing for presentation purposes.

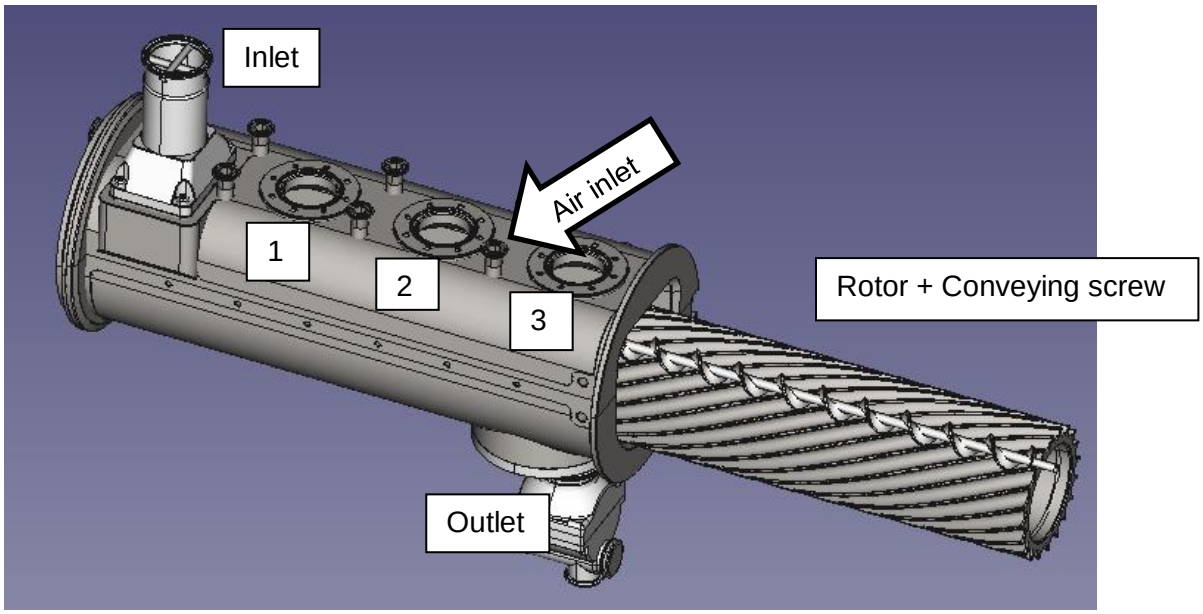

Figure 44. CAD-Model of the dryer, with the rotor pulled out. No filter or sensors are shown. The possible filter positions are 1, 2 and 3. The air inlet is between positions 2 and 3.

The initial test runs are summarized in Table 15. All test runs were performed with a mass flow of 2 kg/h on a dry basis and with an initial moisture of about 30 wt. %. The first test run was performed using di-calcium phosphate since it changes its flowability depending on the moisture content. The temperature in this test run was 85 °C, the rotational speed was 2 rpm and the air flow was 3.6 Nm^3/h, i.e., approximately the same as in the majority of paddle dryer test runs. In this test run no outlet insert was used. After it, the material was changed to ibuprofen. The temperature was decreased to 60 °C due to ibuprofen's low melting point and the air flow was increased to 4.8 Nm^3/h to improve the drying performance. Next, a diagonal Teflon plate was installed (Figure 42b1) and, to evaluate its influence on the drying process, the rotational speed was reduced to 50%. Finally, the half-chute was mounted (Figure 42c1), the air flow was changed to counter-current and the temperature was raised to 70 °C.

Table 15. Tested dryer configurations for the new dryer prototype. Air inlet and filter positions are shown in Figure 44. Outlet configurations are depicted in Figure 42.

Material [-]	**Air inlet + Filter position** [-]	**Outlet Configuration** [-]	$\dot{m}_{dry,in}$ [kg/h]	$w_{H2O,feed}$ [wt.%]	**Water bath temperature** [°C]	**Air flow** [Nm³/h]	**Rotational speed** [rpm]
Di-calcium phosphate	1 -3	a	2	29.9	85	3.6	2
Ibuprofen	1 - 3	a	2	29.7	60	4.8	2
Ibuprofen	1 - 3	b	2	29.8	60	4.8	1
Ibuprofen	3 - 1	c	2	33.6	70	4.8	1

3.5 Results and Discussion

The results for the paddle dryer (Section 4.1) and the outcome of the initial test runs for the new dryer (Section 4.2) are presented below. The relevant findings are discussed, and the drying efficacy is evaluated.

3.5.1 Paddle Dryer

Figure 46 shows the results of the test run with the best paddle configuration for the paddle dryer: 18 double-peaked paddles glued in 3 rows with 120° offset. To prolong the residence time in the dryer, one of these rows was installed in the backward direction. Additionally, two rectangular paddles were positioned in each row to facilitate the material ejection. The air-hole above the outlet was open in this test run and, to reduce the hold-up within the system, plates covered with a Teflon foil were inserted in front of and behind the rotor. This configuration is illustrated in Figure 45.

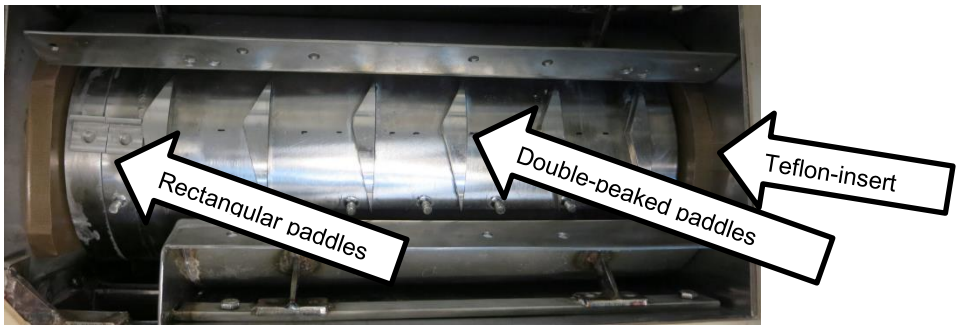

Figure 45. Paddle dryer configuration in the test run with the best process performance.

For this test run, a mass flow of 1.25 kg/h of wet material (a residual moisture of 9.5 wt. %) was used, resulting in approximately 1.13 kg/h of dry material. The process airflow was set to 3.7 Nm^3/h. The temperature in the water bath that heated the housing, and the shaft was set to 55 °C. The top lid (55 °C), the filter and the outlet (40 °C each) were heated electronically. The shaft speed of the rotor was 60 rpm. Figure 46 depicts problems with the paddle dryer encountered when drying cohesive materials. While the ingoing mass-flow was rather constant, small fluctuations occurred due to bridging inside the feeder. The product mass flow was very unstable. Moreover, it took 180 minutes to achieve a steady state. The beginning of the steady state was assumed to take place when the mass flow started fluctuating around the mean value. However, since at no point the outgoing mass flow equaled the feed mass flow, the holdup increased to 1.56 kg based on dry ibuprofen with a rate of up to 200 g/h. In addition, the product mass flow had significant fluctuations between 0.8 to 1.2 kg/h on a dry basis, which were caused by the aperiodic breaking-off of the material accumulations and the subsequent build-up of new accumulations.

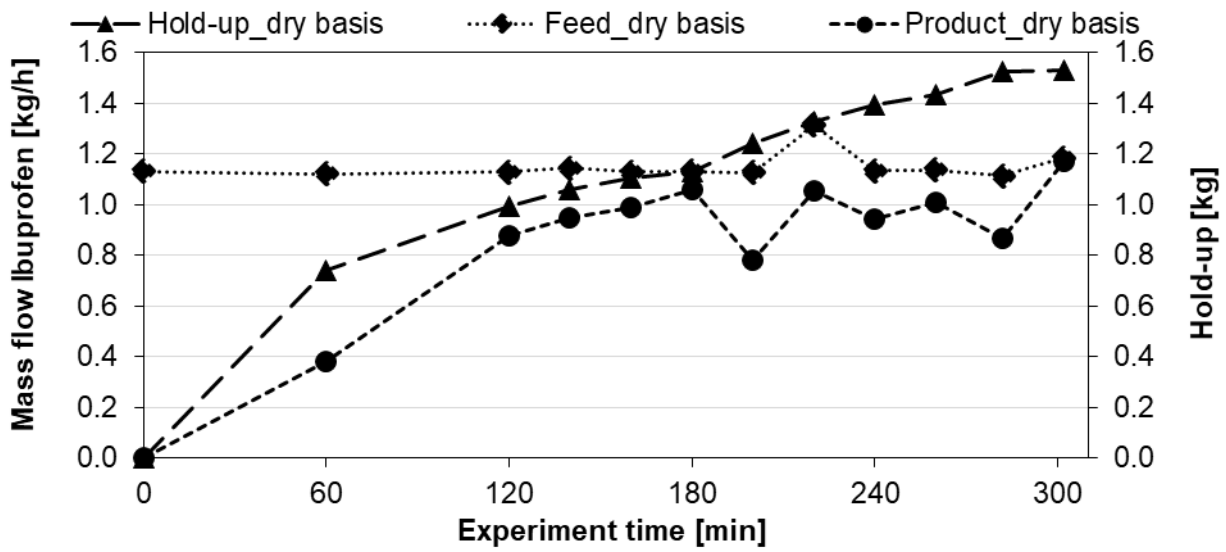

Figure 46. Hold-up data with the feed and product mass flows in the paddle dryer. Data from test run 13.

On the positive side, the obtained product was very dry (Figure 47). The measurements started after 2 hours, when a stable product mass flow was achieved. For the measurements after the defined steady state, all moisture levels were below 0.5 wt. % water. In this configuration, the calculated mass of evaporated water equals 112.6 g/h.

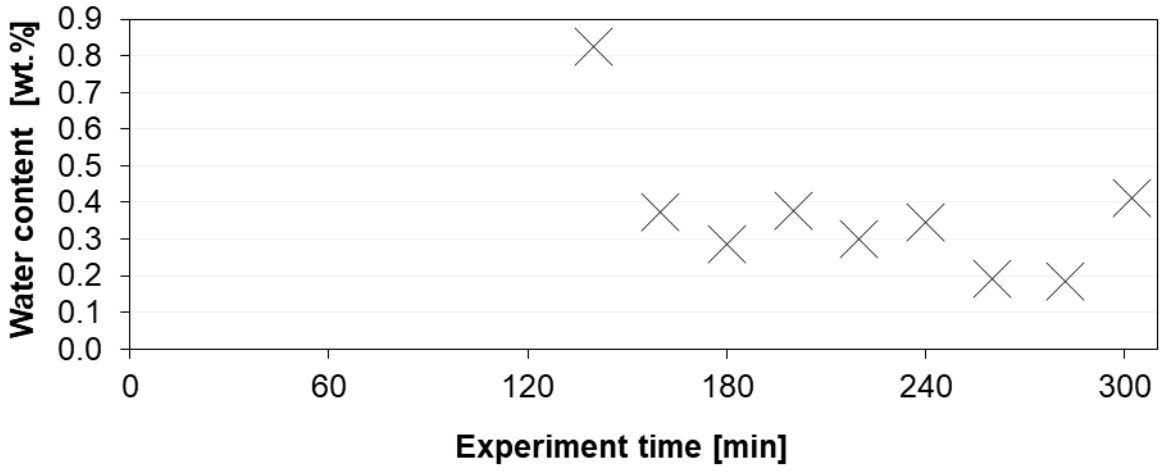

Figure 47. Measured residual moistures of the best paddle dryer configuration.

Previous measurements for all types of paddles suggested that the paddle configurations do not alter the PSD of ibuprofen. Figure 48 shows the results of PSD measurements with a similar paddle configuration (double peak paddles in 3 rows at 120° offset, all in the forward configuration)

and comparable moisture levels. Clearly, the results for all samples are alike, indicating that neither fines nor agglomerates were produced during processing.

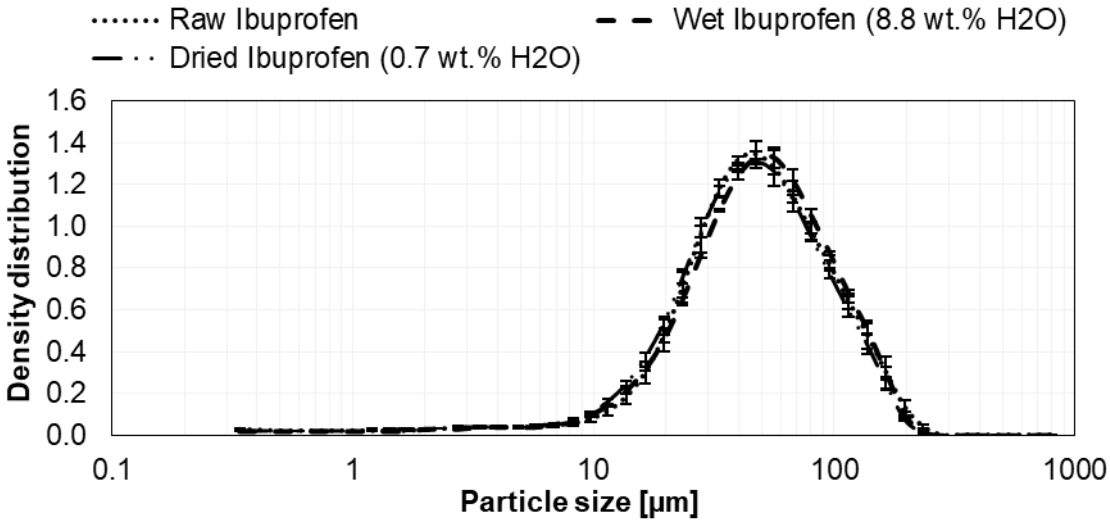

Figure 48. PSD of raw, wet and dried ibuprofen measured using the HELOS KR/CUVETTE system. The results are from the first test run with the 3-row 120° double-peak paddle.

A summary of all results for the 3-row paddle configuration is provided in Table 16, which shows that the reproducibility of the test runs is not achieved, and complete blockage of the system occurs frequently. After optimizing the inlet and the outlet, this behavior improved. However, the generated amount of hold-up was still very high and the mass flow of dried product was very unstable. Additionally, in none of the test runs a steady state was obtained since the hold-up still increased at the end of each one of them.

Table 16. Test run configurations for 3 row, 120° paddle test runs. *Test run stopped since the out- or inlet was completely blocked.

Test run [-]	Setup [-]	Moisture content [wt. %]	Mass flow wet [kg/h]	Shaft speed [rpm]	Water temperature [°C]	Air flow [Nm³/h]	Residual moisture [wt. %]	Mass flow dried [kg/h]	Hold-up [kg]	Evaporated water [g/h]
1	*3F, no air holes	8.8	2.5	60	60	3.7	0.7	-	1.86	-
2	3F, no air holes	16.0	2.5	60	60	3.7	9.6	2.23	1.09	185.9
3	*3F, no air holes	8.4	2.5	60	60	3.7	3.0	-	1.21	-
4	3F, no air holes	22.9	2.5	60	60	3.7	16.7	2.27	1.00	193.41
5	3F, small air holes	7.06	1.25	60	55	3.7	1.25	1.11	1.54	74.4
6	*3F, small air holes	7.73	2.5	120	55	3.7	3.7	-	3.59	-
7	*3F, small air holes	9.38	1.25	120	55	3.7	0.33	-	3.14	-
8	3F, small air holes	9.49	1.25	60	55	1.8	2.79	1.13	1.48	87.1
9	3F, small air holes	29.67	1.25	60	55	3.7	19.32	1.03	0.96	171.9
10	3F, small air holes	19.32	1.25	60	55	3.7	10.16	0.96	1.39	144.0
11	3F, small air holes	10.16	1.25	60	55	3.7	2.10	0.95	1.52	107.1

12	2F+1B, small air holes	8.86	1.25	60	65	1.8	3.74	1.10	1.49	69.6
13	2F+1B, air hole open	9.46	1.25	60	65	3.7	0.36	0.88	1.56	115.1
14	2F+1B, air hole open	10	1.25	60	75	3.7	0.28	0.58	3.76	123.4
15	2F+1B, air hole closed	9.8	1.25	60	85	3.7	0.47	0.85	2.06	118.5
16	3F, air hole closed	9.82	1.25	60	85	3.7	0.52	1.05	1.93	117.3

Based on these results, the focus shifted towards reducing the hold-up and its stabilization in order to obtain reproducible residence time distributions. The configurations depicted in Figure 34 provided the hold-up results shown in Figure 49. In these two test runs dry ibuprofen was fed at 5 kg/h to evaluate if the process stability significantly improved compared to the previously tested paddle configurations. The high feed rate was chosen to decrease the process time. The hold-up with the half rings is lower by approximately 500 g. The hold-up plateau is reached already after 25 minutes, while the screw and paddle configuration required 45 minutes. Despite being relatively low in the half-ring design, the hold-up was still increasing until the outlet was blocked after 57 minutes. The optimization of the paddle dryer was discontinued, since all the easily implementable possibilities were exhausted. In this case, only severe design changes could lead to a significant process amelioration.

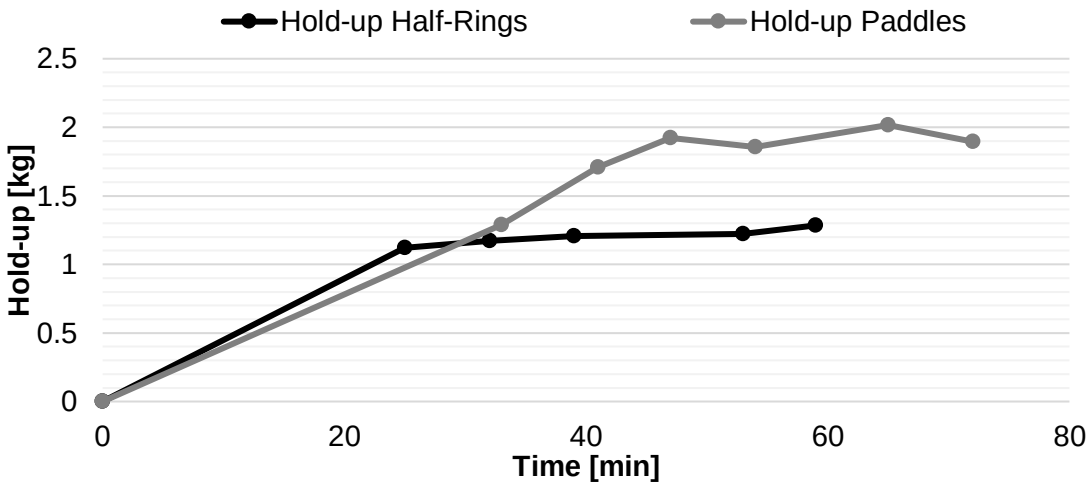

Figure 49. Hold-up results for the test runs with the conveying screw in the paddle dryer.

Based on these findings, the design optimization described in Section 3 was implemented in the new dryer prototype. The results of the first test runs are described in the Section 4.2 below.

3.5.2 **New Prototype**

Initial testing of the new prototype was executed using di-calcium phosphate. Since its flowability and cohesiveness change significantly depending on the moisture level, it is perfectly suited for evaluating the process behavior inside the new dryer. The data depicted in Figure 50 is for a process with 30 wt. % moisture content. The feed mass flow was set to 2 kg/h on a dry basis, which equals 2.857 kg/h of wet material. The temperature in the heating baths was set to 85 °C, and the process air was set to 3.6 Nm^3/h. The air was not preheated and passed the material in the co-current direction. The rotational speed of the large rotor was 2 rpm, and the outlet zone had a free open space at the end of the rotor (Figure 42a). After 13 minutes the first material was discharged. The hold-up and outgoing mass flow were very stable compared to the paddle dryer. The hold-up only increased by 13 g in the last 30 minutes of the process, which is very low considering that no auxiliary insert at the outlet was used in this test run. The fluctuations in the feed mass flow were caused by bridging within the feeder, and the product mass flow variations are probably due to the material accumulation at the end of the process chamber, which occasionally break off. The product had an average moisture of 13.5 wt. %, i.e., of 857 g/h of water introduced 640 g/h evaporated. Considering that di-calcium phosphate has a much higher density than ibuprofen, the resulting 650g of dry material represent a significant improvement to the high hold-ups achieved with the paddle dryer. The corresponding picture to this test run is Figure 39b.

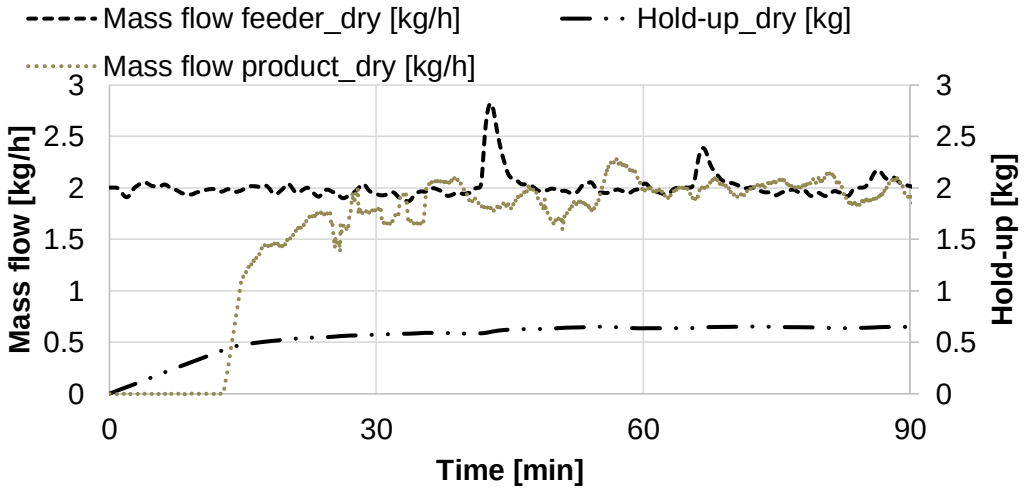

Figure 50. Mass flows and hold-up of a test run with DICAFOS A150 in the new dryer prototype, co-current air flow and no outlet insert.

To assess the system's behavior with ibuprofen, a test run was performed using similar process parameters with 30 wt. % moisture content added to the raw ibuprofen. The air flow was increased to 4.8 Nm^3/h to increase the drying capacity of the system. The temperature was reduced to 60 °C to assure that no ibuprofen could melt during the process. The rotational speed of the large rotor was maintained at 2 rpm. The outcome of this process is shown in Figure 51. The filling up of the system took 13 minutes, i.e., the same time as in the di-calcium phosphate test run. The hold-up showed a slight increase of around 50 g/h towards the end of the process, possibly due to the material's accumulation at the end of the process chamber. Despite the lower density of ibuprofen, more mass (around 765 g) was measured for the hold-up. This was caused by the cohesive nature of the material and its tendency to adhere to the walls. Therefore, more volume of the grooves was filled and the surrounding walls were covered as well (in contrast to the DICAFOS test run, in which the dry material had relatively good flow behavior). This explains why ibuprofen accumulates at the end of the process chamber, while most of the di-calcium phosphate is ejected. These effects are shown in Figure 52.

Surprisingly, the outgoing mass flow was more constant and less fluctuating than the di-calcium phosphate data. The residual moisture measured was 21 wt. %. Only 363 g/h of water evaporated, nearly 300 g/h less than for DICAFOS A150. This may be due to the tendency of ibuprofen to form a paste-like substance, providing less surface area for the drying process. In addition, a lower temperature of the system hinders evaporation, while a higher air flow should facilitate the drying process. The corresponding pictures for this test run are in Figure 42a and Figure 42b.

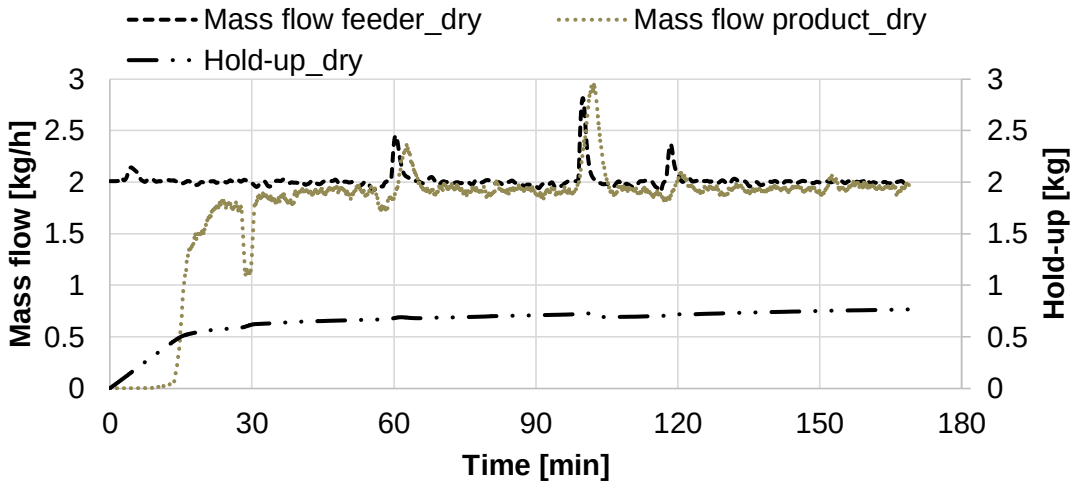

Figure 51. Mass flows and hold-up of a test run with Ibuprofen 25, co-current air flow and no outlet insert.

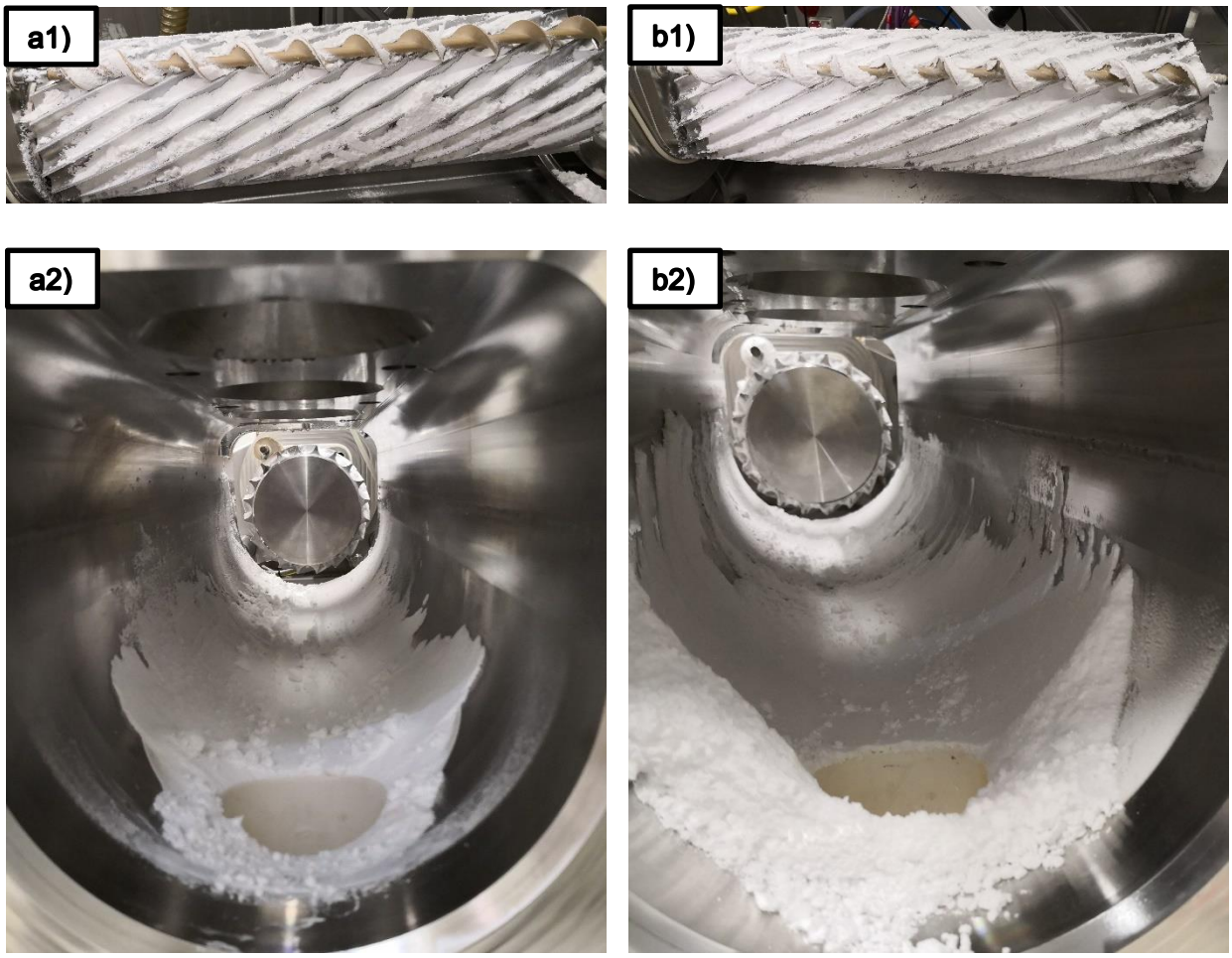

Figure 52. Pictures of the rotor (a1, b1) and the process chamber (a2, b2) after drying test runs with (a) di-calcium phosphate and (b) ibuprofen. No outlet insert was used in these test runs (configuration a1 in Figure 42).

To lower the hold-up further, this test run was repeated with an addition of a diagonal Teflon plate inlay, as shown in Figure 42c. Half of the former rotational speed (1 rpm of the large rotor) was chosen to evaluate the influence on the start-up time and the drying performance of the system. The other process parameters were kept constant. The outcome is shown in Figure 53, which indicates that despite setting the rotational speed to half the speed (1 rpm) the start-up time only took 2 minutes longer (15 minutes vs. the previously measured 13 minutes). The mass flow out of the dryer was very constant and did not fluctuate considerably. The product had a mean residual moisture of 20 wt. %, resulting in 404 g/h of evaporated water, which is approximately 10 % higher than at a higher rotational speed. The hold-up was only lower by approximately 17 g (748 g vs. 765 g). As such, a decision was made to elaborate the outlet design to minimize the stagnant areas shown in Figure 42d.

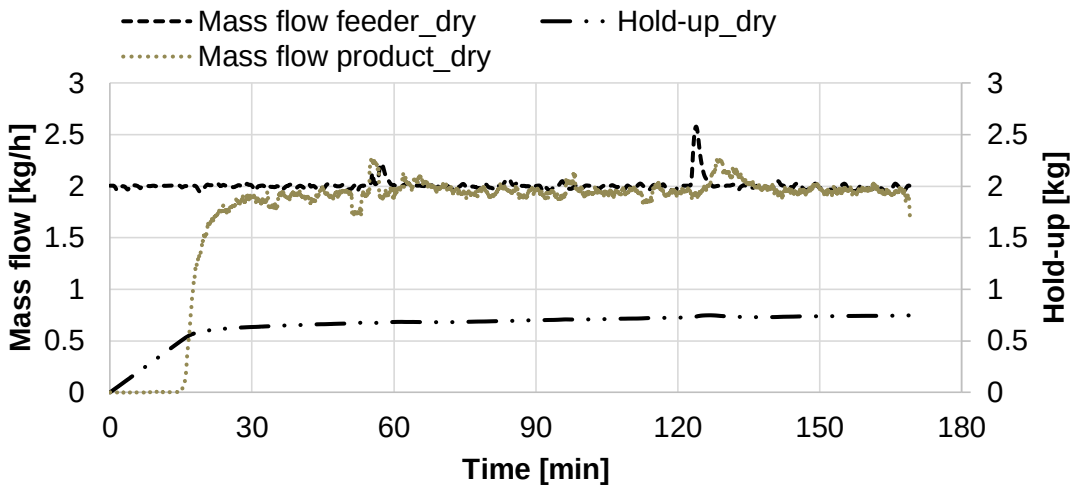

Figure 53. Mass flow and hold-up in the test run with Ibuprofen 25, with a co-current air flow and a diagonal outlet insert.

As a further design adaption to the system, in addition to the half-chute inlay (Figure 42c) towards the back-zone of the dryer, the air flow direction was changed to counter-current and the filter position was moved from above the outlet close to the inlet, which corresponds to a change from position 3 to position 1 in Figure 44. Moreover, the process air was pre-heated to 70 °C, as previously described in Section 2.2. The inlet moisture was slightly higher (34 wt. % instead of 30 wt. %) than before, causing a fluctuating inlet mass flow at the beginning. The rotational speed was maintained at 1 rpm, and the temperature of water baths was set to 60 °C once again. The start-up time is reproducibly 15 minutes until the first material emerges out of the dryer. After the same time as in the previous test runs (approximately 170 minutes), the hold-up was only slightly above 500 g, which was a significant improvement compared to the first designs. It was decided to run the process for 330 minutes to evaluate the long-term stability of the equipment. Despite the nearly doubled process time, about 100 g less of the material accumulated inside the system (649 g compared to 747 g). The fluctuations in the product mass flow are due to the sample taking for PSD measurements and replacements of the product bin. The hold-up was corrected by the sample mass. The residual moisture of the product was equal to 22 wt. %, resulting in a total of 438 g/h of evaporated water, an additional 10 % to the previous test run. The configuration and the outcome are shown in Figure 42e and Figure 42f.

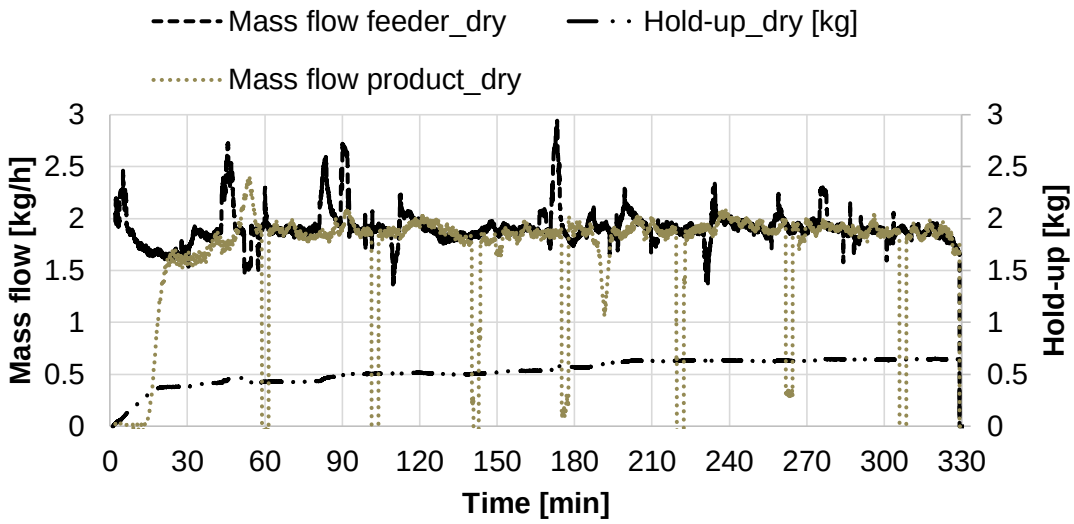

Figure 54. Mass flows and hold-up of a test run with Ibuprofen 25, with a counter-current air flow and a half-chute outlet insert.

A summary of all configurations tested is provided in Table 17, which indicates that the hold-up is very low compared to the results of the paddle dryer and that more water evaporated in this system. Moreover, in contrast to the paddle dryer test runs, the hold-up increase is negligible.

Table 17. Tested dryer configurations with the new dryer prototype. Air inlet and filter positions are shown in Figure 44. Outlet configurations are depicted in Figure 42.

Material [-]	**Air inlet + Filter position** [-]	**Outlet Configuration** [-]	$\dot{m}_{dry,in}$ [kg/h]	$w_{H2O,feed}$ [wt.%]	**Water bath temperature** [°C]	**Air flow** [Nm³/h]	**Rotational speed** [rpm]	**Hold-up** [kg]	**Residual moisture** [wt. %]	**Hold-up increase** [kg/h]	**Evaporated water** [g/h]
Di-calcium phosphate	1 -3	a	2	29.9	85	3.6	2	0.686	13.5	0.08	640
Ibuprofen	1 - 3	a	2	29.7	60	4.8	2	0.765	21.4	0.05	363
Ibuprofen	1 - 3	b	2	29.8	60	4.8	1	0.748	20.0	0.04	404
Ibuprofen	3 - 1	c	2	33.6	60	4.8	1	0.649	21.7	-0.01	438

PSD-measurements of the last test run are shown in Figure 55. The values are the mean value based on triplicate measurements, with the respective standard deviations. Clearly, the particle size does not change significantly during processing since all measurements are within a very narrow band. Therefore, it can be assumed that no particles are destroyed and no stable agglomeration occurred during the processing. To measure loose particle agglomeration, another method should be developed, since the manner in which the samples are prepared for wet dispersion measurement causes a de-agglomeration of the particles. Developing such a method is planned for the future.

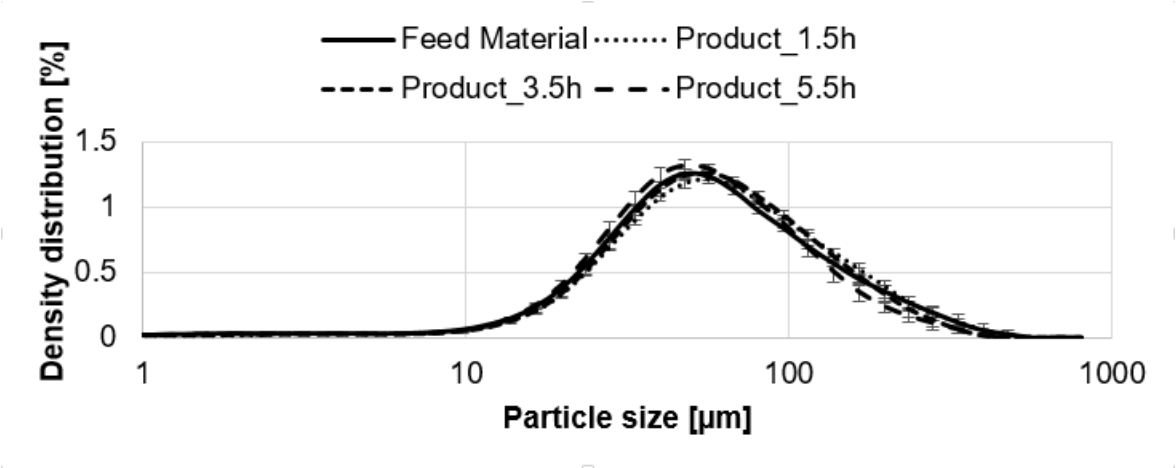

Figure 55. PSD of the test run of the feed and the product after 1.5, 3.5 and 5.5 h of processing.

Since the final design offered significant improvements to the previous configurations, it was decided to use it as a basis for further investigations under atmospheric pressure.

3.6 Conclusion and Outlook

In this work, a dryer for continuous processing of cohesive materials was developed. To that end, experiments with ibuprofen in a paddle dryer were carried out using various paddle configurations. The resulting issues and findings were used to develop a new dryer, subsequently leading to a new patented technology (Patent NL2020740B1[28]). The test substances were classified according to their PSD, morphology and basic flow properties to show the cohesive nature of the material. The worst flowability was measured for 10 wt. % moist ibuprofen, while dry DICAFOS A150 had the best flowability of the substances in question.

To develop the final design, an existing paddle dryer was tested and evaluated. Several paddle designs and configurations were assessed, and the results were used for optimizing the flow behavior in the new drying prototype. With regard to the paddle dryer, it

was shown that ibuprofen with a water content of 10 wt. % could be dried to below 1 %. However, all measured hold-ups of the system were at least around 1 kg or often even higher and still increasing, i.e., too high to be applied to very valuable substances often used in the pharmaceutical industry. Since ibuprofen would accumulate in every free space available, special attention was paid to eliminating the void spaces and implementing a gentle forced flow to move the material out of the process chamber. Since first test runs with the paddle dryer with a conveying screw installed on top of the rotor delivered promising results for dry ibuprofen, the design was further optimized. An interlocking screw mechanism was developed, with the material conveyed from groove to groove via a small conveying screw. The same principle was used to establish self-cleaning in- and outlet configurations.

Once the new prototype design was finalized, several test runs with di-calcium phosphate and ibuprofen were performed and final adjustments to the design and air-flow configurations were implemented. This new design was tested with ibuprofen and di-calcium phosphate. Adjustments to the rotational speed of the rotor, the temperature and the air flow were performed, and the inserts were altered or created. The processes were evaluated according to their stability, the amount and increase of hold-up and the amount of water evaporated. Thereby, it was possible to reduce the hold-up to roughly 650g of ibuprofen on a dry basis, which is significantly lower than in the initial paddle dryer. The final design involved a Teflon half-chute at the end to facilitate the material's falling down and pre-heated process air in the counter-current mode. This configuration had no effect on the particle size distribution of ibuprofen within the system, and significantly more water evaporated per hour. It was shown that the dryer is capable of processing both cohesive and better flowing powders, such as dried di-calcium phosphate.

The next step is to classify the dryer according to its limitations and the governing mechanisms during the process, which will be presented in a follow-up publication. In addition, since many materials in the pharmaceutical industry are thermosensitive or not water-based, the applicability of the dryer under vacuum and with solvents must be investigated to improve the drying performance at low temperatures. Moreover, the particle morphology during the process needs to be evaluated to determine if there are changes in the product quality.

3.7 Nomenclature

BFE	Basic flowability energy / mJ
C	Compressibility / %
C^*	Compressibility without water / %
E_i	Energy of total cycle i / mJ
$E_{i,up}$	Energy of upward cycle i / mJ
f	Correction factor
ffc	Flow function
FRI	Flow rate index
H_2O	Water
$Hold-up_{dry}$	Hold-up on a dry basis / kg
m	Sample mass / g
m_t	Total sample mass / g
$\dot{m}_{dried,out,i}$	Dried mass flow out of the system in time step i / kg/h
$\dot{m}_{evap}$	Mass flow of evaporated water / kg/h
m_{dry}	Dry mass / g
$\dot{m}_{wet,in,i}$	Wet mass flow into the system in time step i / kg/h
SE	Specific energy / mJ/g
SI	Stability index
SMD	Sauter mean diameter / µm
$V_{start,t}$	Total volume at start / cm³
$V_{end,t}$	Total volume at end / cm³
$V_{start,p}$	Powder volume at start / cm³
$V_{start,l}$	Liquid volume at start / cm³
$V_{end,p}$	Powder volume at end / cm³
$V_{end,l}$	Liquid volume at end / cm³
VMD	Volume mean diameter / µm
w	Weight percent of water within the feed/product / %
w_{feed}	Weight percent of water in the feed / %
w_l	Weight percent of liquid / %
$w_{product}$	Weight percent of water in the product / %
ρ_l	Density of the liquid phase / kg/m³
ρ_p	Powder density / kg/m³

σ_c	Major principal stress / kPa
σ_1	Unconfined yield strength / kPa

3.8 Abbreviations

API	Active pharmaceutical ingredient
CM	Continuous manufacturing
FDA	U.S. Food and Drug Administration
FI-A	Flow indicator air
FI-W	Flow indicator water
PSD	Particle size distribution
PTFE	Polytetrafluorethylen
M	Motor mixer
PI	Pressure indicator
RTD	Residence time distribution
SE	Specific energy
SEM	Scanning electron microscope
Teflon	Polytetrafluorethylen
TI	Temperature indicator
TI-A	Temperature indicator air
TC	Temperature control
TC-E	Temperature control electric
H&TI	Humidity and temperature indicator
PR	Pressure regulator

3.9 Acknowledgements

This work has been funded within the Austrian COMET Program under the auspices of the Austrian Federal Ministry of Transport, Innovation and Technology (BMVIT), the Austrian Federal Ministry of Economy, Family and Youth (BMWFJ) and by the State of Styria (Styrian Funding Agency SFG). COMET is managed by the Austrian Research Promotion Agency FFG. We acknowledge the support of Craig Hauser, Sarah Koller, Jelena Milinkovic, Michael Piller, Patrick Vorraber and Daniel Wiegele (all RCPE).

3.10 References

(1) FDA. Guidance for Industry PAT: A Framework for Innovative Pharmaceutical Development, Manufacuring, and Quality Assurance; 2004.

(2) FDA. Pharmaceutical CGMPs for the 21s Century - A Risk-Based Approach. FDA Off. Doc. 2004, No. September, 32.

(3) Badman, C.; Cooney, C. L.; Florence, A.; Konstantinov, K.; Krumme, M.; Mascia, S.; Nasr, M.; Trout, B. L. Why We Need Continuous Pharmaceutical Manufacturing and How to Make It Happen. J. Pharm. Sci. 2019, 108, 3521–3523.

(4) Nasr, M. M.; Krumme, M.; Matsuda, Y.; Trout, B. L.; Badman, C.; Mascia, S.; Cooney, C. L.; Jensen, K. D.; Florence, A.; Johnston, C.; et al. Regulatory Perspectives on Continuous Pharmaceutical Manufacturing: Moving From Theory to Practice: September 26-27, 2016, International Symposium on the Continuous Manufacturing of Pharmaceuticals. J. Pharm. Sci. 2017, 106, 3199–3206.

(5) Plumb, K. Continuous Processing in the Pharmaceutical Industry: Changing the Mind Set. Chem. Eng. Res. Des. 2005.

(6) Li, M.; Gogos, C. G.; Ioannidis, N. Improving the API Dissolution Rate during Pharmaceutical Hot-Melt Extrusion I: Effect of the API Particle Size, and the Co-Rotating, Twin-Screw Extruder Screw Configuration on the API Dissolution Rate. Int. J. Pharm. 2015, 478, 103–112.

(7) Kreimer, M.; Aigner, I.; Sacher, S.; Krumme, M.; Mannschott, T.; van der Wel, P.; Kaptein, A.; Schroettner, H.; Brenn, G.; Khinast, J. G. Mechanical Strength of Microspheres Produced by Drying of Acoustically Levitated Suspension Droplets. Powder Technol. 2018, 325, 247–260.

(8) Coelho, M. C.; Harnby, N. The Effect of Humidity on the Form of Water Retention in a Powder. Powder Technol. 1978, 20, 197–200.

(9) Crouter, A.; Briens, L. The Effect of Moisture on the Flowability of Pharmaceutical Excipients. AAPS PharmSciTech 2014, 15, 65–74.

(10) Bejan, A.; Kraus, A. D. Heat Transfer Handbook; 2003.

(11) Aubin, A.; Ansart, R.; Hemati, M.; Lasuye, T.; Branly, M. Determination of PVC

Powder Drying Kinetics at Particle Scale: Experimental Study and Modeling. Dry. Technol. 2016, 34, 2000–2023.

(12) Aubin, A.; Ansart, R.; Hemati, M.; Lasuye, T.; Branly, M. Modeling and Simulation of Drying Operations in PVC Powder Production Line: Experimental and Theoretical Study of Drying Kinetics on Particle Scale. Powder Technol. 2014, 255, 120–133.

(13) Li, W. Drying of Pharmaceutical Powders Using An Agitated Filter Dryer, University of Leeds, 2014.

(14) Kougoulos, E.; Chadwick, C. E.; Ticehurst, M. D. Impact of Agitated Drying on the Powder Properties of an Active Pharmaceutical Ingredient. Powder Technol. 2011, 210, 308–314.

(15) Tamrakar, A.; Gunadi, A.; Piccione, P. M.; Ramachandran, R. Dynamic Agglomeration Profiling during the Drying Phase in an Agitated Filter Dyer: Parametric Investigation and Regime Map Studies. Powder Technol. 2016, 303, 109–123.

(16) Mujumdar, A. S. Handbook of Industrial Drying, Fourth Edition; 2014.

(17) Mujumdar, A. S.; Huang, L. X.; Dong Chen, X. An Overview of the Recent Advances in Spray-Drying. Dairy Sci. Technol. 2010, 90, 211–224.

(18) Wu, J.; Wu, L.; Wan, F.; Rantanen, J.; Cun, D.; Yang, M. Effect of Thermal and Shear Stresses in the Spray Drying Process on the Stability of SiRNA Dry Powders. Int. J. Pharm. 2019, 566, 32–39.

(19) Wust, K. M.; Beck, T. S.; Hennemann, B. L.; Villetti, M. A.; Frizzo, C. P. Thermal and Oxidative Decomposition of Ibuprofen-Based Ionic Liquids. J. Mol. Liq. 2019, 284, 647–657.

(20) Jain, M.; Lohare, G.; Bari, M.; Chavan, R.; Barhate, S.; Shah, C. Spray Drying in Pharmaceutical Industry: A Review. Res. J. Pharm. Dos. Forms Technol. 2012, 4, 74–79.

(21) Gursch, J.; Hohl, R.; Dujmovic, D.; Brozio, J.; Krumme, M.; Rasenack, N.; Khinast, J. Dynamic Cross-Flow Filtration: Enhanced Continuous Small-Scale Solid-Liquid Separation. Drug Dev. Ind. Pharm. 2016, 42, 977–984.

(22) Liu, L. X.; Marziano, I.; Bentham, A. C.; Litster, J. D.; E.T.White; Howes, T. Effect of Particle Properties on the Flowability of Ibuprofen Powders. Int. J. Pharm. 2008, 362, 109–117.

(23) Garzón, L. C.; Martínez, F. Temperature Dependence of Solubility for Ibuprofen in Some Organic and Aqueous Solvents. J. Solution Chem. 2004, 33, 1379–1395.

(24) Co, J. C. Safety Data Sheet: Calcium Phosphate Dibasic, Anhydrous https://www.jostchemical.com/documentation/SDS/Calcium Phosphate Dibasic, Anhydrous (7757-93-9).pdf (accessed Oct 8, 2019).

(25) Kreimer, M.; Zettl, M.; Aigner, I.; Mannschott, T.; Van der Wel, P.; Khinast, J. G.; Krumme, M. Performance Characterization of Static Mixers in Precipitating

Environments. Org. Process Res. Dev. 2019, 23, 1308–1320.

(26) Krantz, M.; Zhang, H.; Zhu, J. Characterization of Powder Flow: Static and Dynamic Testing. Powder Technol. 2009, 194, 239–245.

(27) Schulze, D. Powders and Bulk Solids, 1st ed.; Springer Berlin Heidelberg: Berlin, Heidelberg, 2008.

(28) van der Wel, P.; Kaptein, A.; Krumme, M.; Mannschott, T.; Aigner, I.; Kreimer, M.; Zettl, M. Drying Device, Rotary Valve and Drying Method. NL2020740B1, October 16, 2019.

„A theory is something nobody believes, except the person who made it. An experiment is something everybody believes, except the person who made it."

Albert Einstein (1879 - 1955)

4 Characterization of a Novel Drying Technology for the Continuous Processing of Cohesive Materials

Manuel Zettl[1], Isabella Aigner[1], Thomas Mannschott[2], Peter van der Wel[3], Hartmuth Schröttner[4,5], Johannes Khinast[1,6], Markus Krumme[2,*]

[1] Research Center Pharmaceutical Engineering (RCPE) GmbH, 8010 Graz, Austria

[2] Novartis Pharma AG, 4056 Basel, Switzerland

[3] Hosokawa Micron B.V., 7005 BL Doetinchem, Netherlands

[4] Graz University of Technology, Institute for Electron Microscopy and Nanoanalysis, 8010 Graz, Austria

[5] Austrian Centre for Electron Microscopy and Nanoanalysis (FELMI-ZFE), 8010 Graz, Austria

[6] Graz University of Technology, Institute for Process and Particle Engineering, 8010 Graz, Austria

*Corresponding author: M. Krumme

Adapted and published in Organic Process Research and Development: https://doi.org/10.1021/acs.oprd.0c00413

TOC-Graphic

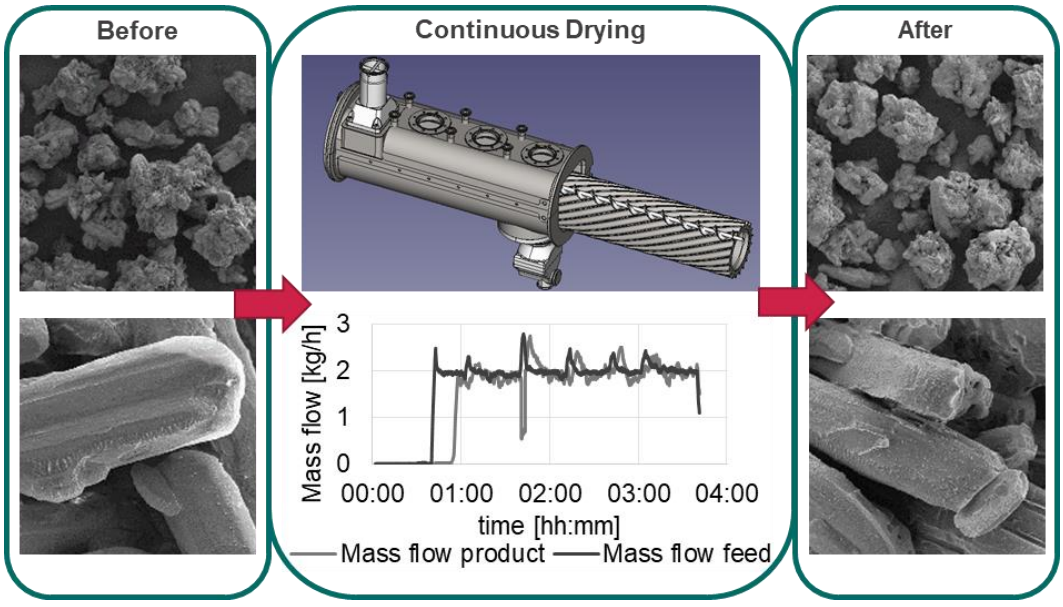

4.1 Abstract

The presented work dealt with the influence of several process parameters and two different test substances on a novel drying device, issued under the patent NL2020740B1. The to-be-dried substance is conveyed through the grooves of a large rotor, by an interlocking screw design. Therefore, a gentle, forced flow is created, avoiding agglomeration and attrition. This enables the new technology to continuously dry poorly flowable substances, as are often encountered in the pharmaceutical industry. Therefore, drying test runs are performed with water-wetted ibuprofen, a non-steroidal, anti-inflammatory drug with poor material flow properties, as well as one test run with di-calcium phosphate, which changes its flow characteristics with its moisture content. The test substances were tested according to their size, shape and flow properties prior to the test runs. The tested process parameters are temperature, mass flow, air flow, rotational speed and initial moisture. Additionally, test runs to estimate the RTD, the drying mechanism, the long-term process behavior, as well as re-processing tests of the substance Ibuprofen are performed. It was shown that the dryer shows very good performance for cohesive materials (continuous process times of up to 10 hours were possible with evaporation rates of up to 688 g/h). The process is very robust, with a few drawbacks for materials that are prone to tribocharging.

Key words: Continuous manufacturing, drying, cohesive materials, temperature sensitive, agglomeration, equipment development

4.2 Introduction

Driven by the U.S. Food and Drug Administration (FDA)[1,2], the pharmaceutical industry has only started to shift towards continuous processes in the 21st century. As manufacturing was done in batch mode previously, a hesitancy to implement new processes can be observed, despite the numerous advantages of continuous processes, such as higher product quality by better process understanding, ecological benefits and decreased production times. Drawbacks include the high investment costs, unclear regulations and the non-availability of suitable equipment. In order to continue the transition from batch-wise manufacturing towards continuous production lines, new equipment is needed. Existing equipment from the oil and chemical industry usually operates at a much larger scale and often cannot be scaled down due to geometrical constraints, therefore new equipment has to be developed.[3,4]

One of the processes that lacks suitable equipment is continuous drying, especially of pasty or very cohesive and powdery material streams. As active pharmaceutical ingredients (APIs) are usually produced and crystallized for optimal bioavailability, their flow properties are very often poor. Additionally, many of these substances show thermal degradation or show agglomeration or attrition tendency, so a gentle way of drying at low temperatures is needed. [3–6] As thermal drying is very energy intensive, as much moisture as possible is removed mechanically , usually by filtration [7–9]. In this context, a technology which is able to continuously process and dry such slurries or powders with high moisture content after filtration could prove to be very beneficial for the pharmaceutical industry. Thereby reducing the residence time in comparison to batch processes which helps to minimize the risk of thermal degradation[10]. Furthermore, in the future this will enable linking API production with the production of solid dosage forms, such as tablets.

Drying is an especially complicated process, as heat and mass transfer occur simultaneously, and several different mechanisms contribute to the outcome of the drying process. The heat is induced either via convection (by a drying agent) or conduction (via a hot surface). Most dryers use a combination of both mechanisms to enhance the drying performance[11,12]. To avoid agglomeration and attrition of the particles while drying, special care needs to be taken during the processing. Attrition occurs due to particle-particle or particle-surface collisions[13–17], as shear is induced, or due to pressure or temperature gradients during the process[18–20]. The tendency towards attrition is strongly dependent by the particle morphology and shape.[21–23] On the other hand, agglomerates are formed due to forces between particles[24–26], such as solid or liquid bridges, van der Waals forces or electrostatic effects. With increasing solubility of the particles in the liquid phase, the agglomerates get stronger due to the forming of solid bridges.[27]

Based on the findings described in Zettl et al.[6], a new contact-convective dryer prototype is investigated in this study. Ultimately, the described equipment shall be able to dry and process under vacuum, enabling it to be used with organic solvents and within harsh chemical environments. As initial testing before further tightness optimization, the working principle and main process influences are analyzed. The investigated influencing parameters are air flow, mass flow, temperature, inlet moisture, rpm variations and influence of different materials. Additionally, a long-term test run with material refeeding was analyzed and the different contributions to the drying performance are discussed. The residence time distribution (RTD) was also evaluated. At first the used materials and process equipment are described, followed by the methodology of the test runs. The performed test runs are described subsequently, before the results are shown. Finally, a conclusion is given and an outlook for future work is provided.

4.3 Materials and methods

4.3.1 Process equipment

The used setup is depicted in Figure 44 and Figure 57. After the feed preparation, the wet powder was filled into the gravimetric feeder (K-Tron KT20, Coperion GmbH, Stuttgart, Germany), which was used to feed the wet material into the dryer. The material was conveyed via the inlet rotary valve, interlocking with the large rotor over a small conveying screw. Through the rotation of the small conveying screw, the pockets of the inlet rotary valve are scraped out and gently forced into the grooves of the large rotor. After one rotation of the large rotor in these grooves the material is reaches the small conveying screw which transports the material to the next groove. After several of these conveying steps, the material falls at the end of the process chamber, onto the outlet rotary valve, where it is finally transported out with a similar principle, as at the inlet. The material falls on top of the large rotor of the outlet rotary valve and the small conveying screw scrapes the dried powder out of the pockets of the larger rotor. A detailed description of the design is given in Zettl et al[6]. and visible in Figure 44.

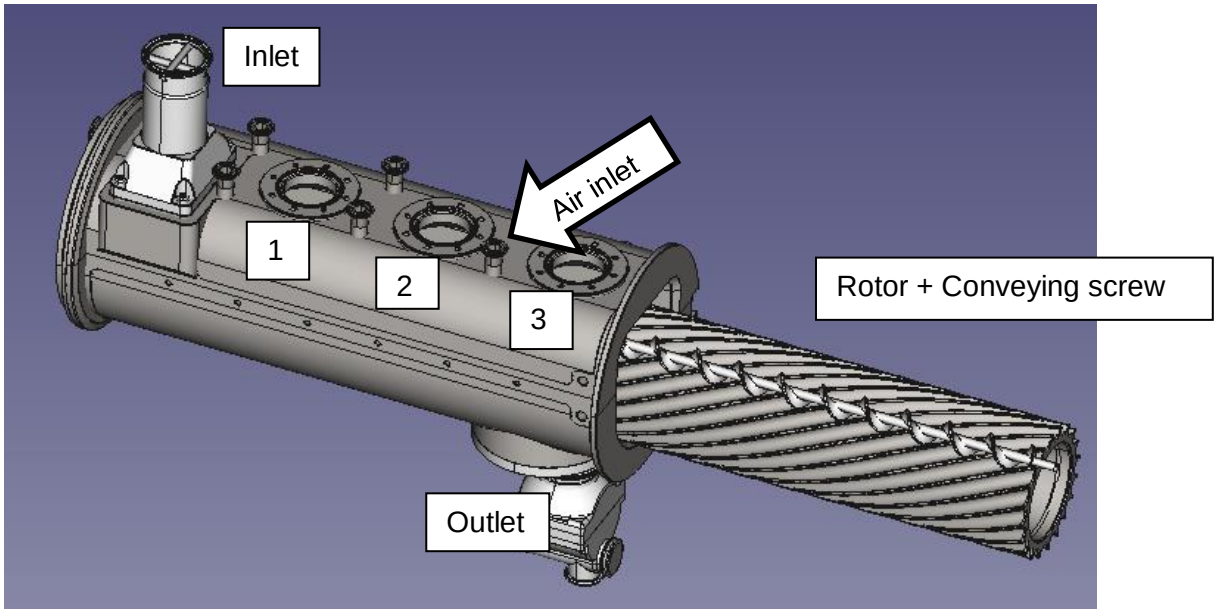

Figure 56. CAD-Model of the dryer, with the rotor pulled out, filter and sensors not visible. Filter position for the described test runs was position 1[6].

The used heating baths were of type HL-4 (Julabo GmbH, Seelbach, Germany) for the heating of the dryer and F25 (Julabo GmbH, Seelbach, Germany) for the heating of the air. The

dryer was heated in two separate heating circuits, one for the trough and the rotor and the other for the filter and the top, each pumping at a rate of 200 l/h. The heated air, serving as a drying agent, moved in a counter-current flow over the material, and left the system via the installed filter. The temperature of the air was logged with a T176-T4 temperature logger (Testo GmbH, Vienna, Austria). After the material is ejected from the process chamber, it is either collected directly in a bucket on a scale ML 4001 (Mettler Toledo GmbH, Vienna, Austria), or moved over a conveyor belt for visual inspection prior to the balance. The outgoing air was measured in terms of relative humidity and temperature by a Vaisala HMT 337 Humicap (Vaisala, Vantaa, Finland). The material humidity was measured with a HC103 moisture analyzer (Mettler Toledo GmbH, Vienna, Austria).

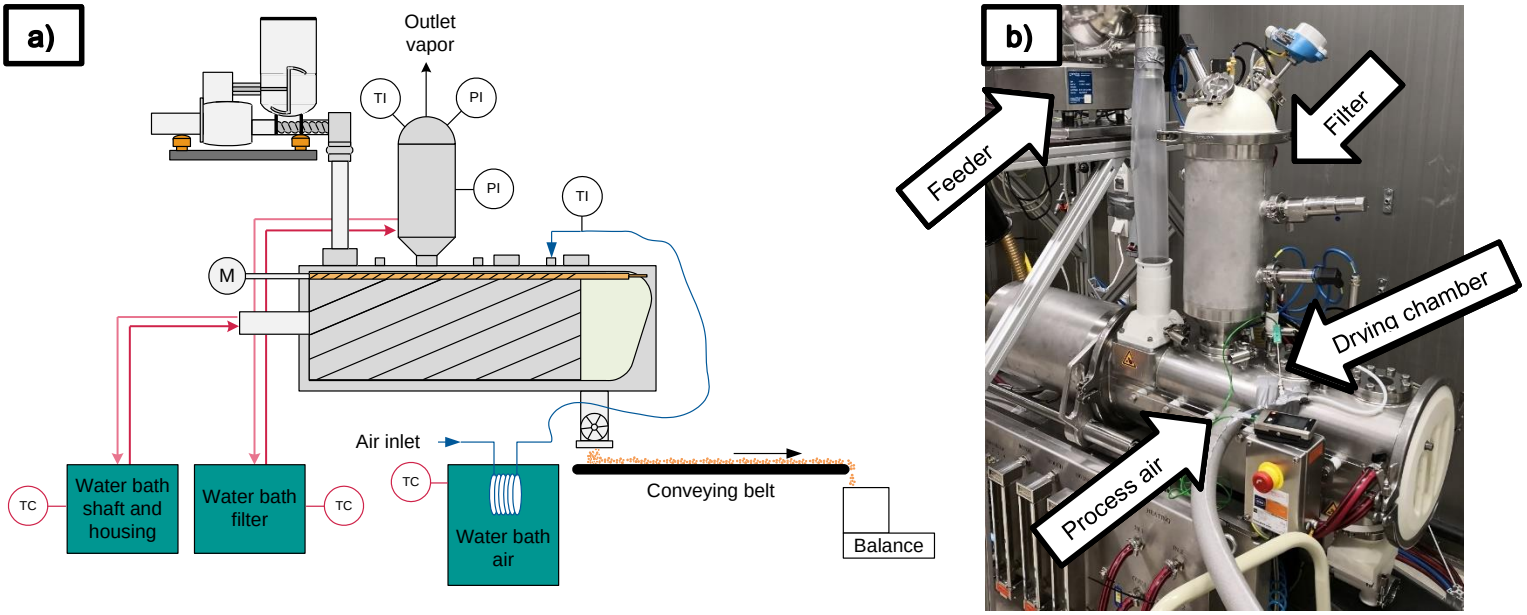

Figure 57. Process flow sheet of the contact-convective dryer (a) and picture of the process setup (b) [6].

4.3.2 **Materials**

For all but one test run Ibuprofen 25 (BASF SE, Ludwigshafen, Germany) was used as the test substance, as it hardly dissolves in water (solubility at 25 °C is 21 mg[28]) and shows poor flow properties for all observed moisture contents[6]. For the comparability between different substances one test run with di-calcium phosphate (DICAFOS A150 Chemische Fabrik Budenheim KG, Budenheim, Germany), was executed, which shows improving flow properties with decreasing moisture content[6]. As moisture levels 10, 20 and 30 wt. % of water were used for Ibuprofen, and 18.9 wt. % for DICAFOS A150. The ratio for DICAFOS was chosen so as to show the same

volumetric ratio as the run with 2 kg/h Ibuprofen. The goal was to compare the flow in the chamber, not the productivity by mass. The true density of both substances differs quite significantly. While the true density of Ibuprofen was reported to be 1.11 g/cm³ [29], di-calcium phosphate is significantly denser with 2.789 g/cm³ [30]. The differences of the measured tapped and bulk densities are reported in Zettl et al.[6], and it is shown that di-calcium phosphate with a certain moisture level is 1.5 to 2 times denser than the corresponding Ibuprofen substance, with a mean value of 1.9. Key material properties of the raw materials are given in Table 18. To evaluate the particle size and morphology, the particle size distribution (PSD) was measured for the raw materials and scanning electron microscopy (SEM) pictures were taken at all moisture levels, to additionally evaluate the agglomeration tendency of the feed substances. The test substances were tested according to their size, shape and flow properties prior to the test runs.

Table 18. Characteristic properties of the used raw substances.

Material [-]	Bulk Density [g/cm³][6]	Tapped Density [g/cm³][6]	True Density [g/cm³]	Solubility in Water at 25°C [mg/kg]	Melting Point [°C]
Ibuprofen 25	0.337	0.540	1.11[29]	21[28]	75-78[31]
DICAFOS A150	0.719	0.904	2.789[30]	100[32]	>450[32]

4.3.2.1 PSD

The PSDs of the raw and feed materials are shown in Figure 58. The measurements were undertaken in a HELOS KR (Sympatec GmbH, Clausthal-Zellerfeld, Germany). The CUVETTE unit was used to disperse the particles within distilled water, stirred at 100 rpm to avoid sedimentation. Additionally, one droplet of Tween 80 was used, to increase the wettability of Ibuprofen and create a stable suspension. The measurements were taken at the ideal optical concentration range of the system, being around 10 %. It is visible that for Ibuprofen the particle size already increases during mixing with water, and agglomerates are formed. As the measurement is nearly identical for all different moisture levels, the agglomerates are possibly broken up during the measurement in wet dispersion and all agglomerates larger than a critical size are broken up. For di-calcium phosphate it can be seen that the amount of fines increases slightly by the mixing step, most probably due to fines de-agglomerating from the larger chunks visible in Figure 59b and Figure 61.

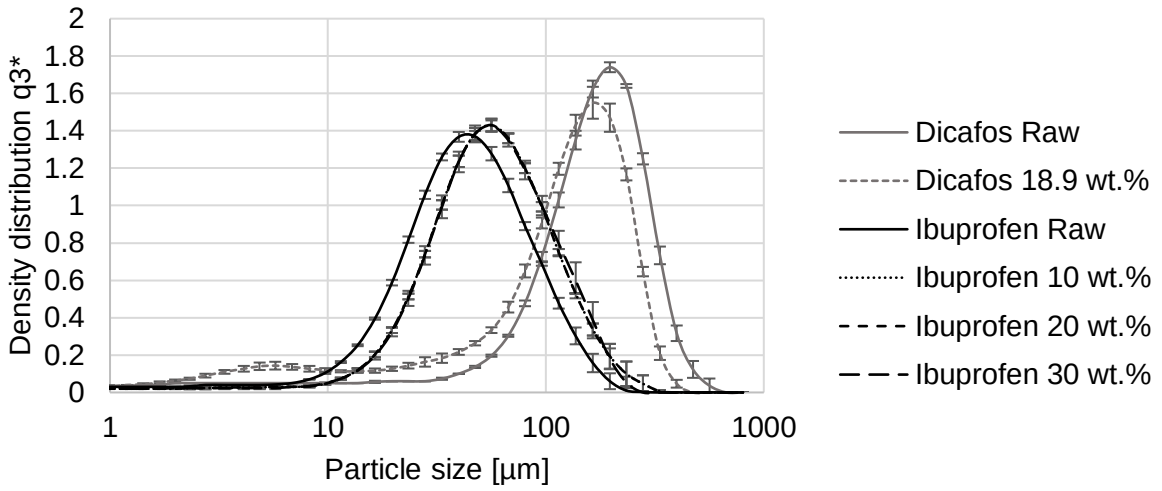

Figure 58. Measured particle size distributions (PSD) for raw and feed materials.

4.3.2.2 SEM

In order to be able to evaluate changes in the particle morphology and if attrition and/or agglomeration occurs within the mixing and drying process, SEM-measurements were performed. The samples were taken after the feed preparation. Therefore, the samples were dried at 200 mbar chamber pressure and 60 °C for at least seven days, to ensure that no moisture was left before putting them inside the SEM-device (Zeiss Ultra 55, Carl Zeiss AG. Oberkochen, Germany). The used Everhart-Thornley detector was set to an acceleration voltage of 5 keV, and the samples were prepared in a sputter coater (EM ACE 600, Leica Camera AG, Wetzlar, Germany) and coated with an 80/20 gold/platinum coating with a thickness of 15 nm. The single particles of the raw materials are shown in Figure 59. The rod-shaped needles of Ibuprofen are visible in Figure 59a, and the agglomerated lumps of di-calcium phosphate are depicted in Figure 59b.

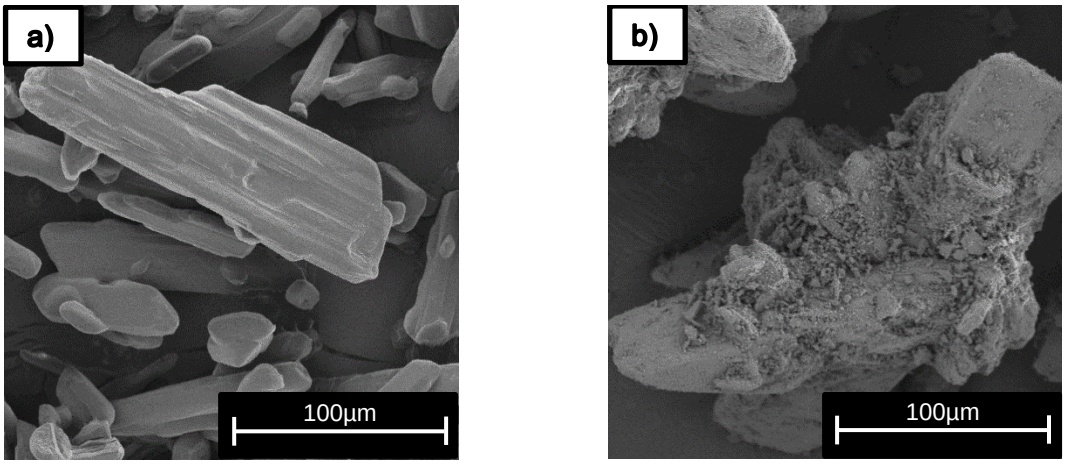

Figure 59. Single particles of raw Ibuprofen (a) and di-calcium phosphate (b)[6].

The agglomeration tendency of Ibuprofen is shown in Figure 60. While no agglomerates are visible for the raw Ibuprofen (Figure 60a), agglomerates already start to form at 10 wt.% of water (Figure 60b), and increase in size when going to higher moisture levels, such as 20 wt.% (Figure **60**c) and 30 wt.% (Figure 60d).

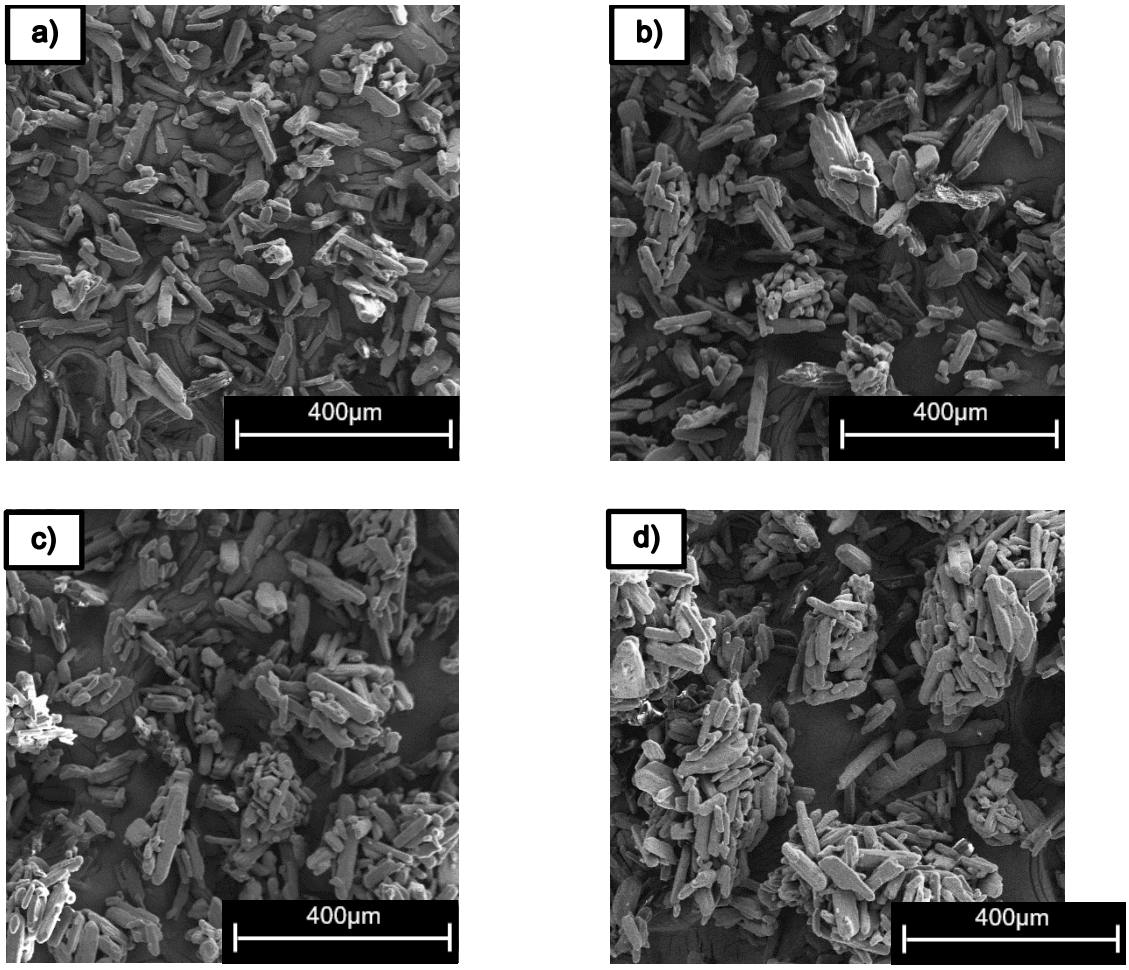

Figure 60. SEM pictures of raw (a) Ibuprofen and the used Ibuprofen feeds with initial water contents of 10 (b), 20 (c) and 30 (d) weight percent.

In contrast to the Ibuprofen particles, DICAFOS A150 exhibits different behavior. The particles seem to get smaller during the mixing step. This can be explained by the inherently different particle structure. While raw Ibuprofen consists more or less of single particles, the used di-calcium phosphate is built from small chunks forming large agglomerates. The raw material is shown in Figure 61a and in Figure 61b di-calcium phosphate with a previous water content of 18.9 wt. % is shown.

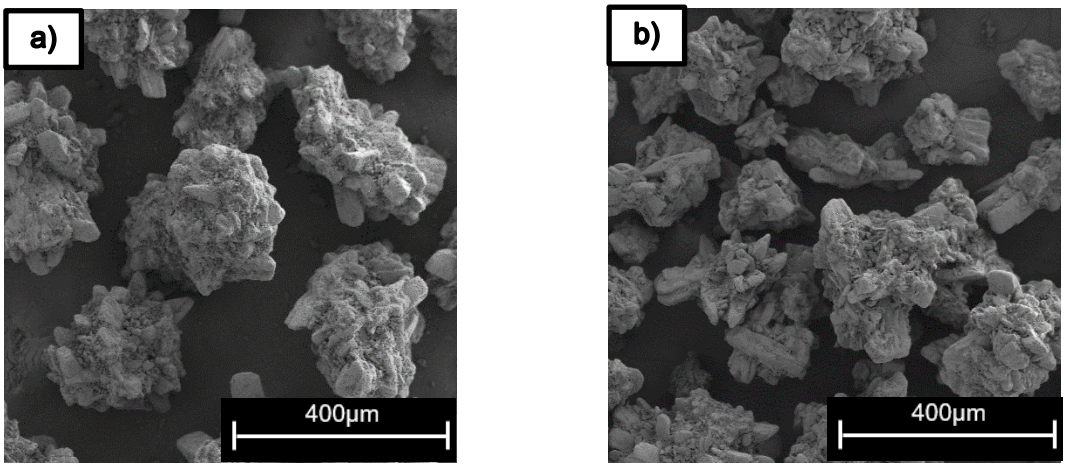

Figure 61. SEM pictures of DICAFOS A150 before (a) and after the addition of 18.9 wt.% water (b).

4.3.2.3 Flow Properties

The characterization of the used substances is described in Zettl et al.[6] and is summarized subsequently. The measurement results were obtained by a FT4 rheometer (Freeman Technology, Tewkesbury, United Kingdom) and Ibuprofen 25 and DICAFOS A150 were analyzed at varying moisture levels. In general, the energy needed to bring the material to flow increases with higher moisture levels, Ibuprofen with 10 wt. % water being an exception. The more often the Ibuprofen mixtures are brought to flow, the lower the needed energy becomes. Concerning the compressibility measurements, it was shown that the addition of water increases the compressibility for both test substances. This indicates that it will get worse, with increasing moisture content. The data from the shear-cell experiments showed that the flow function (ffc) decreases when water is added. The higher the ffc is the better the material flows. The material with the best flow behavior was raw di-calcium phosphate. Using the classification from Schulze[33] it is visible that the used materials are either classified as cohesive (raw Ibuprofen, all measured DICAFOS A150 materials) or very cohesive (the Ibuprofen-water mixtures) [6].

Additionally, the bulk and tapped densities were measured for the raw materials and at 10, 20 and 30 wt. % water in a Pharma-Test PT-TD200 (Pharma Test Apparatebau AG, Hainburg, Germany). While Ibuprofen showed the expected behavior (increasing density with increasing moisture), di-calcium phosphate showed unpredictable behavior at higher moisture levels. This was most likely caused by trapped air bubbles within the measurement vessel. However, all water-solid mixtures had a higher density than the respective raw material.[6]

4.3.3 Experimental procedure

In this chapter the experimental procedures and used setups are described in detail. At first, the methods for the preparation of the feed material are explained, followed by the moisture measurements and the experimental plan to investigate the influence of various process parameters.

4.3.3.1 Material Preparation

In order to obtain a sufficient amount of wet feed material, at first the raw Ibuprofen was weighed into a large container. Afterwards, the solids were stirred with a helical ribbon impeller, mounted to a drilling machine. During the agitation of the solids the necessary amount of water was added slowly to the container. This ensured a homogenous mixture inside the container and enabled the production of up to 20 kg feed material at once. After mixing the moisture of the material was analyzed and if the resulting moisture matched the intended amount, the material was fed into the feeder for further processing.

4.3.3.2 Moisture Measurement

To obtain the results of the residual moisture in a fast and efficient way, a moisture analyzer was used (HC103, Mettler Toledo GmbH, Vienna, Austria). At least 1.5 g of material were placed on an aluminum tray and the drying temperature for the Ibuprofen samples was set to 60 °C, due to the low melting point of Ibuprofen. The di-calcium phosphate samples were measured at 85 °C. The stopping criteria for both materials was that the absolute change of weight of the sample within 90 seconds was less than 1 mg. To heat up the sample, a halogen unit was used. The mean measurement time was approximately 20 minutes under these conditions for Ibuprofen, and 15 minutes for di-calcium phosphate.

4.3.3.3 Process Parameter Recording and Hold-up calculation

For the logging of the relevant process parameters the sensors of the drying unit were connected to two RSG45 (Endress+Hauser AG, Reinach, Switzerland) units and then collected via an OPC-Server in a LabView routine. The scale was connected with a serial RS232 connection and the gravimetric feeder was read out with an OPC server over a Profibus connection. The process data was logged each second, and for some test runs every 50 or 20 ms to be able to distinguish between metal and powder temperature signals. The hold-up was calculated by balancing the weight signal of the scale with the mass flow loss of the feeder. To filter out the disturbances (i.e. feeder refilling, product container exchange, process vibrations) an overall hold-

up was calculated at distinctive time points in the process. The process data was then fitted to match the manually measured hold-up points. The mass of the taken samples was subtracted from this curve at the relevant times, to obtain the real hold-up value. To be able to compare the hold-up at different moisture levels, it was calculated on a dry basis, with equations 2.1 to 2.3 (see Zettl et al.[6]). The hold-up is the summation of the dry material entering and leaving the system (2.1), the evaporated water is therefore the difference between the amount of liquids at the in- and outlet (2.2). The weight percent are calculated with formula 2.3[6].

$$Hold-up_{dry} = \sum_{i=1}^{N}((\dot{m}_{wet,in,i} * (1 - w_{feed}) - \dot{m}_{dried,out,i} * (1 - w_{product})) \quad \textbf{(4.1)}$$

$$\dot{m}_{evap} = \dot{m}_{wet,in} * w_{feed} - \dot{m}_{dried,out} * w_{product} \quad \textbf{(4.2)}$$

$$w = \frac{m_{wet} - m_{dry}}{m_{wet}} \quad \textbf{(4.3)}$$

4.3.3.4 Experimental Procedure

After the process parameter recording started, the heating baths and the process air were turned on at the desired temperature. To compensate for the leakage of process air, a suction unit was turned on after the filter, and equilibrated with the air flow, so that a small amount of air was sucked into the system. When the recorded temperature of the in- and outgoing water leveled (i.e. change in temperature over 5 minutes less than 0.1 °C) the feeder was started at the desired mass flow and the rotors were turned on. The temperature profiles and the start of the feeder of an example test run are shown in Figure 62 and Figure 63. After the heating up of the process chamber was finished (Period 1), the feeder was turned on at the desired mass flow and the filling phase started (Period 2). When a stable mass flow was reached, the filling of the process chamber started. It took some time before steady state was reached, depicted as period 4. When the measured mass flow going out of the dryer matched the incoming mass by ±5 % (i.e. 100 g/h for a mass flow of 2 kg/h of dry solids) for 10 minutes, steady state was assumed (Period 4). To calculate the mass flow going out of the dryer, the values were corrected by the moisture levels of the taken samples. It was important, that when steady state could be reached, it lasted for at least 10 minutes, so that a meaningful balance could be calculated for the analysis of the drying performance. Samples for the moisture measurement were taken at least three times per hour,

and samples for the particle size distribution and SEM- measurements at least twice during the process, unless stated otherwise.

The sample test run visible in Figure 62 and Figure 63 was set to 70 °C as the heating bath temperature, with a solid mass flow of 2 kg/h on a dry basis. The fluctuations of the mass flow of the feeder are due to bridging and refilling of the feeder, and for the product mass flow due to sampling and container exchanges. For the later shown process data, the time-axis starts with period 2, the moment when the feeder was started being minute 0. All samples for the moisture and particle size measurements were taken in time period 3 and 4.

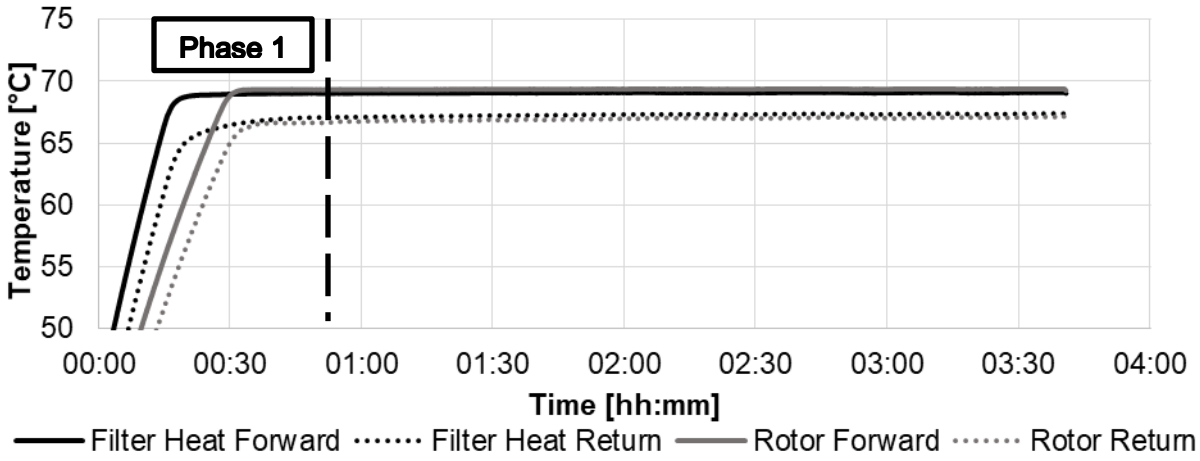

Figure 62. Temperature profiles of the in- and outgoing heating water for a sample test run, set to 70 °C drying temperature.

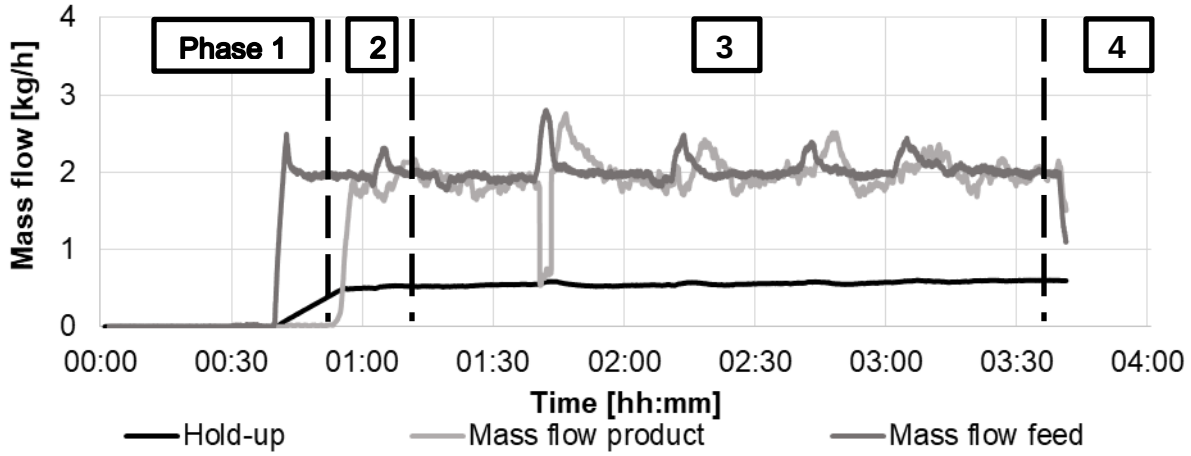

Figure 63. Feed and product mass flows with corresponding hold-up of a sample test run, set to 2 kg/h on a dry basis.

For the evaluation of the test runs, the hold-ups of the relevant test runs will be compared, as this is the best indication for the stability of the process.

4.3.3.5 Residence Time Distribution

To estimate the residence time distribution (RTD) of the powder in the dryer, a test stand, visible in Figure 64, was built. After the outlet of the dryer, a conveyor belt was installed. The dried powder was moved slowly over the belt, guided by two Teflon scrapers to obtain a consistent material stream. A camera recorded the passing powder, illuminated by an LED-ring. These images were post-processed in a Matlab script, converting the pictures to the RGB and LAB color scheme. A detailed description of the data processing is given in Kruisz et al[36]. After the dryer was running at steady state, the feeder was turned off for 20 s and 11.9 g of tracer material was added, at a moisture content of 30 wt. %. This corresponds to a dry solid flow of approximately 1.5 kg/h, or 2.14 kg/h on wet basis, which was also the set point of the gravimetric feeder. The water baths for the drying were set to 60 °C and the preheated air (70 °C) was set to 80 Nl/min. The tracer material was produced by dissolving ibuprofen in ethanol and adding a water insoluble colorant (edding T25, red, edding AG, Ahrensburg, Germany). Afterwards, the material was precipitated by adding water, creating a red ibuprofen tracer. The drawback of this method is that the produced material shows different flow behavior than the feed material. The other investigated options (solid tracers like Fe_2O_3, water soluble dyes) either changed the flow properties of the powder in the process chamber completely or diffused throughout the whole process chamber and led to misleading results. Therefore, this approach was used, and will be further optimized in the future. After the tracer was added, the signal was recorded for 90 minutes, to be able to evaluate the tailing behavior of the distribution as well. At the end of the process the dryer was opened and visually inspected for any residual tracer in order to see dead-spots in the powder movement.

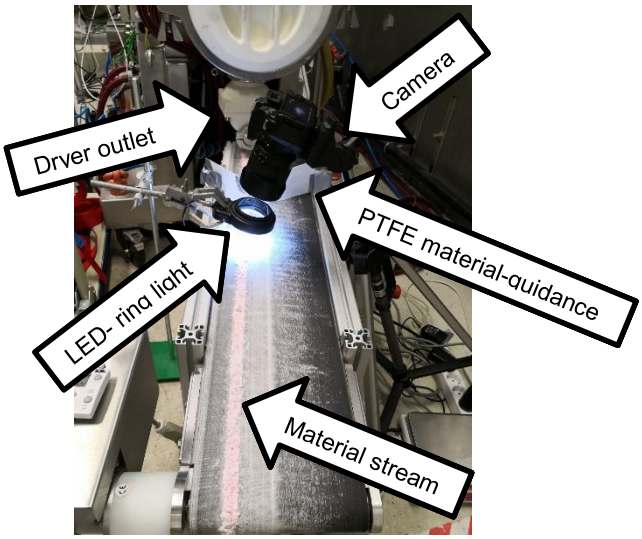

Figure 64. Experimental setup of the residence time distribution test run.

4.4 Results and discussion

In this section the results of the test runs are presented. Initially, the result of the residence time distribution test run is discussed, afterwards the influence of various process parameters (material influence, mass flow, air flow, temperature, inlet moisture, rotational speed) is analyzed. The chapter concludes with the results of test runs to estimate the governing drying mechanisms and a long-term test run, where the material was re-fed twice to obtain a completely dry product and be able to see the effect of processing powder through the dryer. The complete set of test runs is visible in Table 19 with their relevant results.

4.4.1 **RTD**

For the RTD test run a drying test run with a mass flow of 1.5 kg/h on a dry basis was executed (30 wt. % initial moisture, 2.143 kg/h on wet basis). The process duration prior to the tracer addition was 90 minutes, and the process data showed that steady state had been reached. At this point, the residual moisture of the product was at 19 wt. %, which corresponded to an evaporation rate of 320 g/h of water. Sample images of the RTD test are shown in Figure 65, in order of their appearance during the process. At the time when Figure 65a was taken, the tracer was added. The intensity of the reddish color increased steadily, until a maximum was reached after 13 minutes and 30 seconds (Figure 65b). The intensity then declined steadily until after 90 minutes the initial color was almost reached again (Figure 65d). After 70 minutes fluctuations at the feeder outlet occurred, resulting in an unsteady material layer on the conveying belt, and therefore an inaccurate measurement during that time period (Figure 65c). This behavior occurs from time to time and cannot be eradicated completely, but does not influence the process evaluation significantly, as it can easily be determined by looking at the video data if there is tracer present or another distortion occurs.

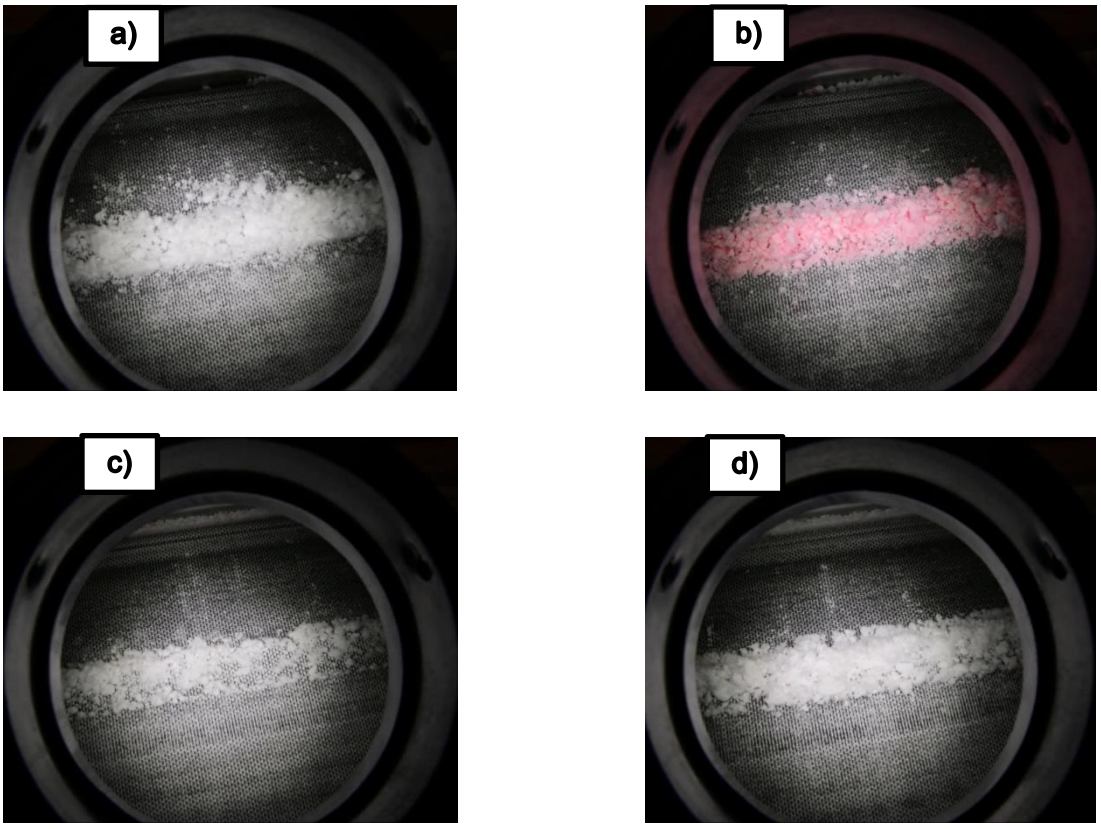

Figure 65. Sample images from the RTD test run. Pictures after 0 minutes, at the time of the tracer addition (a), after 13 minutes and 30 seconds, during the peak of the tracer intensity (b), after 70 minutes, where the mass flow out of the dryer was not constant (c) and at the end of the process (d).

These pictures correspond to the picture analysis routine performed in Matlab. The results of the A-value of the LAB color scheme, where a positive A-value corresponds to red, are depicted in Figure 66. The light grey curve shows all measured values, while the black curve is the mean value over 10 seconds to be able to see the trend of the curve better. It is visible that there is a relatively broad plateau from 11 to 20 minutes of process time, with a maximum at 13 minutes and 30 seconds. After that, the intensity of the tracer diminishes, until only very little is visible after 60 minutes. The increase after 70 minutes is due to the mass flow fluctuations on the conveying belt. Due to the black color of the belt, a wrong A-value is given by the analysis. The same is true for the two small peaks after 80 minutes and 89 minutes, where some material was stuck in front of the camera.

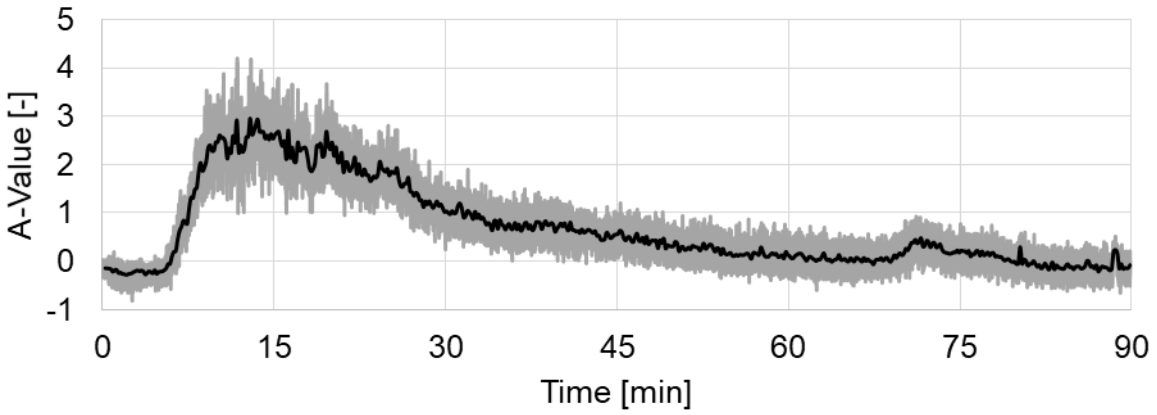

Figure 66. Results of the RTD-measurement.

However, it can be seen from the analysis that the value after 90 minutes is close, but not equal to the initial value. This can be explained by a coloring of the conveying belt itself, but also changing light conditions, which interfere with this measurement method and are invisible to the human eye. The relatively long tailing behavior can be explained by deposits of the tracer material directly after the inlet, as they break off over time and therefore distort the measurement. Also, back mixing inside the dryer could be the reason. These deposits were found after opening the dryer during the cleaning of the equipment, and were probably caused due to problems with the manual addition of the tracer, as its cohesiveness prevented a steady addition.

This method of measuring the RTD of a wet powder through a process seems promising, as the results are meaningful and the flow behavior inside the process chamber stays more or less the same, compared to other tracers. However, to have a meaningful, replicable RTD curve, more effort needs to be taken to optimize the tracer substance and addition, and more experiments need to be performed at several different set points to evaluate the influence of the different process parameters. This was a useful test run for an initial estimate of the powder behavior in the system and future test runs with an optimized setup will be investigated further. For this drying device, a relatively broad residence time distribution, without significant tailing is ideal, as a certain degree of back mixing should be optimal for the drying performance.

Summarizing, the RTD test run (1.5 kg/h dry basis, 30 wt. % initial moisture, 60 °C, 1 rpm, 80 Nl/min) showed a peak after 13 minutes and 30 seconds, and a rather long tail of approximately 75 minutes. The methodology of the RTD measurement needs further improvement, as due to the change in flowability accumulations at the inlet zone occurred, which probably caused the long tail of the RTD curve.

4.4.2 **Air Flow Influence**

To estimate the influence of the air flow and therefore optimal process conditions, three different set points were tested. The air temperature was set at 70 °C, and the other process parameters were kept constant. The chosen air flows were 80 Nl/min (Test run 1), 105 Nl/min (Test run 2) and 130 Nl/min (Test run 3). The results of the test runs with varied air flows are summarized in Table 19. It is easily visible that increasing the air flow only has a minor effect on the drying efficiency, as 105 and 130 Nl/min evaporate more or less the same amount of water, and only around 60 g/h more than with 80 Nl/min. To further investigate the accuracy of the calculations and the amount of false air being sucked into the system, a Vaisala HMT 337 sensor was used for the center point test run. The higher value for the measured air temperature at 105 Nl/min is probably caused by this sensor. As the position of the sensor was slightly different as was the measurement method, it cannot be directly compared to the previous measurement method, which was influenced by condensation on the probe. The measurement device has integrated heating, to avoid condensation on the probe, which most probably explains the higher value for the measurements. The shown values are averaged over the last 30 minutes of the process.

The hold-up behavior is shown in Figure 67. The filling time for the higher air flows is around 16 minutes, in contrast to the 18 minutes for the 80 Nl/min test run. It can be seen that the lowest (80 Nl/min) and the highest (130 Nl/min) air flow, behave very similarly during the process, resulting in a total of 690 g on a dry basis. In contrast, 105 Nl/min showed a considerably lower hold-up of 560 g. This indicates that the air flow has a high influence on the flow behavior in the process chamber. Further investigations to optimize the air flow with a minimal hold-up will be performed, after the dryer is completely tight and a suction unit is no longer required to equilibrate the air flow, inducing false air. The calculated false air for the 105 Nl/min test run was 20 Nl/min, based on the temperature and humidity of the outgoing air. This was calculated by multiplying the air flow with the water loading of the outgoing air, and comparing it to the measured evaporation rate. The measurement of the outgoing air gave 50 °C and 60 % humidity, corresponding to 450 g/h of evaporated water at 105 Nl/min. Therefore, a higher air flow must have been present, to evaporate the additional water. The balance was only possible for the 105 Nl/min test run, as no air humidity was measured for the other test runs. The hold-up increase for the test runs over the last 30 minutes was equal to 20 g/h (80 Nl/min), 16 g/h (105 Nl/min) and 42 g/h (130 Nl/min).

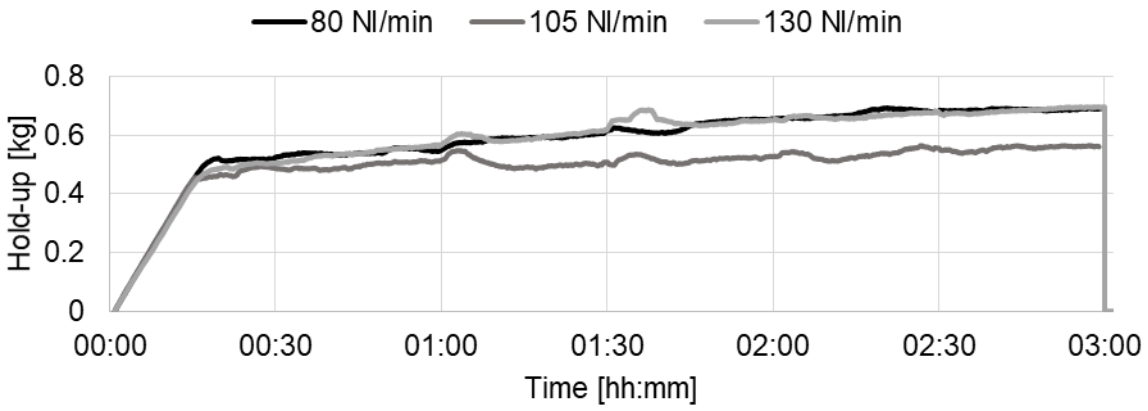

Figure 67. Hold-up profiles of the air-flow variation test runs. The shown data are from the test runs 1 (80 Nl/min), 2 (105 Nl/min) and 3 (130 Nl/min).

The effect of increasing the air flow on the particle size is depicted in Figure 68. It seems like an increased air flow increases the agglomeration tendency during the process slightly. Nonetheless it must be stated that the standard deviations are high, therefore a more or less constant PSD is visible over the process.

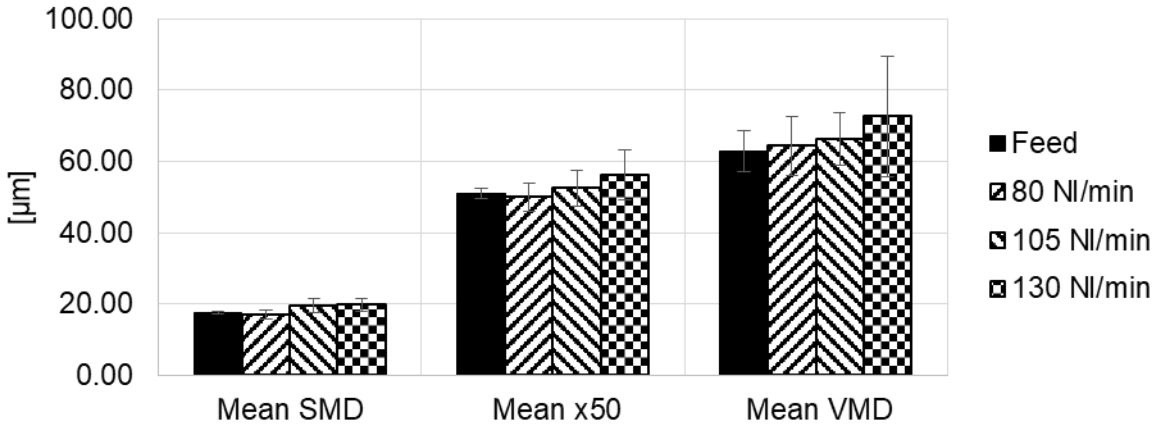

Figure 68. Characteristic PSD values for Ibuprofen: results of air flow influence test runs.

By increasing the air flow, more water could be evaporated, but not in a significant amount. The measurements indicate that the airflow influences the flow within the dryer.

4.4.3 **Mass Flow Influence**

By adapting the mass flow, the drying capacity of the dryer was tested. The feed rate was set at 2 kg/h (Test run 1), 1.5 kg/h (Test run 4), 1 kg/h (Test run 5) and 0.5 kg/h (Test run 6) on a dry basis and the water varied between 857 g/h and 214 g/h, to obtain an initial moisture of 30 wt. % water. The rotor speed was set to 1 rpm and 80 Nl/min of air were used. The set points are summarized in Table 19. The results show that the drying efficiency improves drastically with lower mass flows, as the product of the 1.0 kg/h (dry basis) test run had a residual moisture of 4 wt. %, and the product of the 0.5 kg/h (dry basis) test run was essentially dry, with a residual moisture below 1 wt.%. Again, the calculations were based on the last 30 minutes of each process.

While the product moisture decreases the start-up time increases, as can be seen in Figure 69. The filling times of the higher mass flows are around 18 minutes, while the system with a mass flow of 1 kg/h on a dry basis already needs 34 minutes and the 0.5 kg/h test run takes approximately 70 minutes until the material flow out of the dryer is stable. This can be explained as a certain level of hold-up needs to be reached, and therefore the start-up time significantly increases at lower mass flows. It is also visible that there is no clear correlation between mass flow and hold-up. While the 0.5 and 1.5 kg/h test runs resulted in a comparable hold-up of around 600 g, the 2.0 and 1.0 kg/h test runs showed a slightly higher hold-up of approximately 690 g on a dry basis. This difference can be explained due to other flowability properties and densities at varying moisture levels and temperature. The hold-up increase over the last 30 minutes was between 42 g/h (2.0 kg/h) and 72 g/h (1.5 kg/h).

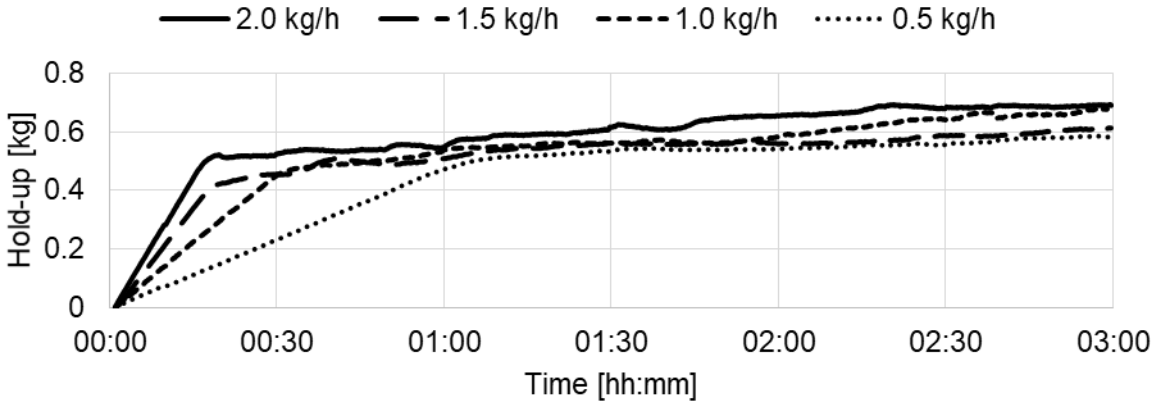

Figure 69. Hold-up profiles during the mass-flow variation test runs. The test runs correspond to test run 1 (2.0 kg/h), test run 4 (1.5 kg/h), test run 5 (1.0 kg/h) and test run 6 (0.5 kg/h).

In Figure 70 the results of the particle size measurements are shown. The VMD tends to be slightly higher for the smaller mass flows, other than that no clear influence of the mass flow on the PSD can be seen.

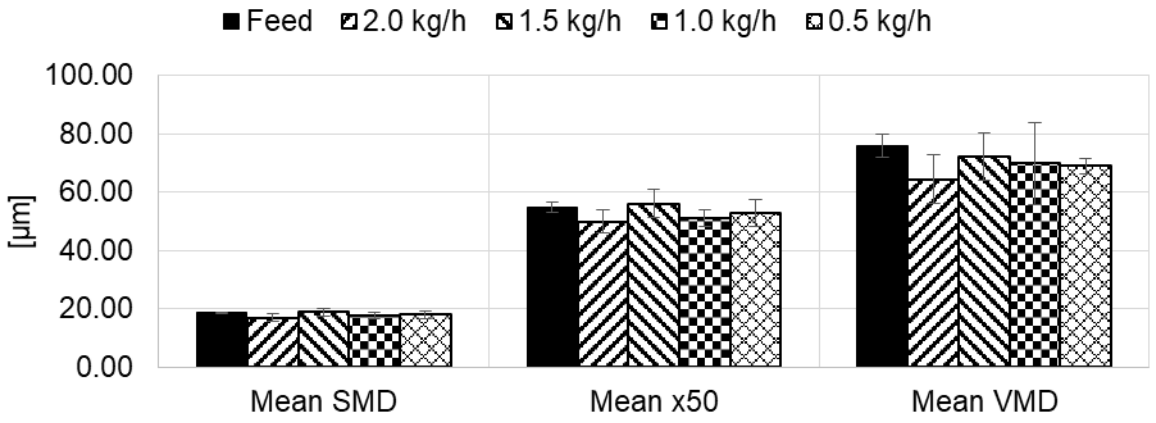

Figure 70. Characteristic PSD values for Ibuprofen: results of mass flow influence test runs.

By lowering the mass flow of Ibuprofen with an initial moisture content of 30 wt. % to 0.717 kg/h on wet basis, the residual moisture of the product could be decreased to below 1 wt. %. This, however, comes at the cost of the filling time of the prototype being prolonged to over one hour. This effect can be overcome by increasing the rotor speed for the filling of the system.

4.4.4 **Temperature Influence**

Another influencing process parameter is the temperature, as it determines the amount of heat which is conducted between the hot steel surfaces and the wet powder. The temperature of the powder can also influence its flow properties[37].[37]. The temperature of the dryer was varied to be 60 °C (Test run 7), 65 °C (Test run 8) and 70 °C (Test run 1) and the temperature of the air was kept at 70 °C, to keep the drying capacity of the ingoing air constant. The rotational speed was set at 1 rpm and the mass flow used corresponded to 2 kg/h on a dry basis. The preheated air flow was set to 80 Nl/min. The influence of the drying temperature is visible in Table 19. Unsurprisingly the temperature of the outlet gas increases at higher drying temperatures, and also more water can be evaporated. The residual moisture of the products was between 22 and 16 wt. %.

A very interesting phenomenon can be observed looking at the hold-up during the processes (Figure 71). While the start-up times are similar between 15 and 20 minutes, the amount of solids in the system at which a stable mass flow out of the drier starts differs

substantially. While at 60 °C only 380 g stay inside, at 65 °C already 430 g and at 70 °C even 510 g on a dry basis stay within the system. This is a strong indication that the powder temperature severely influences the flowability of the product, which decreases when getting closer to the melting point. The powder seems to be stickier, and therefore more is accumulating in the process chamber and the grooves. The lowest hold-up after 3 hours was visible for 65 °C (510 g with a hold-up increase of 20 g/h), followed by 60 °C (570 g with a hold-up increase of 90 g/h) and the already known 690 g (increasing by 20 g/h) from the 70 °C test run.

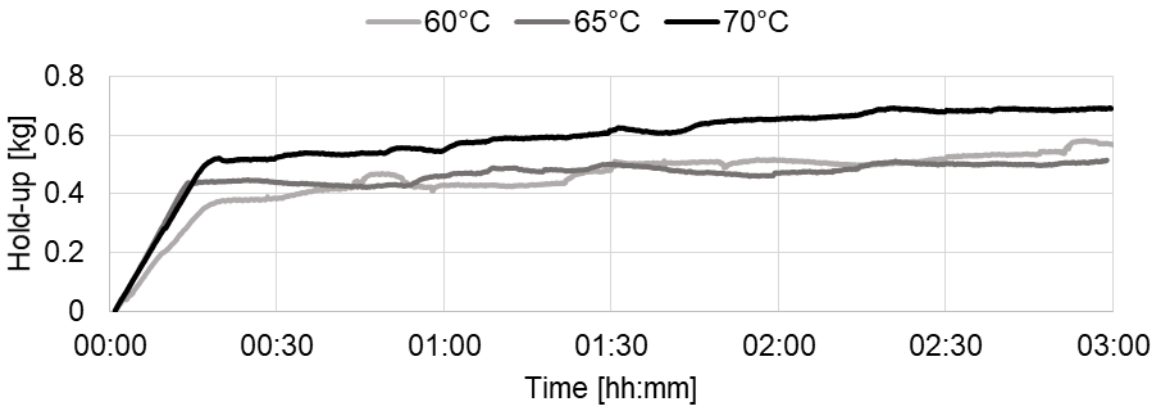

Figure 71. Hold up of the temperature variation test runs. The corresponding test runs are test run 7 (60 °C), 8 (65 °C) and 1 (70 °C).

Looking at the particle size results (Figure 72), it is visible that the process temperature does not influence the particle size after drying, as all results are within the respective standard variations.

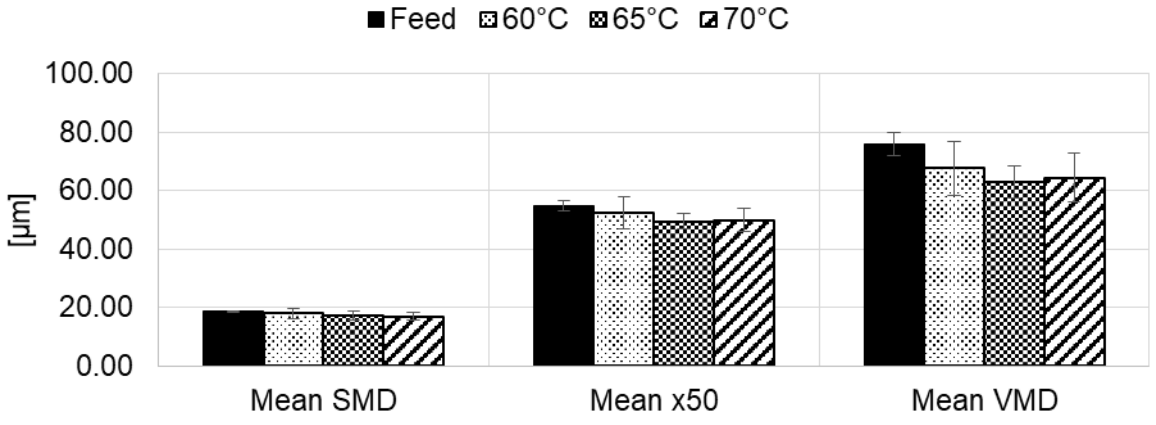

Figure 72. Characteristic PSD values for Ibuprofen: results of temperature variation test runs.

In general, higher temperatures lead to a lower residual moisture, but do not have a strong influence. Also, the higher the temperature, the more hold-up was generated for the tested temperatures.

4.4.5 **Inlet Moisture Variation**

Another investigated factor was the influence of the initial moisture of the material. As the thermal properties, as well as the electrostatic behavior, vary depending on the amount of water present, the water was varied to be 10 wt. % (Test run 10), 20 wt. % (Test run 9) and 30 wt. % (Test run 1), at 2 kg/h mass flow on a dry basis. The rotational speed was 1 rpm and the air flow was set to 80 Nl/min. The remainder of the process parameters and the relevant results are shown in Table 19. For the test runs with 20 and 10 wt. % moisture content, the evaporated water was calculated as if the mass flow out of the dryer was constant at 2 kg/h of dry solids. As it is visible in Figure 73, no stable hold-up plateau was reached for these test runs, therefore the usual calculation would result in a large error.

Regarding the hold-up curves in Figure 73, it is obvious that reducing the inlet moisture has a negative influence on the process stability. In this case, a lot of tribocharging was visible, and therefore more material accumulated in the process chamber. This could also explain the longer filling times for the lower initial moistures. In comparison to the 18 minutes filling time of the 30 wt. % test run, it took 20 minutes for the 20 wt. % test run and around 25 minutes for the 10 wt. % test run. For the 10 wt. % test run, the hold-up was still increasing significantly until the process end (154 g/h). After 1 hour and 50 minutes of process time the process was stopped due to severe mass flow fluctuations at the outlet, to avoid blockage of the system. These fluctuations were caused by material accumulations above the outlet due to tribocharging. For the 20 wt. % test run, tribocharging was also an issue, however not as severe as for 10 wt. %. This shows in a more or less periodic in- and decrease of the hold-up (increasing by 160 g/ based on the last 30 minutes of the process). During the decrease larger amounts of the accumulated material broke free, therefore reducing the hold-up.

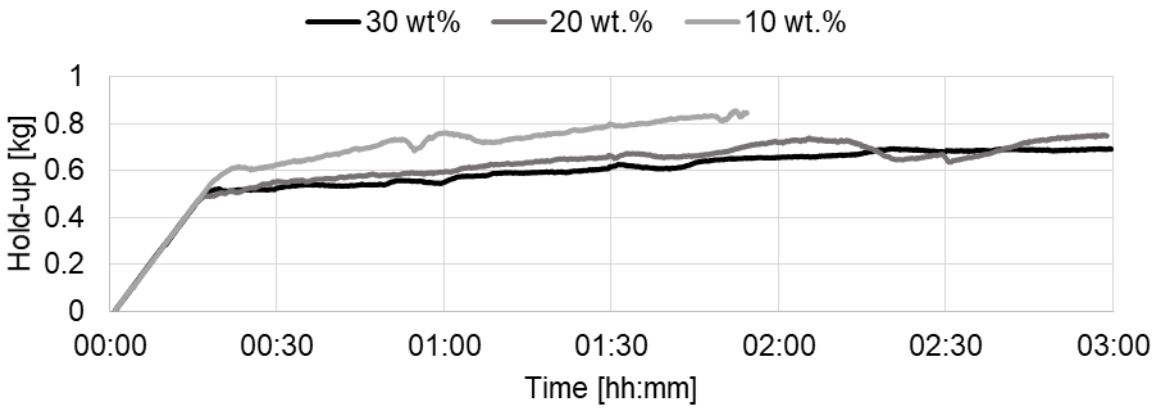

Figure 73. Hold-up profiles of the inline moisture variation test runs. The corresponding test runs are test run 1(30 wt. %), 9 (20 wt. %) and 10 (10 wt. %)

In contrast to the previous test runs, a change of the particle size was visible for the reduced inlet moisture contents (Figure 74). Each measurement is shown next to the relevant feed material. It can be seen that all diameters decrease with decreasing moisture content. This might indicate that attrition occurs, possibly also leading to the tribocharging caused by the increased friction.

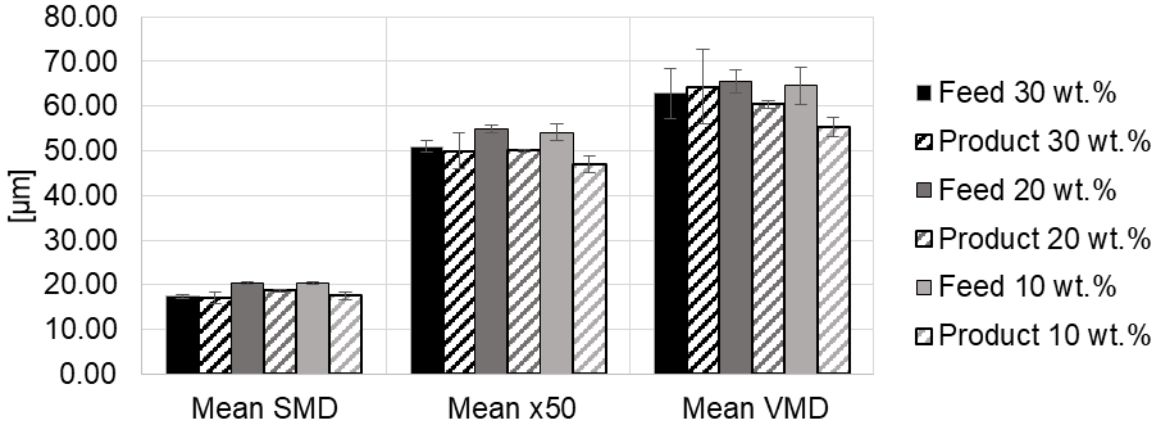

Figure 74. Characteristic PSD values for Ibuprofen: results of inlet moisture variation test runs.

By lowering the initial moisture of the feed material, more accumulations and tribocharging inside the process chamber could be observed. Therefore, it is advised for this setup to have high inlet moistures to minimize the adverse effects.

4.4.6 **RPM Variation**

For these test runs the rotational speed was varied and set to 1 rpm (Test run 1), 3 rpm (Test run 11) and 5 rpm (Test run 12) of the big rotor respectively. The other process parameters, such as the air flow (80 Nl/min) and mass flow (2 kg/h on a dry basis), were not changed. A summary of the configuration and the shaft speeds is visualized in Table 19. The test run with a rotor speed of 5 rpm was stopped early due to problems with the data acquisition. For the calculation of the evaporated water the last 30 minutes of each process were taken.

It is visible in Figure 75 that with higher speeds, material is ejected from the dryer faster, however not to the same extent. Therefore, an increase of the rotor speed by factor 5, only reduced the fill-up time from 18 to 12 minutes, and to 16 minutes with a rotor speed of 3 rpm. The hold-up is less for higher speeds, as the grooves are not filled as much anymore, and material is flowing faster through the dryer. For the 5 rpm test run, the hold-up started to increase, as the high rotor speed led to accumulations due to charging of the Ibuprofen particles.

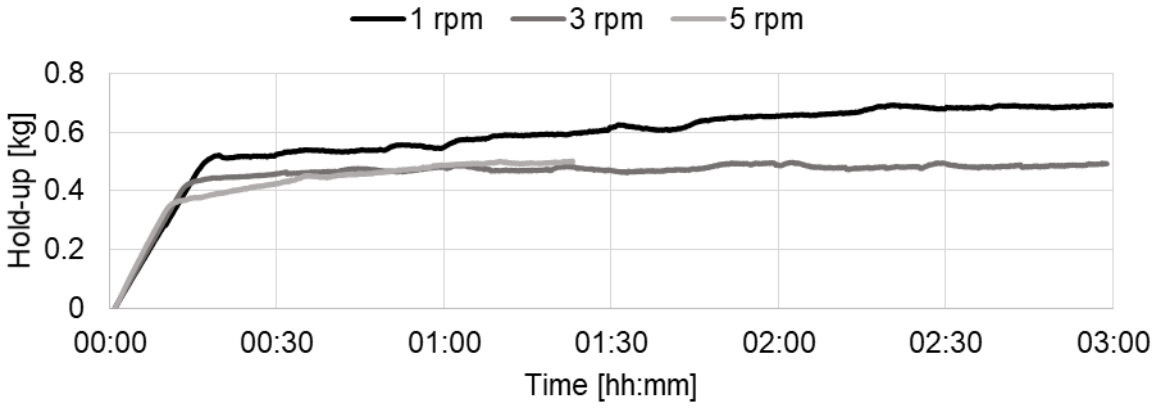

Figure 75. Hold-up of the rpm-variation test runs at 30 wt. % initial moisture. The corresponding test runs are 1 (1 rpm), 11 (3 rpm) and 12 (5 rpm).

The PSD results of the test runs are visible in Figure 76. While the PSD decreases for 3 rpm, no significant change is visible for the 5 rpm test run. This might be due to the shorter processing time of the 5 rpm test run. Regardless, the results from the 3 rpm test run indicate that increasing the rotational speed might lead to attrition and therefore an effect on the final product. This needs to be confirmed with more test runs in the future.

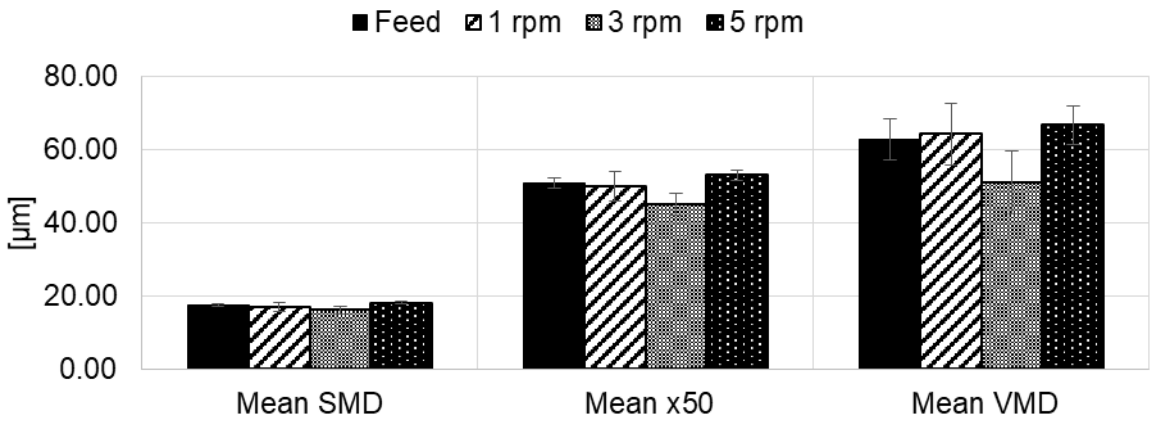

Figure 76. Characteristic PSD values for Ibuprofen: results of rotational speed variation test runs.

By elevating the rotational speed of the dryer rotor, more accumulations and tribocharging inside the process chamber could be observed. Therefore, it is advised to keep the rotational speed as low as possible.

4.4.7 **Drying Capacity Estimations**

To estimate the governing influences on the drying performance, three test runs were performed. In the first one, the dryer was not heated up additionally, and only the preheated air was blown into the dryer as a drying agent (Test run 13). In the second test run, the filter and the top were heated additionally, so that no condensation could occur and to have an estimate where the necessary heat for evaporation is conducted (Test run 14). In the final test run, which was conducted directly after test run 15, the process air was turned off, and the dryer was heated up to 70 °C (Test run 15). In this way it was investigated how much moisture could be removed by just exposing the heated powder to the air inside the process chamber, and the short distance after the outlet, before being measured. All test runs were performed with 2 kg/h on a dry basis and a rotational speed of 1 rpm. Looking at the results in Table 19, it can be seen that the influence of the process air on the drying performance is minimal in comparison to the heat conduction. In the first test run, only 88 g could be evaporated by the process air. By adding heat at the top and the filter, more (144 g) could be evaporated. After heating up the whole system and turning off the process air, even more water was removed, just by diffusion and the small contact area after the outlet with the surrounding air. This is a strong indication that the drying mechanism is mainly conduction, and the drying agent is only needed to remove the moisture from the process chamber. From the different hold-up levels over time (Figure 77) it is visible that the configuration

without heating has a higher hold-up (836 g) than the configuration where only the top of the dryer and the filter was heated (564g). This might be due to a possible flowability change on the top of the rotor at elevated temperatures as also indicated by the results of the temperature variation. A very interesting phenomenon is visible at the test run without process air, and only a heated system. After the rotor heating was turned on and the process air was turned off (after 3 hours of the previous test run with process air and a turned-on filter heating) the hold-up increased by approximately 150 g until the desired temperature level was reached after approximately 3 hours and 40 minutes. This indicates, as already shown at the temperature test runs, that Ibuprofen tends to become more adhesive at higher temperatures.

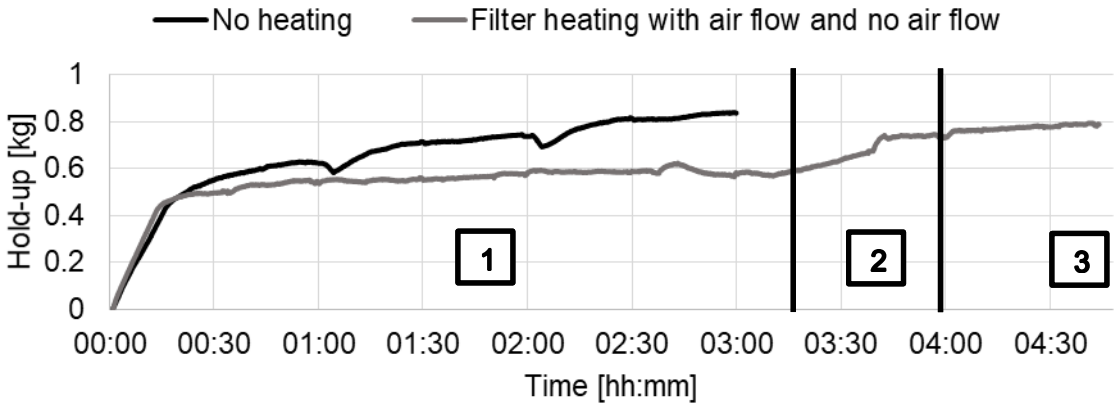

Figure 77. Hold-up profiles of the drying capacity test runs. Corresponding test runs are 13 (no heating, air flow), 14 (top and filter heating, air flow) and 15 (heating, no air flow). The stage 1 corresponds to test run 14, stage 2 is the heating up of the system and stage 3 is test run 15.

As the tested configurations do not represent intended drying processes, no PSD measurements are included for these test runs.

4.4.8 **Long Term Test Run + Refeed Experiment**

After the screening test runs previously described, a long-term experiment followed by refeeding test runs were undertaken. This was to evaluate the stability of the process over a long time period, as well as to see the influence of refeeding the material. To have sufficient material, the second test run was also conducted over a longer time period. The goal was to obtain a product with a residual moisture below 1 wt. % of water. The mass flow was set to 1.5 kg/h on a dry basis and the inserted airflow was 80 Nl/min. The process set points and corresponding results are

shown in Table 19. To be able to evaluate morphology changes of the Ibuprofen, samples were taken after the test runs and analyzed via SEM. It is visible that the evaporated water decreases with decreasing inlet moisture, but after the third processing of the material, dry material with a residual moisture around 0.2 wt. % could be obtained. With decreasing residual moisture of the product, the temperature of the outlet gas increases.

In Figure 78 the hold-ups of the different processes are shown over time. It is clearly visible that the test run with highest initial moisture (31 wt. %) resulted in the lowest and most stable hold-up. The fill-up period of this test run lasted around 20 minutes, after which around 480 g of dry Ibuprofen had accumulated within the system. At the process end, the total hold-up amounted to 692 g, which results in a total hold-up increase rate of 21.9g/h over the 9 hours and 40 minutes process duration. The hold-up increase shown in Table 19 is based on the last 30 minutes of each process. Since the amount of hold-up fluctuated towards the end, it is assumed that a plateau was reached at around 680 g of dry Ibuprofen for this process configuration. For the first re-feeding test run another process behavior was observed. The filling time was 24 minutes in which 570 g of dry material deposited in the process chamber. For this test run the hold-up increase was significantly higher with 221 g/h until the process end after 4 hours and 50 minutes. Additionally, the hold-up curve towards the end (after 3 hours of process time) showed exponential growth characteristics, which could eventually lead to a blockage of the dryer. The third test run, where the material was refed the second time, had a filling time of ~34 minutes, with a corresponding hold-up of 670 g of dry Ibuprofen. The calculated hold-up increase until the end of the process was 90 g/h, resulting in a total hold-up of around 890 g, which was very close to the hold-up at this processing time of the first re-feeding test run (870 g). This is an additional indication that lower initial moistures (and therefore higher product temperature) lead to a worse process behavior. Nonetheless, it was shown that the system works for up to 10 hours of processing time. It must be further investigated if the worse process behavior during the refeeding test runs is due to the reprocessing of the material or the lower moisture contents.

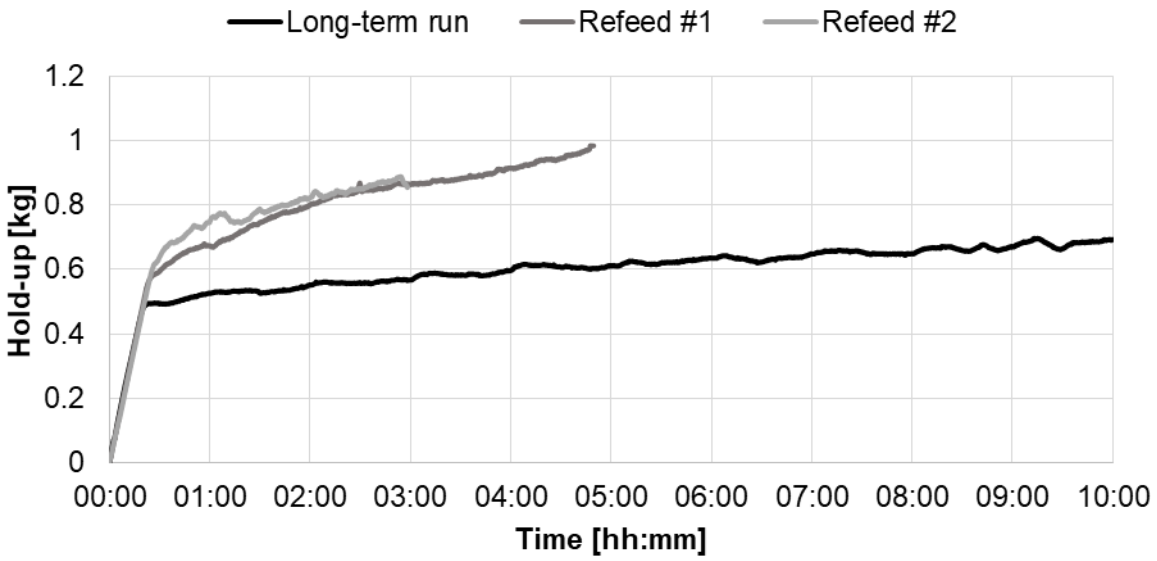

Figure 78. Hold-up results of the long-term and re-feeding test runs. The corresponding test runs are 16 (long-term run), 17 (refeed #1) and 18 (refeed#2).

The PSD measurements visible in Figure 79 show contradicting results. While the SMD and x50 indicate no or very small change of the particle size, the VMD decreases with each processing cycle. To further evaluate this influence, SEM-measurements were made to investigate the change of the particle morphology during processing.

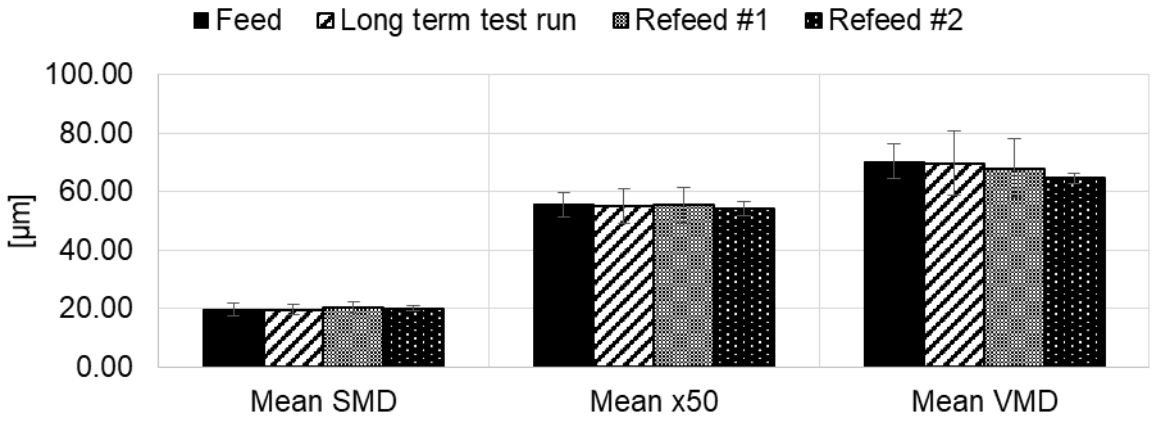

Figure 79. Characteristic PSD values for Ibuprofen: Long term and refeeding test runs.

The results of these SEM-measurements can be seen in Figure 80. While the initial feed has a rather smooth, rounded surface, the obtained product has rather sharp edges, and some fines adhering to larger particles are visible. These fines could explain the decrease of the VMD for the PSD measurements. In general, however, even though the surface seems to be affected

by the processing, the particles are not severely changed by the process. For future experiments, the dissolution behavior before and after the test runs could be analyzed to quantify the impact on the bioavailability of the substance.

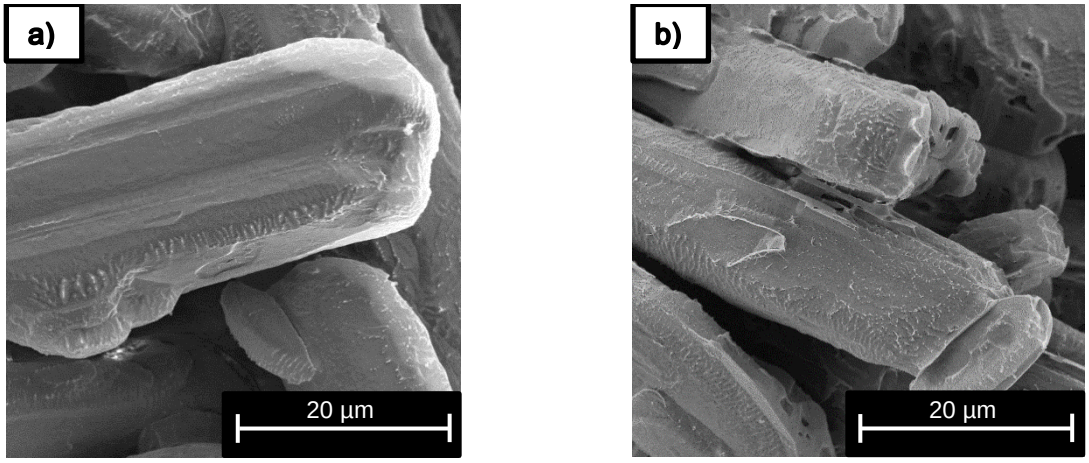

Figure 80.. SEM-images of the feed (a) and the product after being processed in the dryer for three times (b).

The drying capacity test runs indicated that the water is evaporated mainly by conduction, and the drying agent is only needed to transport the moisture away, which might explain the small influence of the amount of drying air on the drying efficacy. By investigating the long-term test run and the two subsequent refeeding test runs, it is visible again that lower initial moisture has a negative impact on the process behavior. The SEM and PSD measurements indicate that a small amount of fines are produced during processing.

4.4.9 **Material Influence**

It was assumed that the influence of the flow properties of the material for this drying technology is substantial. Therefore, two screening test runs were performed, one with di-calcium phosphate (Test run 19 in Table 19) and one with Ibuprofen (Test run 1). To account for the density difference between the materials, the mean factor between bulk and tapped density was computed, for the raw materials, as well as the materials at 10, 20 and 30 wt. % moisture content. The average of these factors was subsequently calculated, being 1.9^6. This procedure was chosen, as neither the true density nor the moisture profile inside the dryer was known previously, and by using this approach the filling degree of the grooves was assumed to remain constant. Therefore, the mass flow of di-calcium phosphate was set to 3.8 kg/h, in contrast to the 2 kg/h test run with ibuprofen. The amount of water present was the same for both test runs (857 g/h). Both

test runs were performed at a rotational speed of 1 rpm of the big rotor, and the speed of the outlet rotary valve was set to the maximum, being 6 times as high. The temperature of the process was elevated for the di-calcium phosphate, as it only decomposes at around 370 °C, to maximize the heat transfer to the powder.

A summary of the obtained results of the two test runs is shown in Table 19 (Test runs 1 and 19). The most obvious difference is the higher evaporation rate for di-calcium phosphate, being 205 g/h higher than for Ibuprofen. This can be explained by the higher drying temperature, and therefore more energy for the evaporation. The results are calculated over the last 30 minutes of the process.

The resulting hold-up profiles of the material influence test runs are shown in Figure 81. The filling times vary from 10 minutes (di-calcium phosphate) to 18 minutes (Ibuprofen). It can be seen that the Ibuprofen test run reaches a hold-up plateau after approximately 20 minutes at 510 g, which then increases to 4694 g after a process time of 3 hours. The di-calcium phosphate system reaches a similar plateau after only 2 hours and 20 minutes, at 1.804 kg on a dry basis. Correcting this amount with the same density factor (1.9) as before, leads to a comparable hold-up of approximately 947 g of Ibuprofen. Therefore, more volume of the drying chamber is filled with di-calcium phosphate. This can be explained by the accumulation of powder at the inlet-opposing side of the rotor. This material was visible after the test run and was probably blown out of the grooves by the entering process air. As the process air is warmer in the di-calcium phosphate setup, the volumetric flow is slightly higher, and thus the air velocity in the system is increased. This might also explain the long duration until a hold-up plateau was reached.

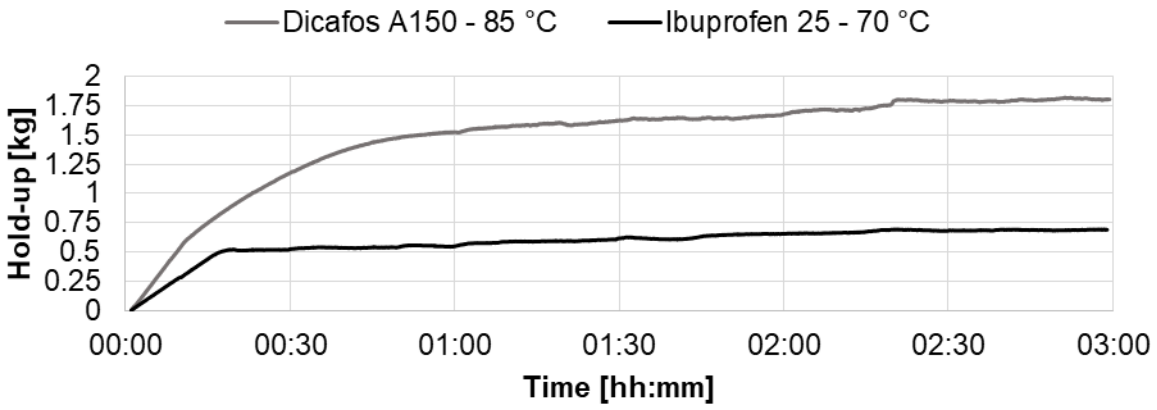

Figure 81. Hold-up results during the compared test runs with Ibuprofen (Test run 1) and di-calcium phosphate (Test run 19).

The results of the particle size measurements are depicted in Figure 82. The Sauter mean diameter (SMD), x50 and volumetric mean diameter (VMD) are shown for the feed and the product. While the Ibuprofen PSD remains more or less constant, an increase of the particle size is visible for di-calcium phosphate. This might be explained by the accumulations in the system, as fines could be accumulating. Further test runs and analyses have to be performed to investigate this effect.

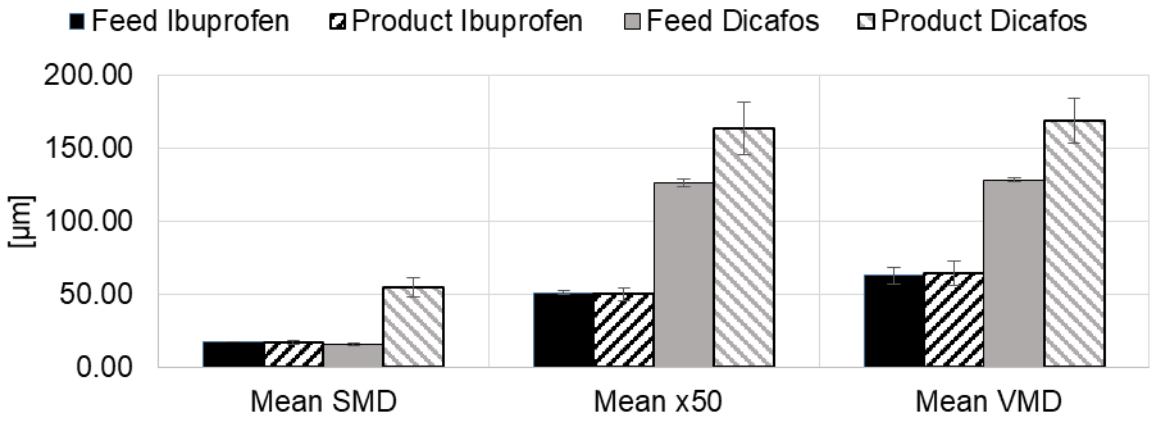

Figure 82. PSD results of the material influence test runs.

The SEM-images for di-calcium phosphate (Figure 83b) do not indicate a change in the PSD due to attrition or agglomeration, however the small amount of particles investigated has to be considered. For Ibuprofen, no change is visible (Figure 83a), compared to the raw material (Figure 59a).

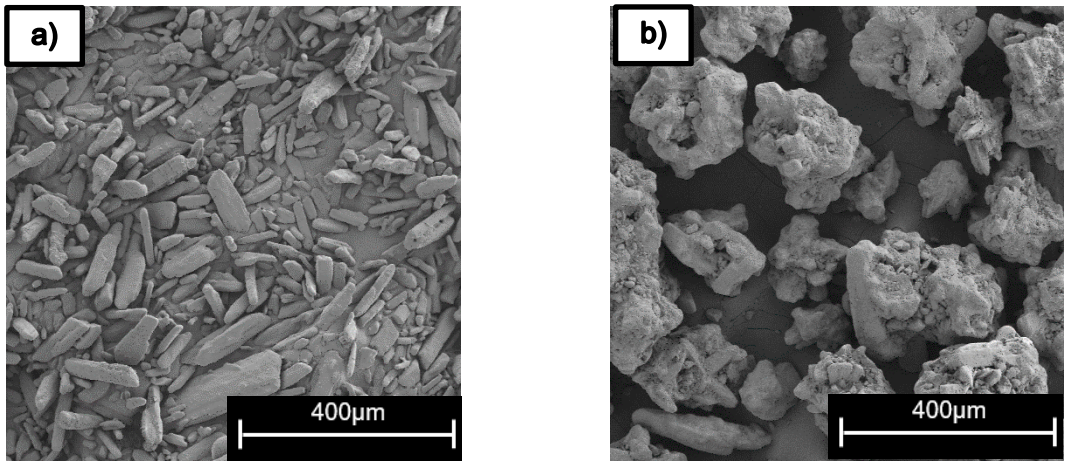

Figure 83. SEM-measurements of Ibuprofen (a) and di-calcium phosphate (b) after the test runs.

The comparison test run between di-calcium phosphate and Ibuprofen show that more water can be evaporated for the di-calcium phosphate system, possibly due to the higher drying temperature. On the other hand, the PSD of di-calcium phosphate increases during drying, while the Ibuprofen particles show more or less the same particle size throughout the experiments.

Table 19. Process parameters and results for the characterization of the influence of various process parameters. Temperatures marked with an asterisk (*) are measured with a Vaisala HMT337, in contrast to a Pt-100 temperature sensor. Evaporated water values marked with an [§] are calculated with an assumed mass-flow out of the dryer being equal to the inlet mass flow. For the drying capacity test run marked with [¥] the first value corresponds to the temperature of the rotor and the trough, and the latter for the filter and the top of the drying chamber. All hold-up increases are calculated over the last 30 minutes of each process.

Test Run [-]	Material [-]	Duration [hh:mm]	Temperature dryer [°C]	Temperature air [°C]	Mass flow wet [kg/h]	Mass flow dry [kg/h]	Rotor rotation speed [RPM]	Air flow [Nl/min]	Temperature outlet gas [°C]	Evaporated water [g/h]	Residual moisture [wt. %]	Hold-up [kg]	Hold-up change [g/h]
1	Ibuprofen 31wt.%	03:00	70	70	2.857	2.0	1	80	44	483	16	0.694	20
2	Ibuprofen 30wt.%	03:00	70	70	2.857	2.0	1	105	50*	542	14	0.563	16
3	Ibuprofen 29wt.%	03:00	70	70	2.857	2.0	1	130	43	541	13	0.698	42
4	Ibuprofen 29wt.%	03:00	70	70	2.143	1.5	1	80	45	467	10	0.677	72
5	Ibuprofen 29wt.%	03:00	70	70	1.429	1.0	1	80	44	403	4	0.613	54
6	Ibuprofen 31wt.%	03:00	70	70	0.714	0.5	1	80	43	220	0.5	0.581	52
7	Ibuprofen 32wt.%	03:00	60	70	2.857	2.0	1	80	41	366	22	0.566	90
8	Ibuprofen 29wt.%	03:00	65	70	2.857	2.0	1	80	42	417	16	0.512	20

9	Ibuprofen 22wt.%	03:00	70	70	2.5	2.0	1	80	50*	390[§]	7	0.746	160
10	Ibuprofen 10wt.%	01:50	70	70	2.222	2.0	1	80	48*	212[§]	0.8	0.847	154
11	Ibuprofen 30wt.%	03:00	70	70	2.857	2.0	3	80	44	414	18	0.492	6
12	Ibuprofen 30wt.%	01:25	70	70	2.857	2.0	5	80	46	401	18	0.500	60
13	Ibuprofen 30wt.%	03:00	-	70	2.857	2.0	1	80	23*	88	27	0.836	50
14	Ibuprofen 31wt.%	03:00	-/70[¥]	70	2.857	2.0	1	80	45*	144	27	0.564	-46
15	Ibuprofen 31wt.%	01:30	70	-	2.857	2.0	1	-	-	157	27	0.789	44
16	Ibuprofen 31wt.%	10:00	60	70	2.148	1.5	1	80	44*	311	17	0.692	40
17	Ibuprofen 17wt.%	04:50	60	70	1.808	1.5	1	80	45*	233	5	0.985	150
18	Ibuprofen 5wt.%	03:00	60	70	1.568	1.5	1	80	47*	68	0.2	0.855	12
19	Dicafos 19wt.%	03:00	85	70	4.657	3.8	1	80	51	688	6	1.804	12

4.5 Conclusion and Outlook

The present work deals with the influence of several process parameters and two different test substances on a novel drying device, issued under the patent NL2020740B1. In general, it was shown that the new drying technology is capable of drying cohesive materials in a continuous way, with only minor effects on the particle morphology. Independent of the process parameters, the particle size distribution remains more or less constant for all investigated processes, showing no signs of agglomeration and only minor attrition occurring. The existing equipment is able to continuously dry Ibuprofen with an initial moisture content of 30 wt. % to below 1 wt. %, at a mass flow of 0.5 kg/h on a dry basis.

The process itself is very robust, as the alteration of different process parameters only showed slight effects on the drying efficacy. Even without a vacuum being applied, the drying of thermosensitive materials is possible with this drying principle. The used model substance Ibuprofen shows very poor flow behavior, which further decreases at higher temperatures. A significant improvement of the process will likely be observable when running the process under vacuum, as lower drying temperatures can be used. An issue to overcome is the occurring tribocharging, which can lead to a blockage of the outlet in the worst case. At the moment, the use of moist materials and low rotational speeds shows a better process behavior.

By further improving the equipment in a vacuum tight way and optimizing the flow behavior within the process chamber, a further improvement of the drying efficacy is expected. Thereby, the driving force for the drying process (i.e. the difference between the partial pressure of the solvent within the drying agent to the vapor pressure at saturation) is elevated. As the air flow variations showed a strong influence on the accumulating hold-up, special considerations must be taken at low pressure levels. Very low air flows already have a large volumetric flow under vacuum, therefore optimization possibilities of the equipment at low vacuum levels need to be investigated. Additionally, the drying performance is usually much higher at low pressures, due to the lower boiling point of the solvents. This should lead to an increase of evaporated solvent, and thereby of the maximum mass flow capacity of the system.

This will be investigated in future work, as well as the possibility to dry directly after mechanical filtration and obtain a dry powder afterwards. By implementing a possibility of directly connecting the thickened suspension after a filtration process to the dryer, a truly continuous process could be achieved. This technology shows great potential to make the continuous production of API’s possible in the future.

4.6 Nomenclature

ffc	Flow function
H_2O	Water
$Hold-up_{dry}$	Hold-up on a dry basis / kg
m	Sample mass / g
$\dot{m}_{dried,out,i}$	Dried mass flow out of the system in time step i / kg/h
$\dot{m}_{evap}$	Mass flow of evaporated water / kg/h
m_{dry}	Dry mass / g
m_{wet}	Wet mass / g
$\dot{m}_{wet,in,i}$	Wet mass flow into the system in time step i / kg/h
SMD	Sauter mean diameter / µm
VMD	Volume mean diameter / µm
w	Weight percent of water within the feed/product / %
w_{feed}	Weight percent of water in the feed / %
$w_{product}$	Weight percent of water in the product / %

4.7 Abbreviations

API	Active pharmaceutical ingredient
BASF	Badische Anilin- & Soda-Fabrik
PSD	Particle size distribution
PTFE	Polytetrafluorethylen
M	Motor mixer
PI	Pressure indicator
RTD	Residence time distribution
SE	Specific energy
SEM	Scanning electron microscope

Teflon	Polytetrafluorethylen
TI	Temperature indicator
TC	Temperature control
PR	Pressure regulator

4.8 Acknowledgements

This work has been funded within the Austrian COMET Program under the auspices of the Austrian Federal Ministry of Transport, Innovation and Technology (BMVIT), the Austrian Federal Ministry of Economy, Family and Youth (BMWFJ) and by the State of Styria (Styrian Funding Agency SFG). COMET is managed by the Austrian Research Promotion Agency FFG. We acknowledge the support of Sarah Koller, Jelena Milinkovic, Daniel Wiegele and Patrick Vorraber (All RCPE).

References

(1) FDA. Guidance for Industry PAT: A Framework for Innovative Pharmaceutical Development, Manufacuring, and Quality Assurance; 2004.

(2) FDA. Pharmaceutical CGMPs for the 21s Century - A Risk-Based Approach. FDA Off. Doc. 2004, No. September, 32.

(3) Plumb, K. Continuous Processing in the Pharmaceutical Industry. Chem. Eng. Res. Des. 2005, 83, 730–738.

(4) Kreimer, M.; Aigner, I.; Lepek, D.; Khinast, J. Continuous Drying of Pharmaceutical Powders Using a Twin-Screw Extruder. Org. Process Res. Dev. 2018, 22, 813–823.

(5) Burcham, C. L.; Florence, A. J.; Johnson, M. D. Continuous Manufacturing in Pharmaceutical Process Development and Manufacturing. Annu. Rev. Chem. Biomol. Eng. 2018, 9, 253–281.

(6) Zettl, M.; Aigner, I.; Hauser, C.; Mannschott, T.; van der Wel, P.; Schröttner, H.; Khinast, J. G., Krumme, M.; Establishing the Missing Link: Development of a Dryer Suitable for Continuous Processing of Cohesive Materials. Journal of Pharmaceutical Innovation, submitted. 2021.

(7) Vaxelaire, J.; Bongiovanni, J. M.; Puiggali, J. R. Mechanical Dewatering and Thermal Drying of Residual Sludge. Environ. Technol. (United Kingdom) 1999, 20, 29–36.

(8) Gursch, J.; Hohl, R.; Toschkoff, G.; Dujmovic, D.; Brozio, J.; Krumme, M.; Rasenack, N.; Khinast, J. Continuous Processing of Active Pharmaceutical Ingredients Suspensions via Dynamic Cross-Flow Filtration. J. Pharm. Sci. 2015, 104, 3481–3489.

(9) Gursch, J.; Hohl, R.; Dujmovic, D.; Brozio, J.; Krumme, M.; Rasenack, N.; Khinast,

J. Dynamic Cross-Flow Filtration: Enhanced Continuous Small-Scale Solid-Liquid Separation. Drug Dev. Ind. Pharm. 2016, 42, 977–984.

(10) Li, M.; Gogos, C. G.; Ioannidis, N. Improving the API Dissolution Rate during Pharmaceutical Hot-Melt Extrusion I: Effect of the API Particle Size, and the Co-Rotating, Twin-Screw Extruder Screw Configuration on the API Dissolution Rate. Int. J. Pharm. 2015, 478, 103–112.

(11) Gursch, J.; Hohl, R.; Armenante, M. E.; Dujmovic, D.; Van Der Wel, P.; Brozio, J.; Krumme, M.; Rasenack, N.; Khinast, J. Continuous Drying of Small Particles for Pharmaceutical Applications - An Evaluation of Selected Lab-Scale Systems. Org. Process Res. Dev. 2015, 19, 2055–2066.

(12) Mujumdar, A. S. Handbook of Industrial Drying; Mujumdar, A. S., Ed.; CRC Press, 2014.

(13) Keey, R. B. Drying of Loose and Particulate Materials. Dry. Technol. 1992, 10, 1139–1141.

(14) Bemrose, C. R.; Bridgwater, J. A Review of Attrition and Attrition Test Methods. *Powder Technology*. 1987.

(15) Neil, A. U.; Bridgwater, J. Attrition of Particulate Solids under Shear. Powder Technol. 1994.

(16) Bravi, M.; Di Cave, S.; Mazzarotta, B.; Verdone, N. Relating the Attrition Behaviour of Crystals in a Stirred Vessel to Their Mechanical Properties. Chem. Eng. J. 2003.

(17) Hare, C.; Ghadiri, M.; Dennehy, R. Prediction of Attrition in Agitated Particle Beds. Chem. Eng. Sci. 2011.

(18) Bika, D. G.; Gentzler, M.; Michaels, J. N. Mechanical Properties of Agglomerates. Powder Technol. 2001, 117, 98–112.

(19) MacLeod, C. S.; Muller, F. L. On the Fracture of Pharmaceutical Needle-Shaped Crystals during Pressure Filtration: Case Studies and Mechanistic Understanding. Org. Process Res. Dev. 2012, 16, 425–434.

(20) Kowalski, S. J.; Rajewska, K.; Rybicki, A. Destruction of Wet Materials by Drying. Chem. Eng. Sci. 2000, 55, 5755–5762.

(21) Bemrose, C. R.; Bridgwater, J. A Review of Attrition and Attrition Test Methods. Powder Technol. 1987, 49, 97–126.

(22) Gahn, C.; Krey, J.; Mersmann, A. The Effect of Impact Energy and the Shape of Crystals on Their Attrition Rate. J. Cryst. Growth 1996, 166, 1058–1063.

(23) Schæfer, T.; Mathiesen, C. Melt Pelletization in a High Shear Mixer. VII. Effects of Product Temperature. Int. J. Pharm. 1996, 134, 105–117.

(24) Seville, J. P. K.; Willett, C. D.; Knight, P. C. Interparticle Forces in Fluidisation.Pdf. 2000, 261–268.

(25) Papadakis, S. E.; Bahu, R. E. The Sticky Issues of Drying. Dry. Technol. 1992, 10,

817–837.

(26) Birch, M.; Marziano, I. Understanding and Avoidance of Agglomeration during Drying Processes: A Case Study. Org. Process Res. Dev. 2013, 17, 1359–1366.

(27) Kreimer, M.; Aigner, I.; Sacher, S.; Krumme, M.; Mannschott, T.; van der Wel, P.; Kaptein, A.; Schroettner, H.; Brenn, G.; Khinast, J. G. Mechanical Strength of Microspheres Produced by Drying of Acoustically Levitated Suspension Droplets. Powder Technol. 2018, 325, 247–260.

(28) Garzón, L. C.; Martínez, F. Temperature Dependence of Solubility for Ibuprofen in Some Organic and Aqueous Solvents. J. Solution Chem. 2004, 33, 1379–1395.

(29) Rasenack, N.; Müller, B. W. Ibuprofen Crystals with Optimized Properties. Int. J. Pharm. 2002, 245, 9–24.

(30) Hentzschel, C. M.; Sakmann, A.; Leopold, C. S. Comparison of Traditional and Novel Tableting Excipients: Physical and Compaction Properties. Pharm. Dev. Technol. 2012, 17, 649–653.

(31) Reinwald, G.; Zimmermann, I. A Combined Calorimetric and Semiempirical Quantum Chemical Approach to Describe the Solution Thermodynamics of Drugs. J. Pharm. Sci. 1998, 87, 745–750.

(32) Co, J. C. Safety Data Sheet: Calcium Phosphate Dibasic, Anhydrous https://www.jostchemical.com/documentation/SDS/Calcium Phosphate Dibasic, Anhydrous (7757-93-9).pdf (accessed Oct 8, 2019).

(33) Schulze, D. Powders and Bulk Solids, 1st ed.; Springer Berlin Heidelberg: Berlin, Heidelberg, 2007.

(34) Di, Y. Y.; Ye, C. T.; Tan, Z. C.; Zhang, G. D. Low-Temperature Heat Capacity and Standard Molar Enthalpy of Formation of Crystalline (S)-(+)-Ibuprofen (C13H18O2)(S). Indian J. Chem. - Sect. A Inorganic, Phys. Theor. Anal. Chem. 2007, 46, 947–951.

(35) Water - Specific Heat https://www.engineeringtoolbox.com/specific-heat-capacity-water-d_660.html (accessed Jan 13, 2020).

(36) Kruisz, J.; Rehrl, J.; Sacher, S.; Aigner, I.; Horn, M.; Khinast, J. G. RTD Modeling of a Continuous Dry Granulation Process for Process Control and Materials Diversion. Int. J. Pharm. 2017, 528, 334–344.

(37) Tomasetta, I.; Barletta, D.; Poletto, M. Correlation of Powder Flow Properties to Interparticle Interactions at Ambient and High Temperatures. Particuology 2014, 12, 90–99.

„An expert is a man who has made all the mistakes which can be made in a very narrow field."
Niels Bohr (1885-1962)

5 Summary and Conclusion

In chapter 1 an overview of the current situation in the pharmaceutical industry is given. An introduction of the relevant topics, which are the basis of the research, are presented in chapters 2-4. The main addressed points are the standing of continuous manufacturing in pharmaceutical processes, as well as the primary and secondary manufacturing chain. Thereby, the differences between batch and continuous production are explained, as well as the integration into primary and secondary manufacturing routes. Furthermore, the pharmaceutical unit operations of purification and drying are investigated in more detail, and commonly used methods to characterize materials and their flow properties are presented.

The second chapter deals with the possibility of a continuous washing strategy within precipitating environments. Based on previous work performed with static mixers, a novel technique is proposed: performing the mixing within an ultrasonic process chamber. Therefore, a suspension of solids within their respective saturated solution was mixed with an anti-solvent, shifting the solubility and precipitating solids from the solution. The investigation of different process parameters shows that the PSD of lactose is increasing, while the Ibuprofen samples do not show such an effect. The process behavior of both substances is substantially different; while lactose adheres to the metal surface, Ibuprofen shows foam build-up within the process chamber. Breakage of particles cannot be observed for this study. The positive influence of ultrasound on the process stability is confirmed in this work, showing that once a certain threshold of power intake is reached, no agglomerates form within the system. In contrast, cooling the system increases the yield but decreases the stability of the process. The ideal initial solid loading is found to be 15 wt. % in terms of process duration and stability. For both model substances, it was possible to successfully run the process for 24 h, with only minor surface adhesion or foaming present in the process chamber. The total amount of processed solids for these test runs is 44.8 kg of lactose (21.6 kg initially suspended, 20.6 kg precipitated and 2.6 kg remaining dissolved) and 30.5 kg of Ibuprofen (21.6 kg initially suspended, 8.4 kg precipitated and 0.5 kg remaining dissolved), which is the desired production range for 24 h of this process. For implementation in the pharmaceutical industry, a cascade of such washing steps with filtration units could be implemented, or if it remains a single step, a second unit could be installed in parallel, to which the process can be switched during

cleaning of the other chamber. To make this process fully continuous, a recurring washing strategy could also be implemented.

Chapter 3 deals with the development of a small-scale, continuously working dryer, being able to process cohesive materials such as pastes or powders. As the flow properties are of crucial importance for the subsequent process steps, the tested materials are characterized according to their flowability at first. This confirms that all tested materials are very cohesive, and therefore especially hard to process. The initial testing before coming up with a new design takes place in an existing paddle dryer. From observed problems at this device, severe design optimization changes are performed, and a completely new dryer design is developed. The conveying principle is interlocking screws, which gently force the material from groove to groove on a large rotor, before being ejected at the end of the process chamber. By these design adaptions, it is possible to achieve stable hold-ups over extended periods of time, in contrast to the previously tested paddle dryer. PSD measurements indicate that the particles are kept intact over the drying process. The hold-up in the new dryer is 40 % less than in the paddle dryer, and also the mass flow out of the dryer was constant and no longer led to blockage. Process times of up to 5.5 hours are possible for the initial test runs, which is considerably longer than the maximum process time of the paddle dryer (i.e. 3 hours). Additionally, the stability of the processes is better by magnitude, and enables further, thorough testing of the device.

In chapter 4 this dryer is investigated in terms of process influencing parameters. Therefore, a test run to estimate the RTD in the dryer is performed, followed by variations of (1) material, (2) air flow, (3) mass flow, (4) temperature, (5) inlet moisture and (6) rotational speed. Further test runs to estimate the governing drying mechanisms as well as long term test runs with refeeding of the processed material were performed. The last test run series was to see the effect of the drying process on the particle properties. It was shown that a higher initial moisture leads to a more stable process, as well as lower rotational speed. While higher temperatures have a slight positive effect on the evaporated water, they can negatively influence the hold-up within the dryer. The drying performance is more or less independent from the air flow, which is supported by the drying capacity test runs, as they identified conduction as the main driving force for this drying process. The RTD test setup showed a peak after 13 minutes and 30 seconds, but as the methodology has not yet been perfected, more test runs must be performed to eradicate the long tailing behavior. The refeeding test runs and the SEM pictures of the product showed that a small amount of fines are produced, but generally the particle morphology is kept intact. The tested configurations for Ibuprofen gave results between 492 g and 985 g of hold-up (based on dry Ibuprofen), whereby the typical amount was around 650 g. The test run with di-calcium phosphate showed a hold up of 1.8 kg of dry powder, but also had accumulations on the

screw-opposing side on top of the rotor, possibly caused by the drying air. This behavior needs to be further investigated. The amount of evaporated water ranged from 68 g to 542 g for Ibuprofen, whereas the small amounts led to a completely dry product. By further improving the dryer to be able to operate under vacuum, the drying capacity can be tremendously improved, and the direct integration into existing production lines is feasible.

„So Einstein was wrong when he said, "God does not play dice." Consideration of black holes suggests, not only that God does play dice, but that he sometimes confuses us by throwing them where they can't be seen."
Stephen Hawking (1942-2018)

6 Outlook

As processes and equipment are emerging, which can fill the existing gaps within continuous manufacturing lines, the shift towards CM will further advance in the pharmaceutical industry. By improved mechanistic understanding of the processes and optimal use of PAT tools, CM can match the flexibility of batch processes without their disadvantages, such as difficult scale-up and scale-down and large energy and storage demands. The main difficulties at the moment are the integration into primary manufacturing, as the flowability is often very poor and process streams are typically small.

Within this thesis, two attempts to provide such puzzle-pieces are presented. The first one is a continuous purification or washing line, working at small scales. Since it is confirmed in the performed work that the particle properties are mostly maintained and the process works stable for at least 24 h, it could be implemented continuously into primary pharmaceutical manufacturing. By adapting the design of the process chamber to withstand higher pressures, and possibly changing the geometry of the chamber itself to optimize the flow pattern, the process could reach even more stability. Also, a washing strategy based on a certain pressure rise could be implemented. Surface optimization of the process chamber could also result in much longer process times, eradicating solidification on the walls. Further investigations and optimizations can therefore lead to a very robust and stable process, with constant product properties. Also, a sophisticated temperature control could be used in front of and after the chamber, to obtain a very narrow PSD by solving and dissolving material on purpose. Further investigations of the needed power supply in different geometries need to be performed, to reduce the energy consumption of the system, with the same process behavior.

For the novel dryer design, the initial testing has proven to be very promising in terms of flow behavior and robustness. If the design is further optimized to be air-tight, it will be possible to operate under vacuum and/or with organic solvents, which will be necessary for an implementation in the pharmaceutical industry. Further test runs to evaluate the process performance and drying capacity under vacuum are part of future investigations. To further reduce hold-up generation and tribocharging, surface treatment of the parts could be looked at. By further adapting the design of some dryer parts (e.g. outlet valve, guidance system) to improve the mounting and cleaning process, a lot of time could also be saved for each

process. To be able to be implemented directly after a filtration unit, the feeding system into the dryer also needs to be adapted, to be able to process pastes. The integration of a control and regulation system to have the dryer as a stand-alone unit must be created for industrial relevance. As the initial testing shows a small amount of fines after processing, further optimization of the conveying screw could be done, to take even more care of maintaining the particle properties. As the existing dryer is very mobile and flexible, integration into modular manufacturing will be rather easy, indicating the huge applicability of the proposed design within pharmaceutical industry.

Future research could investigate the possibility of linking the continuous purification line with a continuously working filtration device, from which the material is fed into the dryer. Achieving process times of up to 24 h in such a system would be a strong indication of the industrial relevance of the purification and the drying step. Finding a working process configuration combining these three-unit operations enables a truly continuous production line in primary manufacturing. As solutions for continuous synthesis and crystallization exist, this could ameliorate existing production by a large extent.

Also, the possibility of integrating the dryer into a direct compaction line will be investigated. While this is not completely relevant for the current status of the pharmaceutical industry, it could provide valuable insights for the continuous feeding of freshly dried, cohesive powder and the influence of process fluctuations on final tablet properties. Additionally, it would serve as proof of concept for manufacturing companies, who might want to connect primary and secondary manufacturing in the future. With the results from these test runs, a PAT strategy could be implemented for the monitoring and the control of the production process.

As one of the influencing factors on the product quality of the final product is the solubility, screening experiments should be performed to make sure that the solubility of the solids in the liquid substance of the feed material is as low as possible, to avoid agglomeration. A certain moisture content however is beneficial, as tribocharging is reduced tremendously. Therefore, further test runs should be performed, looking at the optimal composition of the feed material, taking into account the necessary energy consumption for the drying process. Also, a solvent recycling strategy could be implemented after the drying step. This would reduce waste to a large extent and reduce the running costs of the primary manufacturing route.

In the complex and large field of pharmaceutical manufacturing, robust and qualitatively high processes and equipment need to be developed and implemented. This thesis presented ways to improve continuous purification and washing, as well as drying of

small product streams, maintaining the initial particle properties to a large extent. This work contributes to the transition towards continuous manufacturing in the pharmaceutical industry, by providing easily implementable solutions in the described unit operations.

"Knowing others is intelligence;
knowing yourself is true wisdom.
Mastering others is strength;
mastering yourself is true power.

Laozi (6th–5th century BC)